2012

Design of a Mastication Robot of Lead Screw and Scotch-Yoke Actuation

WEI-LIN CHANG
Lehigh University

Design of a Mastication Robot of Lead Screw and Scotch-Yoke Actuation

By

Wei-Lin, Chang

A Thesis

Presented to the Graduate and Research Committee

of Lehigh University

in Candidacy for the Degree of

Master of Science

In

Mechanical Engineering and Mechanics

Lehigh University

September, 2012

This thesis is accepted and approved in partial fulfillment of the requirements for the Master of Science.

_____

Date

_____

Thesis Advisor

_____

Chairperson of Department

ACKNOWLEDGMENTS

I would like to thank to my advisor Dr. Meng-Sang Chew for providing this opportunity to work on this research. It is with his advice, opinion and support, that I can complete this thesis research and write up. During this process, I learned a lot. I will forever treasure these experiences. I would also a wish to thank my family for their continue support, encouragement and patience during my study here in the United State.

TABLE OF CONTENTS

APPRNDICES

LIST OF TABLES

LIST OF FIGURES

Tables of Nomenclature

K_m	clenching subsystem motor torque constant
R_m	clenching subsystem motor armature resistance
J_m	clenching subsystem motor armature & pinion gear inertia
J_c	bevel gear & lead screw inertia
N_g	bevel gear ratio
L	lead
W	grinding subsystem load
E	lead screw Efficiency
D	displacement of grinding subsystem
$\ddot{\theta_m}$	angular acceleration of motor output
$\ddot{y}_m$	acceleration of grinding subsystem
f_u	required force when the jaw closes,
f_d	required force in mandible opening
f_c	chewing force

Abstract

A three degree-of-freedom mastication robot system is presented. The system utilizes a lead screw subsystem plus a scotch-yoke subsystem to perform some simple human masticatory functions.

A robotic device is required to enable the reproduction of human chewing behavior; therefore, this thesis will briefly review the human mandible structure and masticatory systems which are relevant to masticatory robotics. In order to reduce the actuators using in mastication system, Chasle's theorem is applied in arriving the final design. The design of a masticatory robot which can perform some human masticatory functions is presented. The motion trajectory of the system is experimentally determined and it shows that the robot can indeed perform human-like masticatory motions. To determine the lowest energy consumption by the DC motors of the mastication robot an optimization procedure is also presented.

CHAPTER 1:

INTRODUCTION

1.1 Description of the Project

The objective of this project is to design and build a prototype of a masticatory device which can perform some human masticatory functions and to assist those physically impaired in chewing and eating.

Many researchers have developed a variety of machines and devices to perform the complex functions related to mastication. A simple introduction of developed robots that have been developed is shown on Chapter 2. These are classified into dental training robots, jaw simulation robots and foods chewing robots. The first two types of robots are used in experiment or therapy. In this thesis, the focus is on food-chewing robots since current design are impractical due to their size and weight. The objective of this study is to design a device which can serve both purposes: easy to put on and take off, and help the user in chewing.

The design must meet the following requirements:

i. The design must perform the basic jaw movement and help user in chewing food.
ii. The operation of speed of the device must be similar to normal chewing of a human.
iii. The operational force conforms to the average chewing force applied.

iv. The device must be light in weight.

Details of the design and the characteristics of system are shown in Chapter 3. In Chapter 4, an optimization procedure is used to determine the lowest energy consumption at the DC motors. The power consumption will be lower and the device will still performed adequately.

1.2 Background of Masticatory System

Mastication is a complex process from food taken into the mouth, through crushing and grounding by teeth, and then to clearing and swallowing [1]. This is the first step of digestion and increasing the surface area of foods to allow a more efficient break down by enzyme. In order to carry out this process, the masticatory system is separated into seven parts: bones, teeth, tongue, muscles, ligaments, blood vessels and nerves. Generally, the two types of bones, Maxilla (upper jaw) and mandible (lower jaw), as shown in Figure 1.1 [3], acts as the structural support to the system.

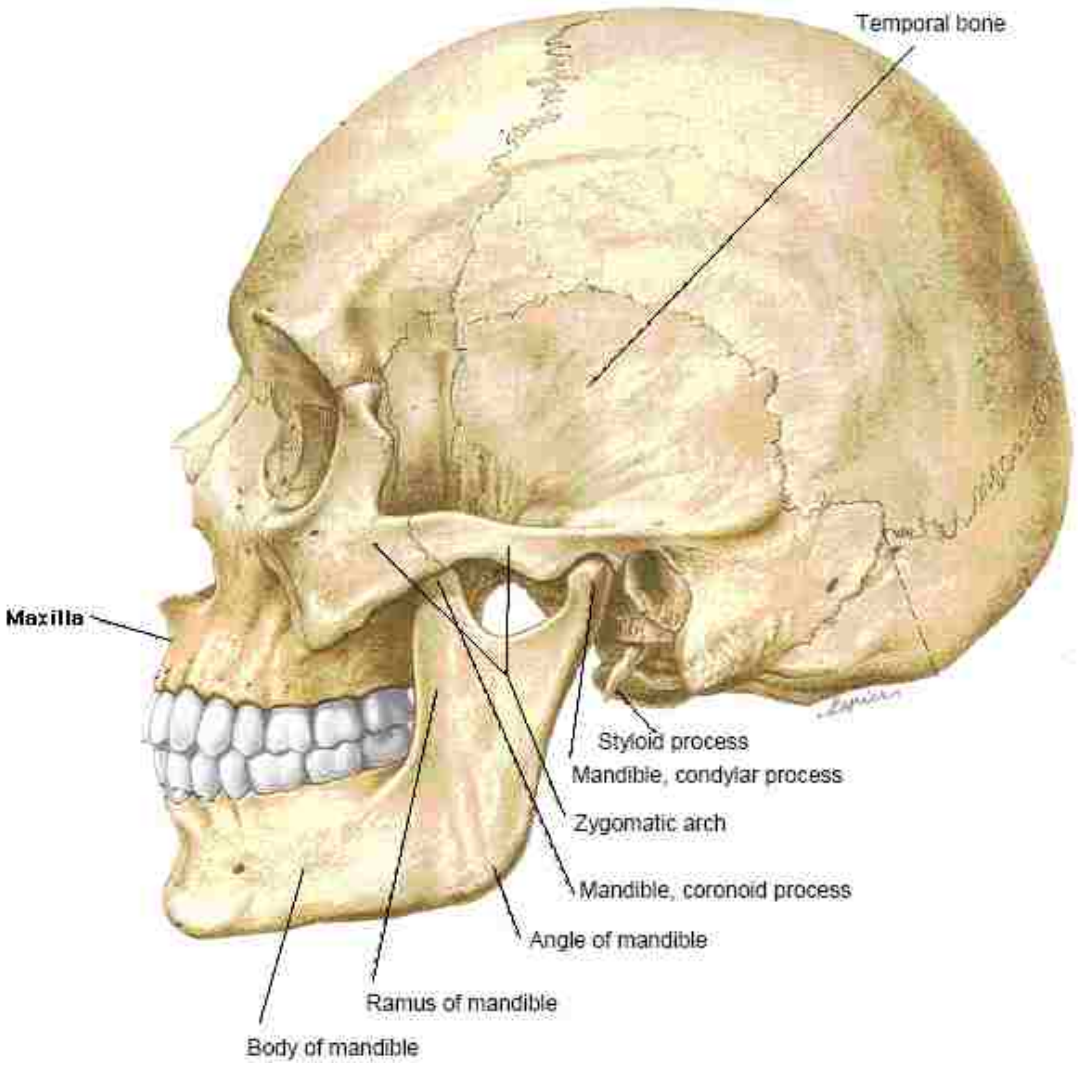

Figure 1.1: Side view of human skull showing masticatory bone structures

Maxilla is the fixed bone structure that which is connected with the temporal bone and makes up the skull. The mandible is pivoted at the condylar and works as a mobile that is controlled by central nervous system to the muscles. The joint drives action cutting and grinding of foods. The function of the tongue is to mix the foods and then deliver them into pharynx. It can be seen that the essence of the process is to control the mandible motion for the complex chewing movement to cut and grind of foods. The details of jaw motion and chewing forces will be discussed in Chapter 3.1.

CHAPTER 2:

PIOR STUDIES OF DEVELOPED MASTICATION ROBOTS

There have been several robots available for different applications in mastication research, such as dental training, jaw simulation and food texture analysis. Each of these types of robots is discussed below.

2.1Dental Training Robots

2.1.1 WY Series Robots

2.1.1.1 Background

WY (Waseda Yamanashi) series robots was developed at Takanishi Laboratory, Waseda University, Japan in 1986 [9]. It was used to treat mastication movement disorder patients for mouth opening training. This method is for the patients who could not open the mouth more than 10mm. Conventional, doctors use mouth opening tool such as wooden screws, bite blocks and clothespins-type apparatus, as shown in Figure 2.1 [9] but these kinds of devices cause pain to the patients and rely greatly on the doctors' experience [10]. Therefore, the dental Robotics Group in Takanishi Laboratory, Waseda University started developing a system which can execute the treatment objectively through the use of actuators, sensors and controller systems.

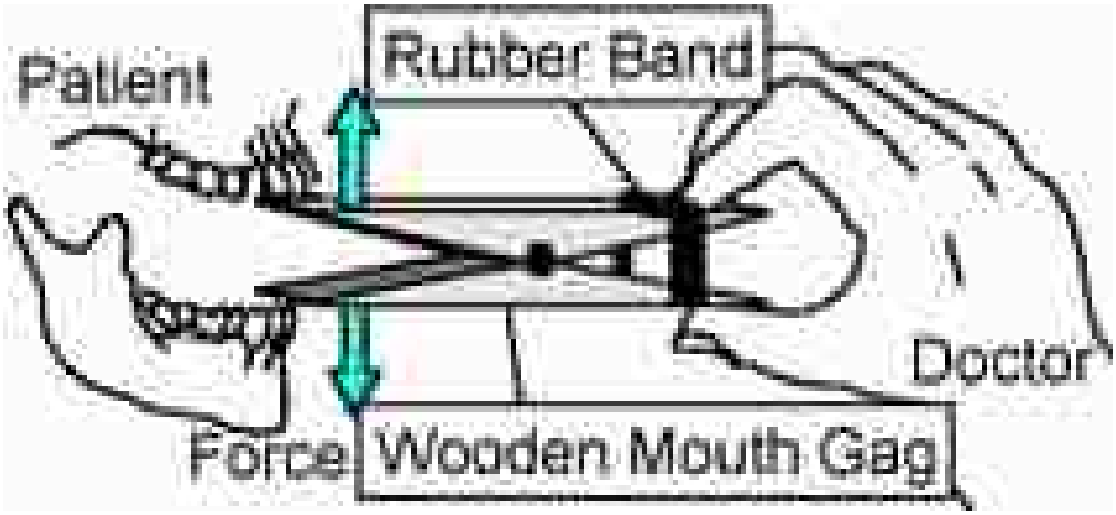

Figure 2.1: Conventional Treatment with Wooden Mouth Gag

2.1.1.2 System composition of WY-5/WY-6 robot

WY-5/WY-6 is the most advanced version of the WY series robots and is shown in Figure 2.2 [9]. This robot system consists of three subsystems: mechanisms, sensors and control subsystems. An outline of these three subsystems follows:

(1) Mechanisms: The robot performs 6 degrees-of-freedom (DOF) and consists of six ball screws which are actuated by six linear motors, as shown in Figure 2.3 [9]. The upper mouth piece holds the patient's upper jaw and patient's lower jaw will be moved accordingly by the robot. This mechanism provides a wider movable range than the human jaw, and is shown in Figure 2.4 [11].

(2) Sensors: The 6 DOF force moment sensor measures the biting forces in the patient on XYZ axes. Each DOF also has displacement and velocity sensors that

correspond to the muscle spindle [11].

(3) Controller: The doctor in the robotic manipulator is the controller, and it connects to the patient robot through a server and client computer via a network using an ISDN line, as shown in Figure 2.5 [9]. The information that the doctor gives, such as mouth opening angle and forward/backward displacement, are sent to the patient side to actuate the robot while at the same time, the force information is also sent back to the doctor side.

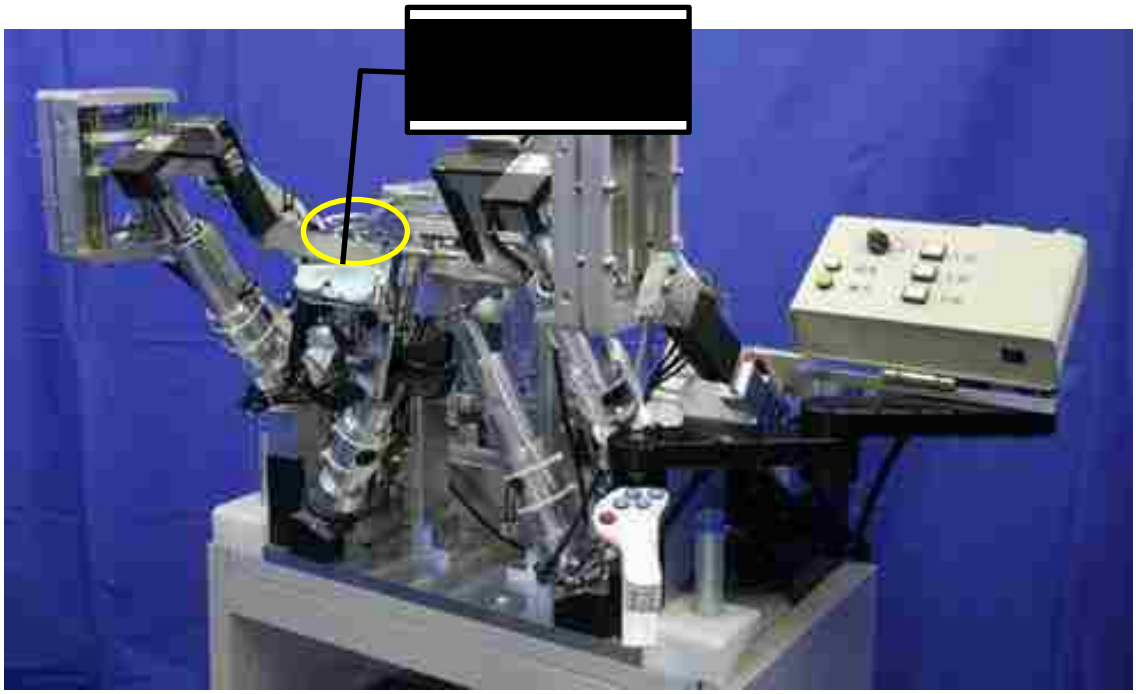

Figure 2.2: Robot WY-5

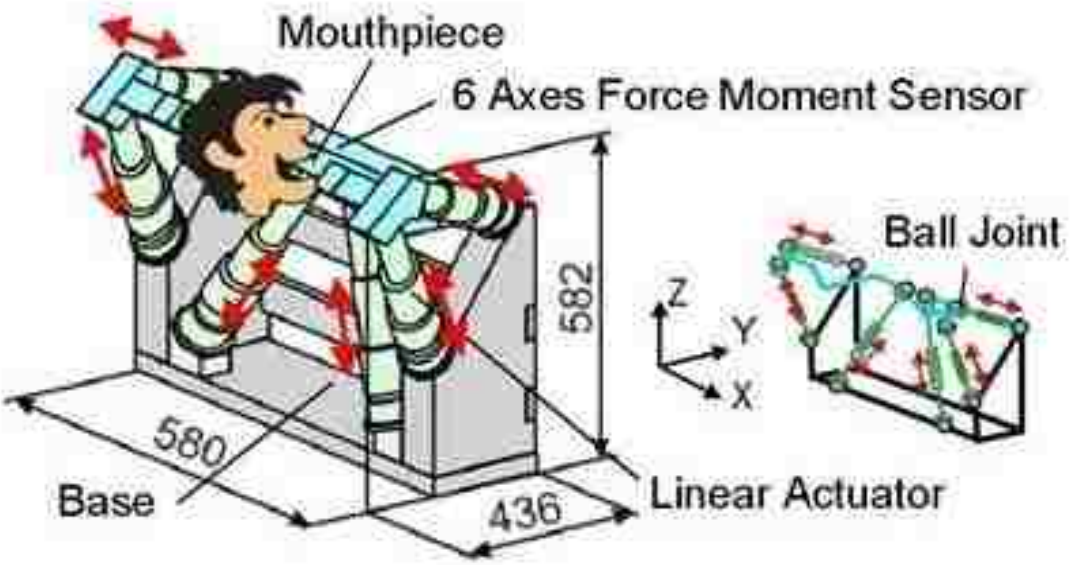

Figure 2.3: Mechanism of WY-5

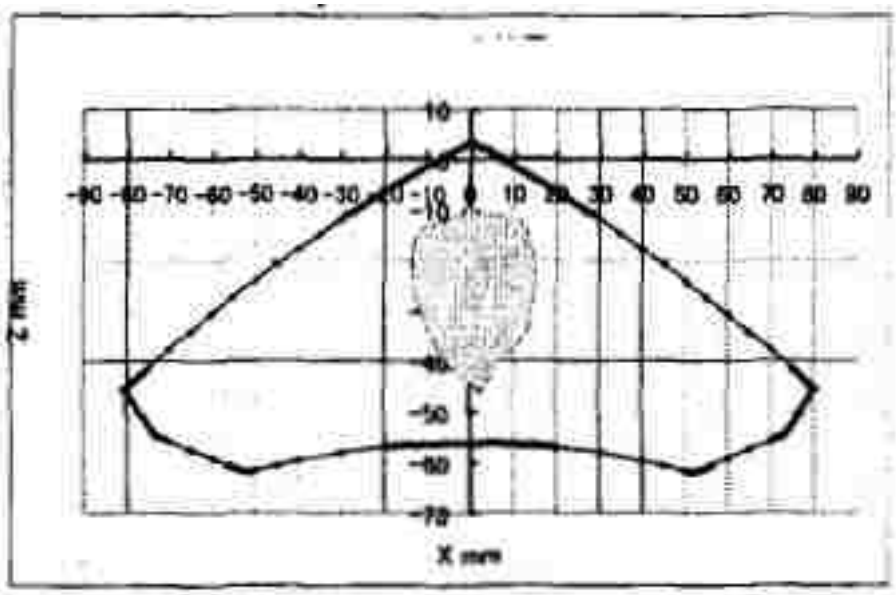

Figure 2.4: Comparison of WY-5 and human jaw movable area (gray part is human area)

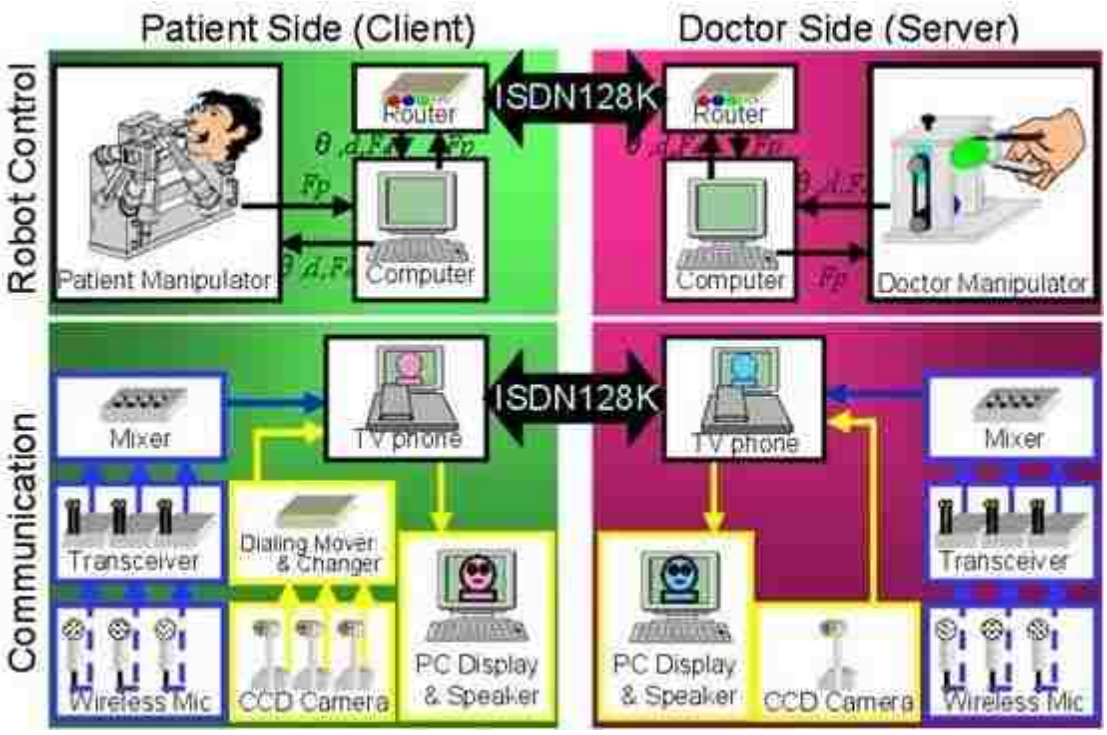

Figure 2.5: Total system configuration of WY-5

2.1.2 WJ series Robot

2.1.2.1 Background

For dental/medical therapy, doctor and patient models are needed to quantify the human model. The mouth opening training robot WY-5 as a doctor model was discussed in 2.1.1. Another robot called WJ (Waseda Jaw) robot series has been used as a patient model. The WJ series robot was developed at the Takanishi Laboratory, Waseda University, Japan and its purpose is working with WY series robot to understand patient's mastication movement and muscle forces during mouth opening and closing. In other words, WJ robot is a mechanical simulator based on a human

mastication system [12], so that the doctor can use this robot to test and analyze the patient's disorders and then decide on the treatment plans.

2.1.2.2 System composition of WJ-2 robot

WJ robots were built under an assumption that the human jaw only has 3 DOFs of movement: open/close, forward/backward and right/left[1], and this is shown in Figure 2.6 [1]. In 1988, Waseda University developed a mastication robot WJ-2 which has 3 DOFs as shown in Figure 2.7 [9]. This robot system consists of four subsystems, mechanisms, artificial-muscle-actuator (AMA) subsystems, sensors and control subsystems. An outline of these three subsystems is as follows:

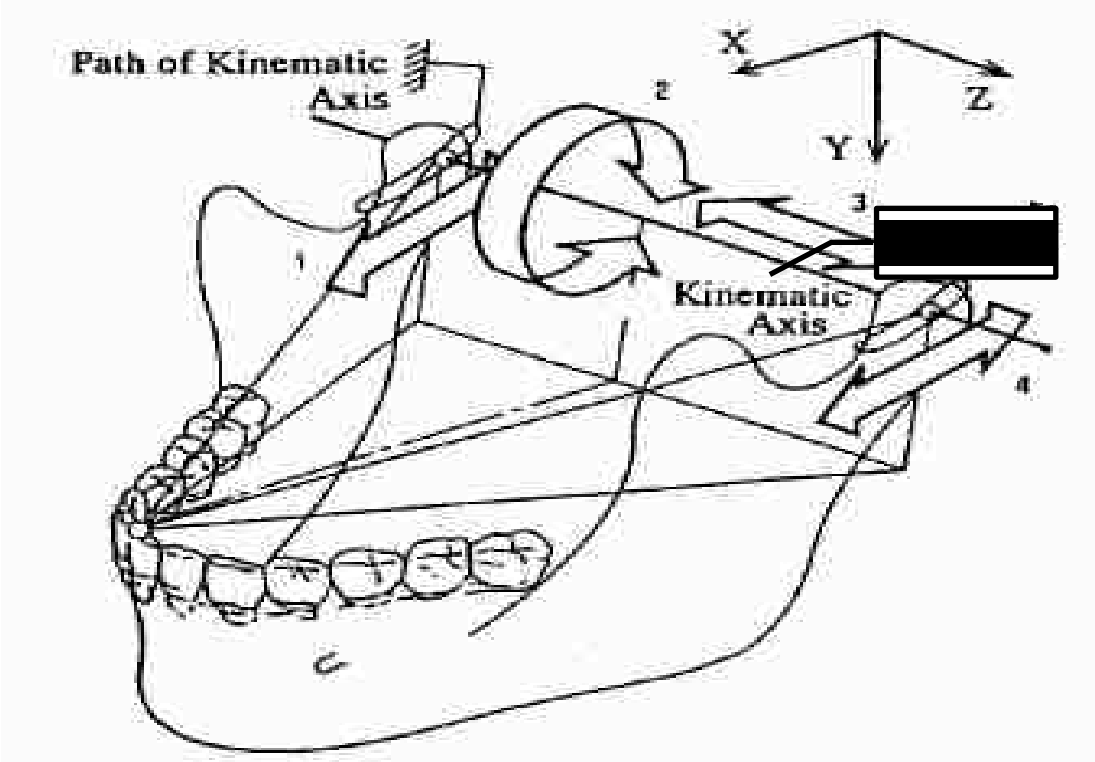

Figure 2.6: Jaw movement of 3 DOFs


Figure 2.7: WJ-2 robot

(1) Mechanisms: Figure 2.8 [13] shows the outline of the mechanism of WJ-2's mandibular joint. A plastic block with a V-groove passes through the right and left condyles and is attached to the upper jaw. Forward/backward motion of this plastic block is inclined 40 degrees from the horizontal plane [13].

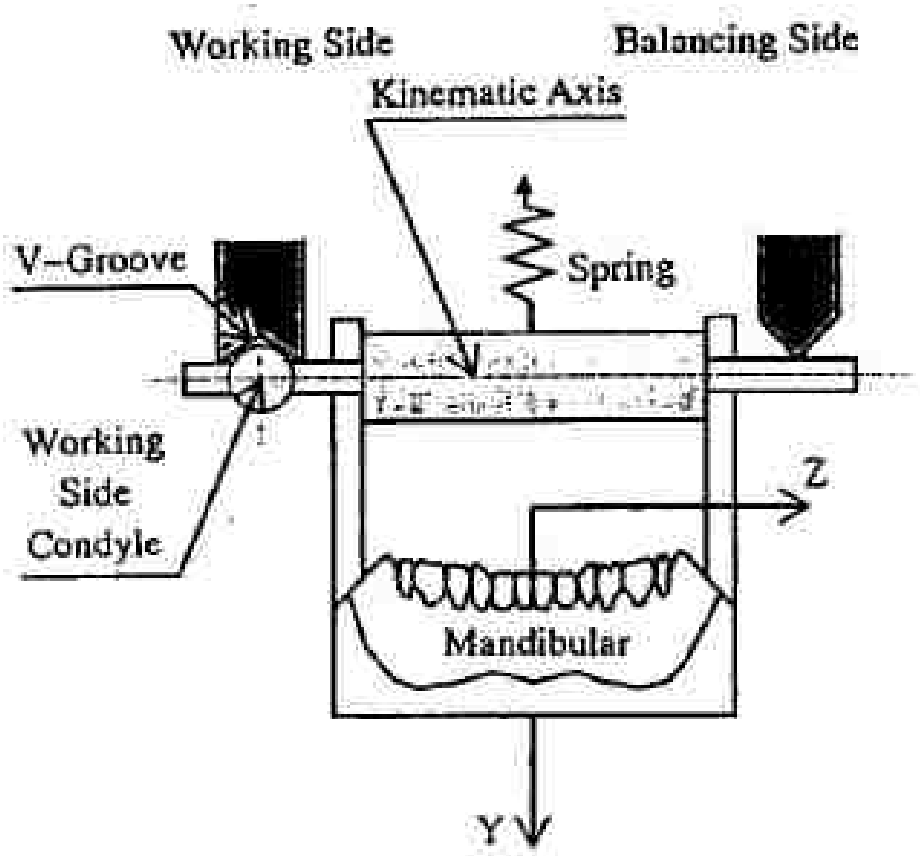

Figure 2.8: Mechanism of WJ-2

(2) Artificial-muscle-actuator (AMA) systems: this actuator is designed to simulate muscular motion. Each AMA is made up of a DC motor, an encoder, a wire and a force sensor. Figure 2.9 [1] shows the detailed design. In the assignment of AMAs, the actuators are placed both on the working side and on the balancing

side symmetrically and one AMA is assigned at the center of the jaw in the frontal plane [13]. Figure 2.10 [13] shows the assignment of AMAs in the WJ-2.

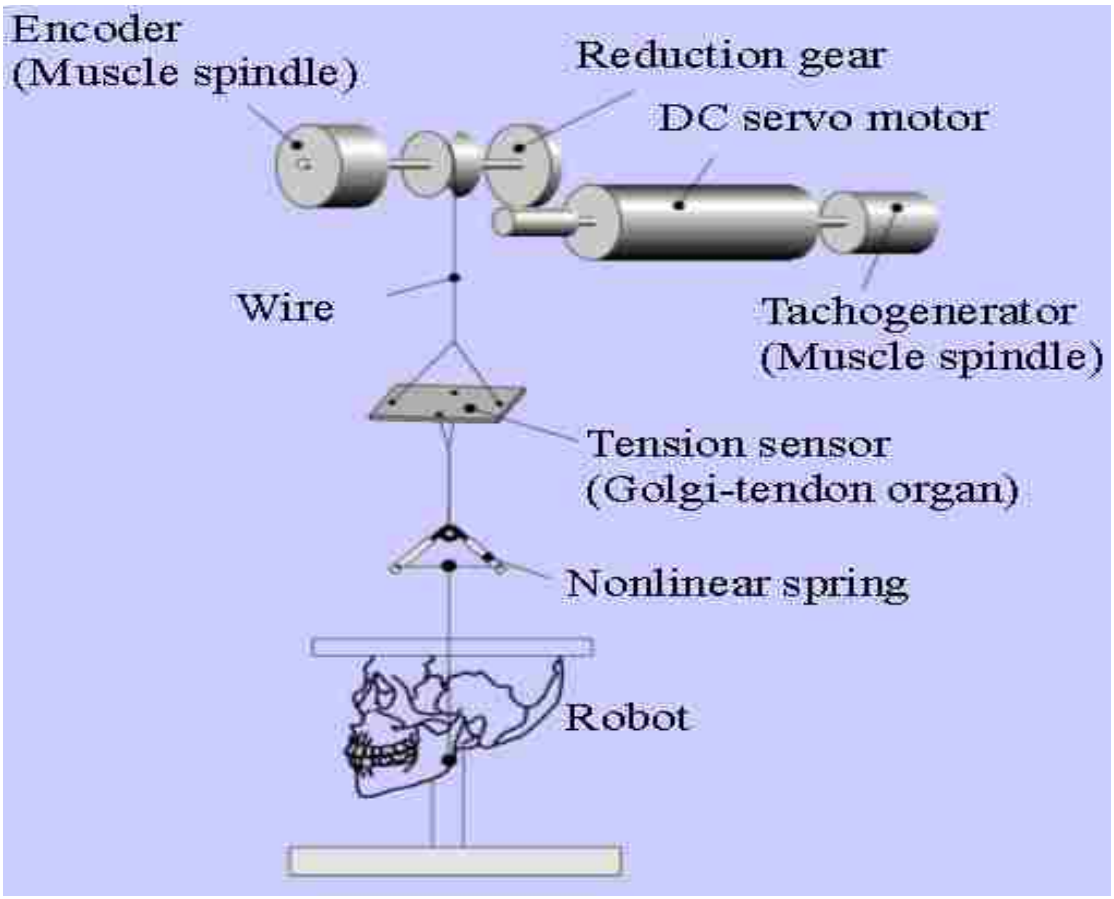

Figure 2.9: Artificial-muscle-actuator

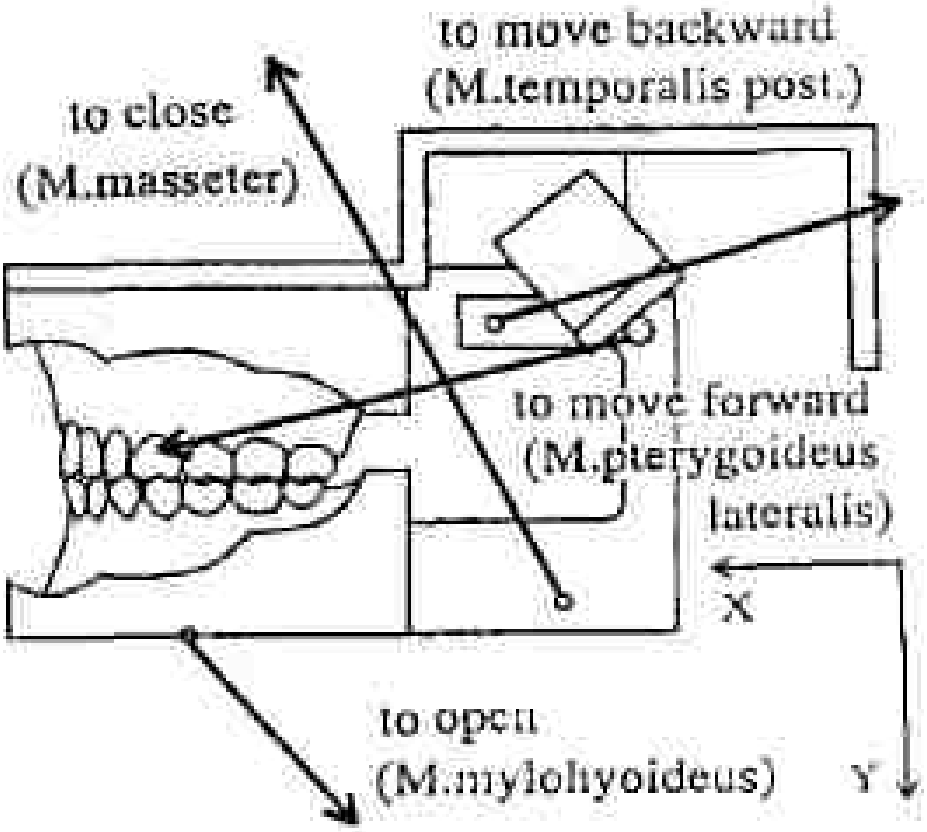

Figure 2.10: Assignment of AMAs in WJ-2

(3) Sensors: There are four types of sensors used in the WJ-2. Potentiometers are used to detect the extension displacements and tachogenerators for detecting the velocities. The third sensor is a strain gauge, which is used to replace the Golgi tendon receptor in human muscle function. A pressure sensor (biting force sensor) is used to detect biting force [13].

(4) Control system: The robot has two levels in the control system. One is the mastication control system which is the upper level system and controls the lower level muscle control system. The mastication control system recreates the

motion pattern of the mandible, and the mastication control sequence is shown in Figure 2.11 [13]. For every mandible motion, the muscle control system controls the AMAs using position and velocity feedback of the muscle spindle [13].

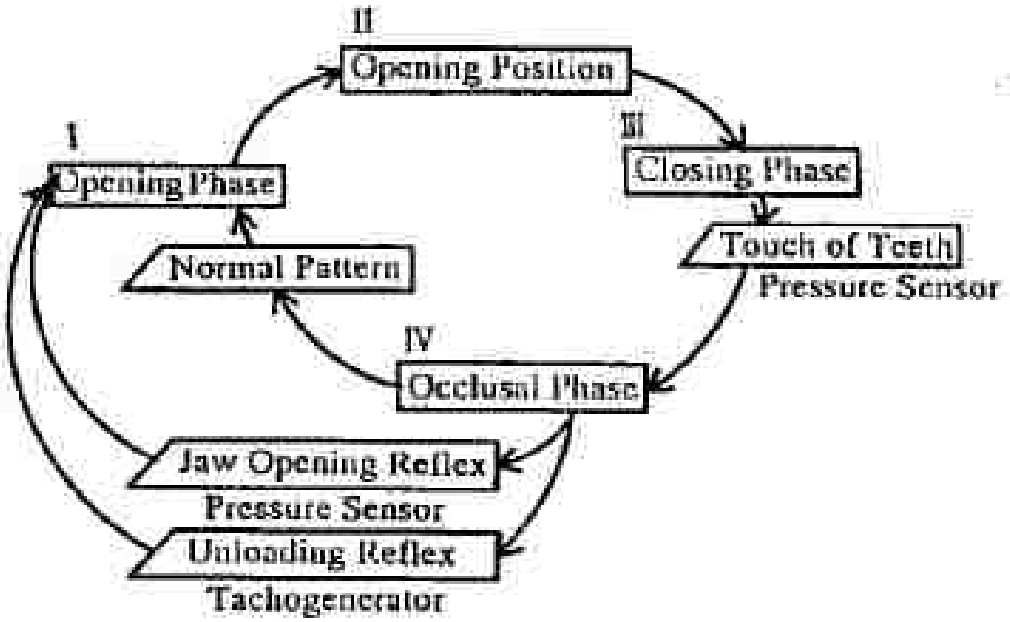

Figure 2.11: Control sequence of WJ-2

2.1.2.2 WJ-2 experiments on foods test

This section shows the results of different foods on WJ-2. Figure 2.12 shows the continuous chewing for tamago-bolo which represents crushable food [13]. Figure 2.13 shows continuous mastication for a jelly candy [13].

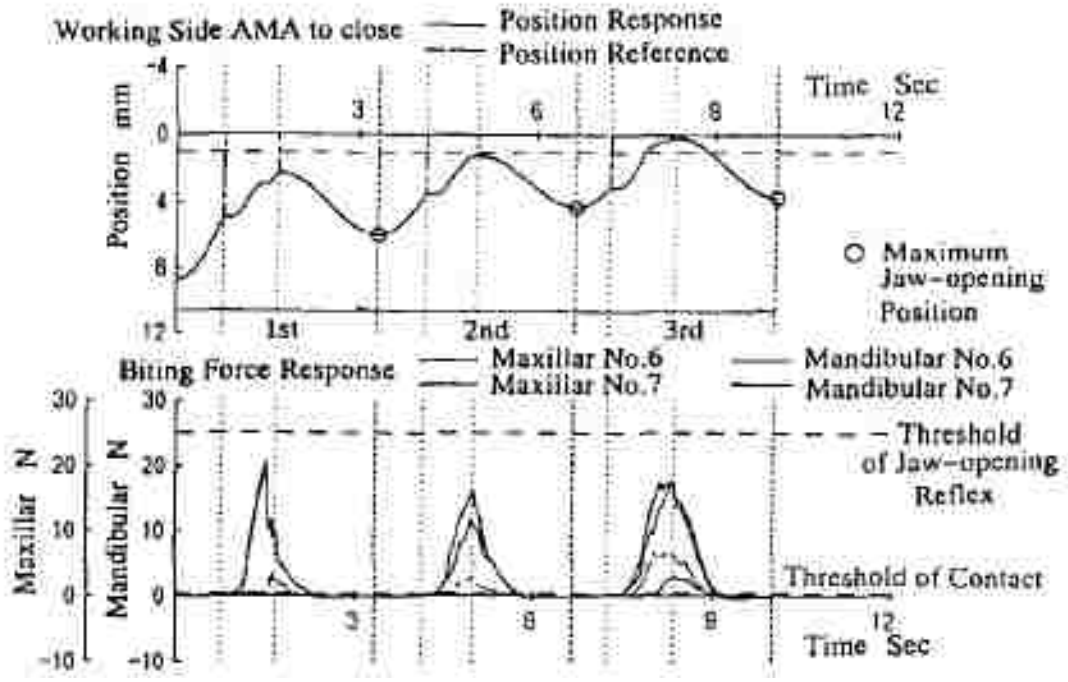

Figure 2.12: Continuous chewing for tamago-bolo

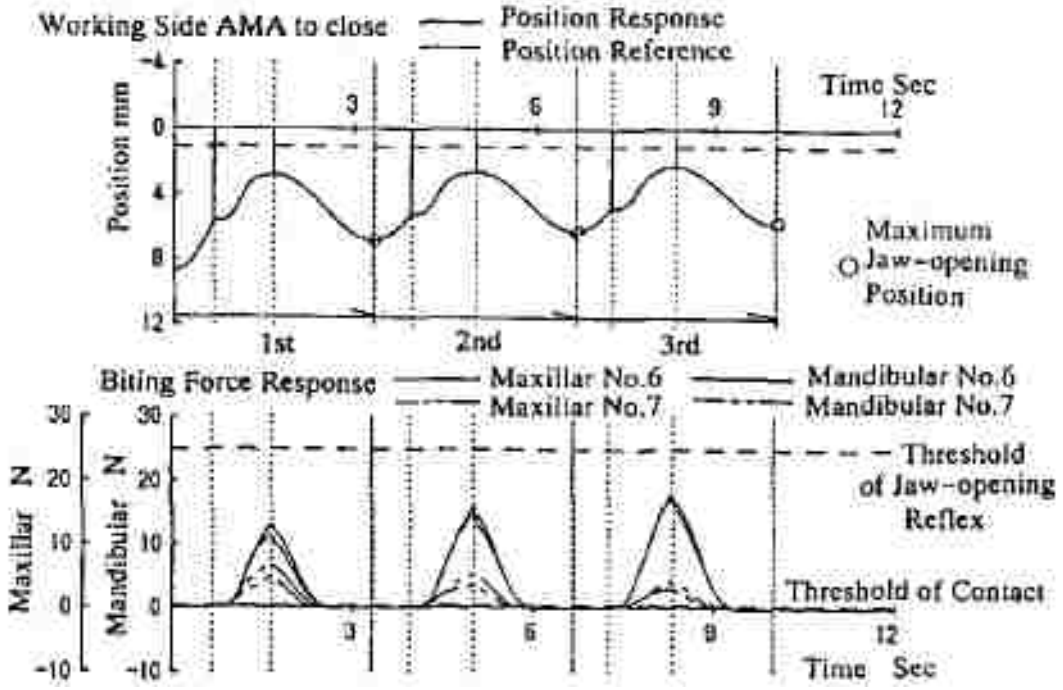

Figure 2.13: Continuous mastication for a jelly candy

2.2 Jaw Simulator Robot

The goal of a jaw simulator robot is trying to simulate the motion and force of the human jaw. A human jaw simulator was developed at Northeastern University, USA [2]. The developers used mechanical components to replace the muscle, ligaments function and to re-produce mandible movement. For this specific robot, the developers focused on simulating the movement of the mouth opening and closing with the LabVIEW user interface [2].

2.2.1 Mechanisms of Jaw Simulator Robot

The robot assists of several parts. First, there are three motors which are used as force actuators for simulating the three muscles on each side of the skull. The second part is a pulleys system which is used to amplify the torques from the motors. This is shown in Figure 2.14 [2]. The third part are wire attachments, and these are used to connect to the pulleys and the skull attachment points. Figure 2.15 [2] shows the system force analysis and position on the mandible, the wires applied to the attachment and anchor points creates the forces and drive the mandible motion. Figure 2.16 [2] shows a skull with the anchor and attachment points. Figure 2.17 [2] shows the final design of the robot.

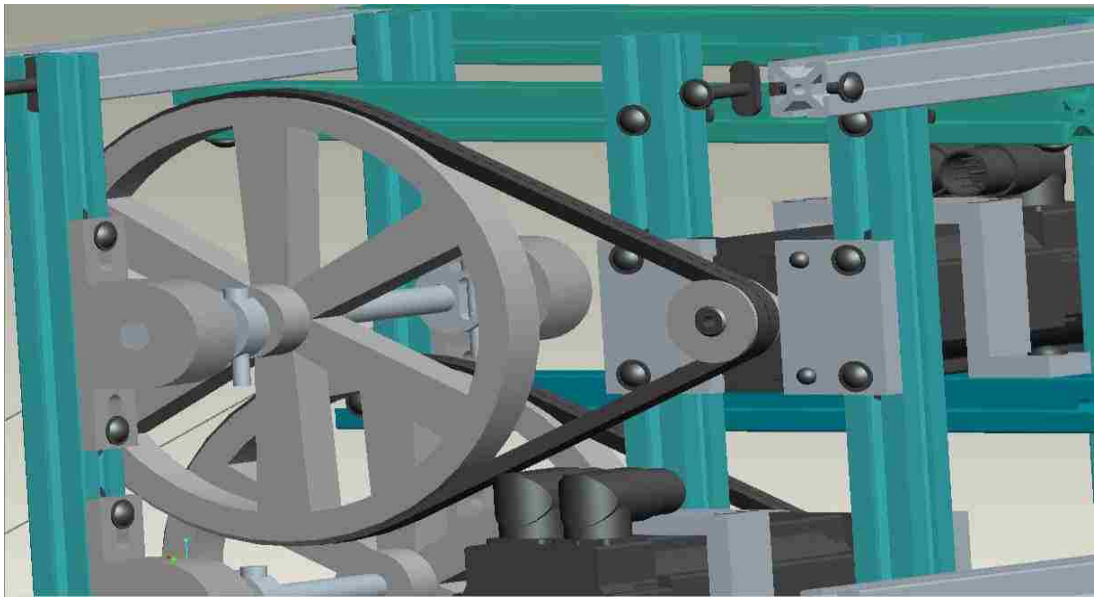

Figure 2.14: Motor and pulley system

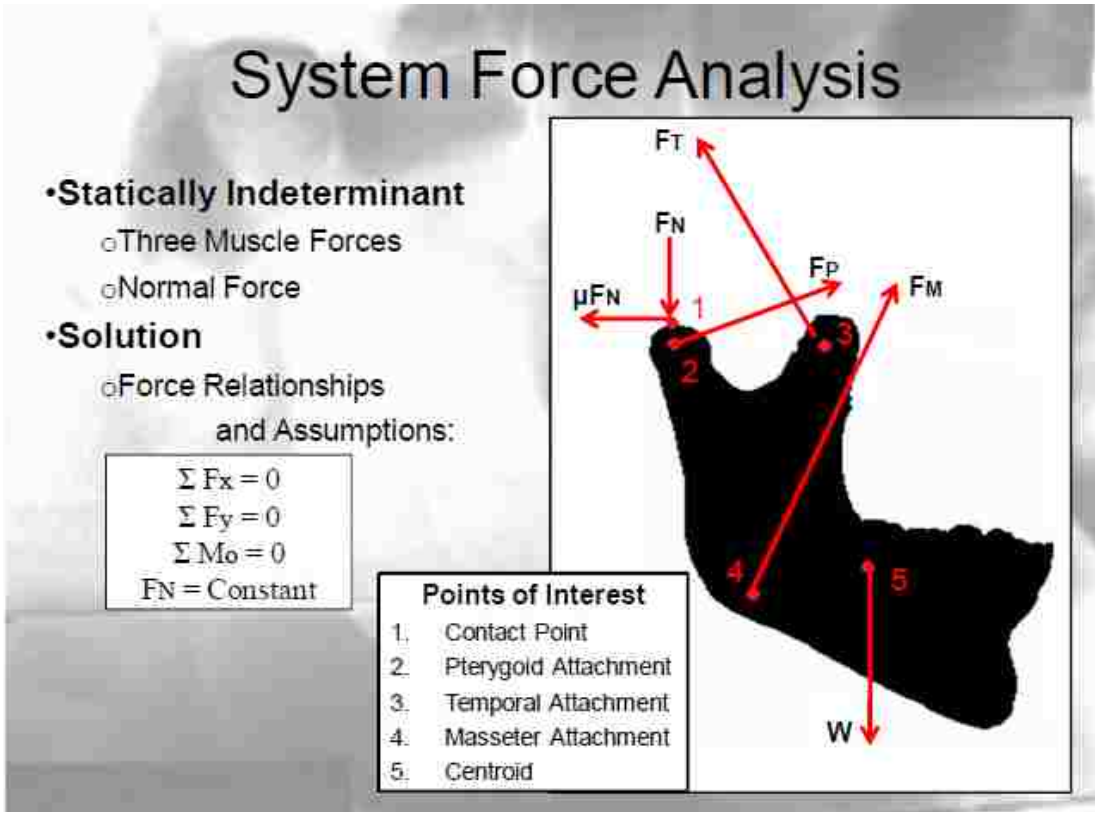

Figure 2.15: Mandible free body diagram

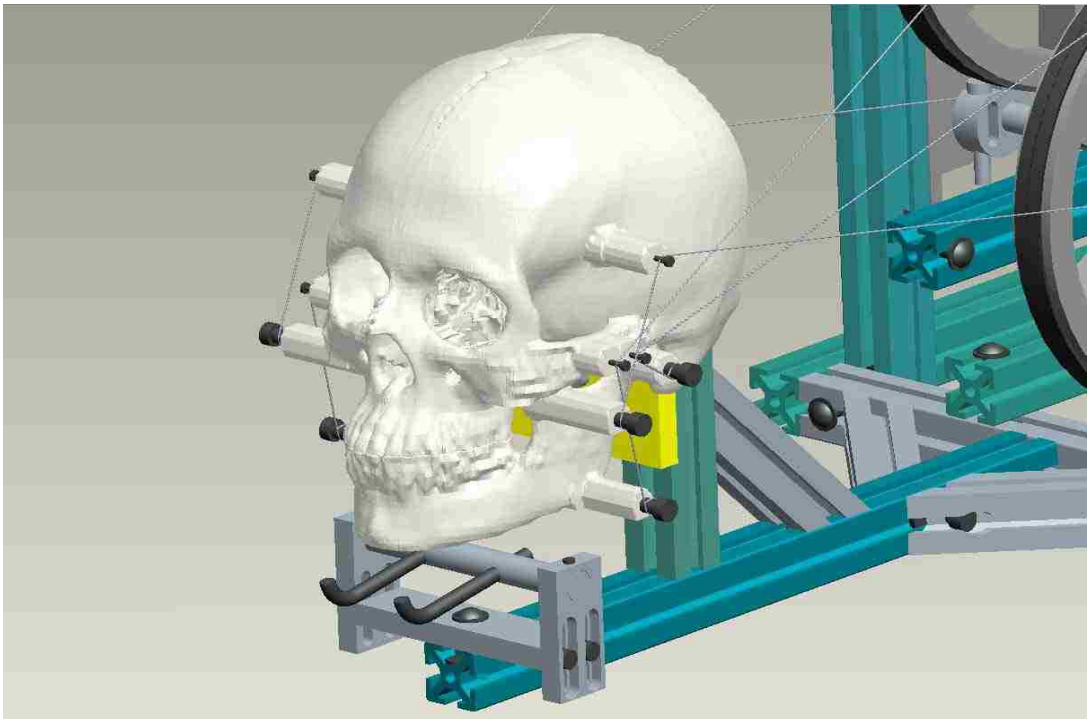

Figure 2.16: Skull with Anchor and Attachment Points

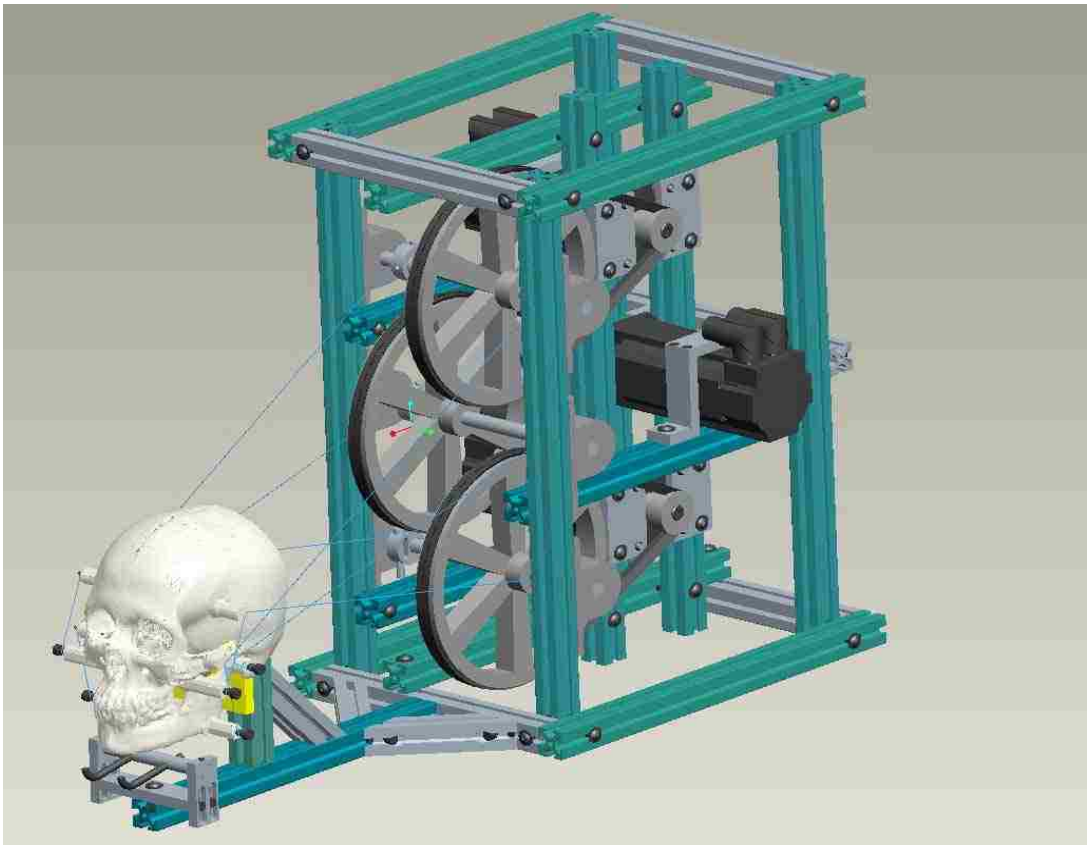

Figure 2.17 Final design of human jaw simulator robot

2.2.2 Simulation results

Figure 2.18 [2] are virtual simulation results that show the mandible motion is close to a translation followed by a rotation [2].

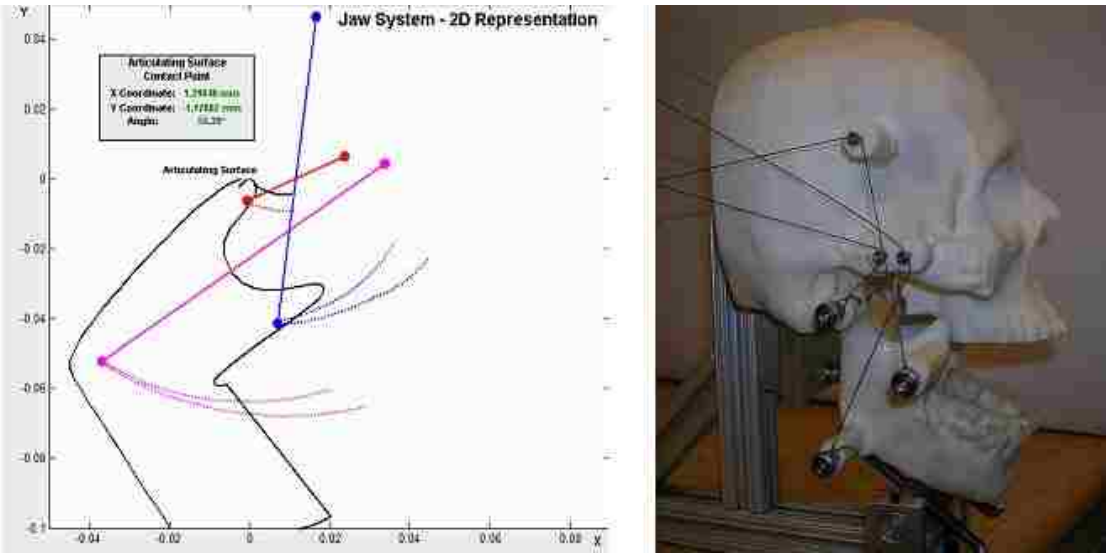

Figure 2.18: Jaw Simulator motion simulation

2.3 Food Chewing Robot

The purpose of the food chewing robot is reproduce movement, velocity and biting forces that simulates the human chewing process before food swallowing. The food chewing robot was developed at Massey University in 2002 and there are two different mechanical models used in the robot. First is a robotic model of linear actuation and the second model is a crank actuation.

2.3.1 Robotic Model of Linear Actuation

2.3.1.1 Mechanism model

According to the mandible model and reference points as shown in Figure 2.19 [1](the reference points represent the places that the three major muscle, temporalis, masseter and pterygoid are attached to the mandible). It used six linear actuators connecting the mandible reference points to the skull, so that the actuators act as the specific muscles to produce biting force and displacement of mandible. Figure 2.20 [1] shows the conceptual model, CAD model and kinematic model.

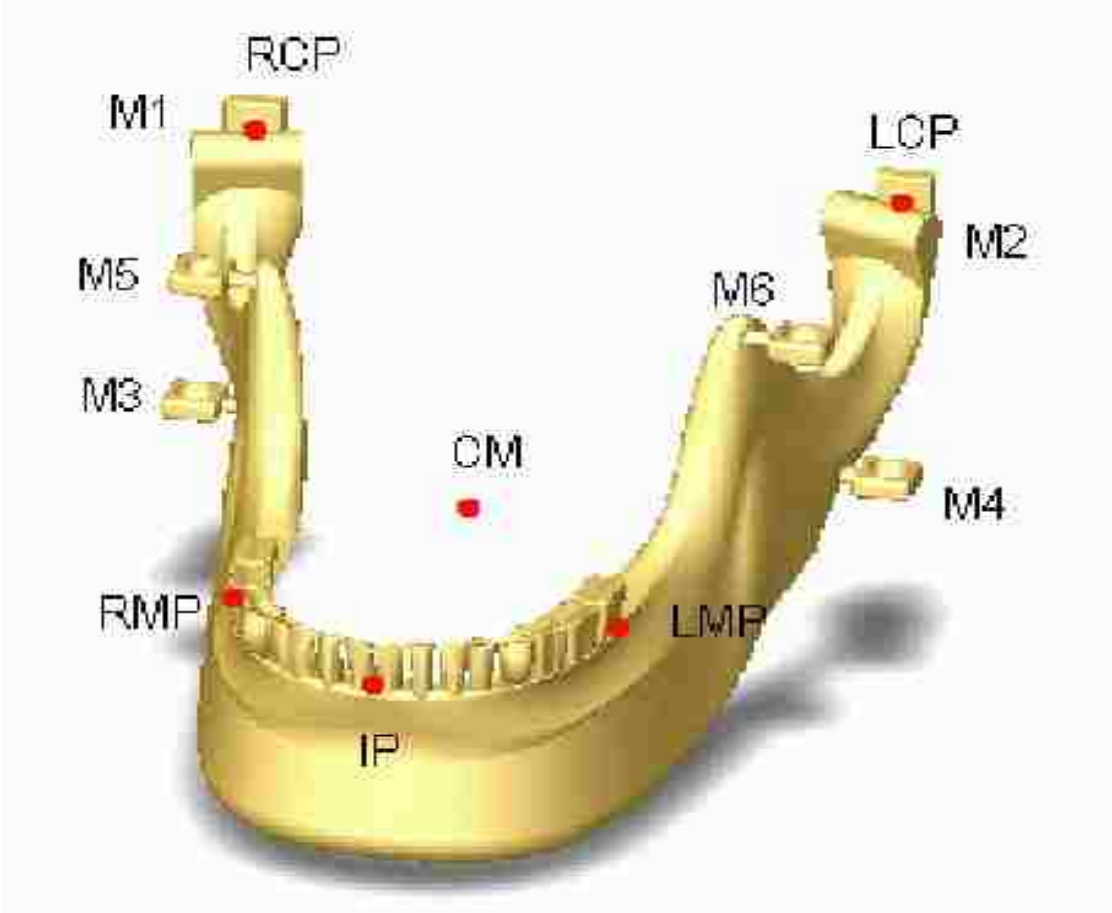

Figure 2.19: A mandible model and reference points

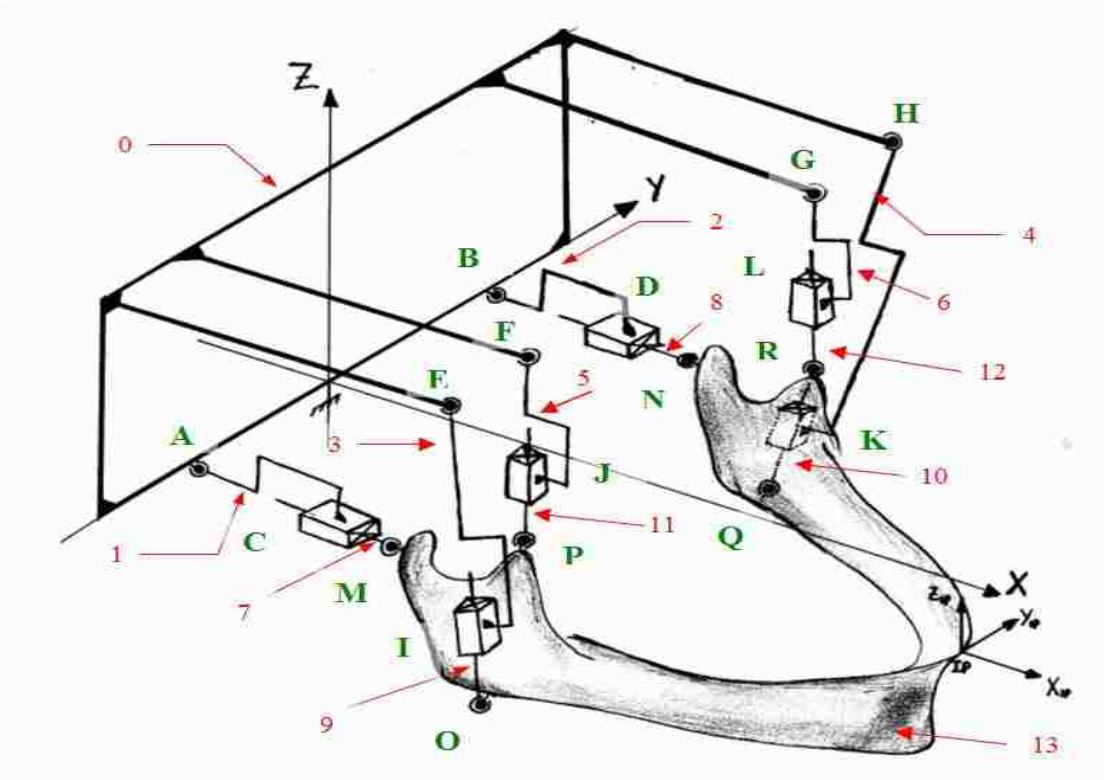

Figure 2.20: Chewing robot model, (a) conceptual model

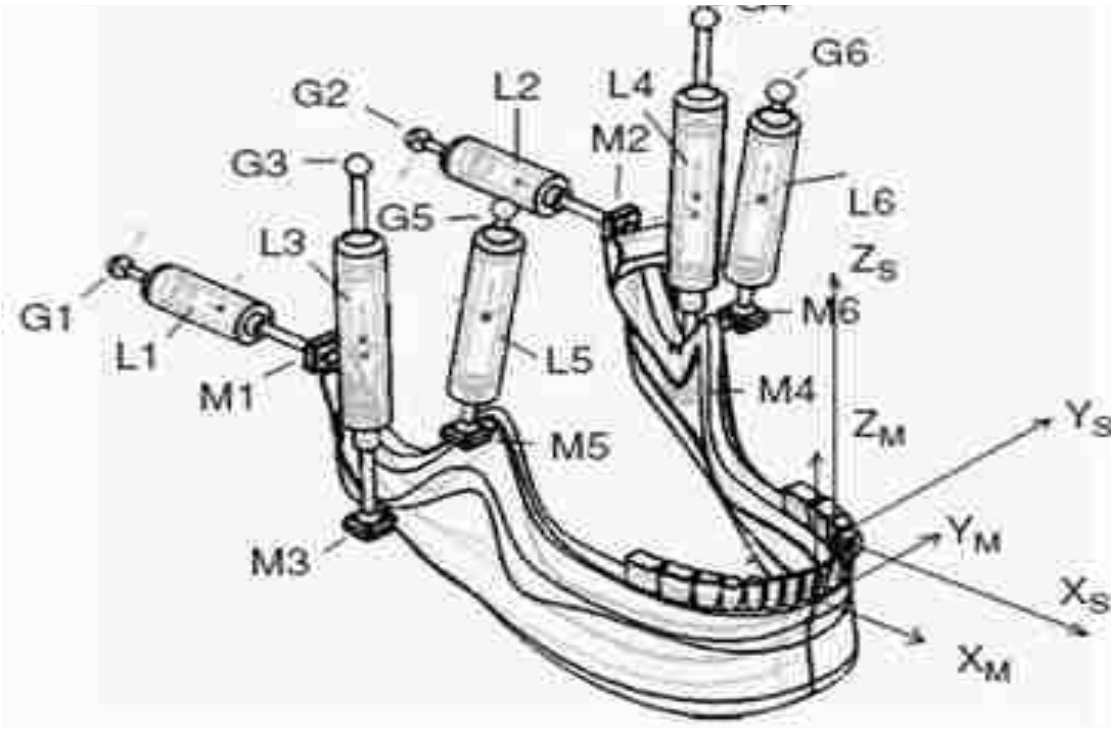

Figure 2.20: Chewing robot model, (b) CAD model

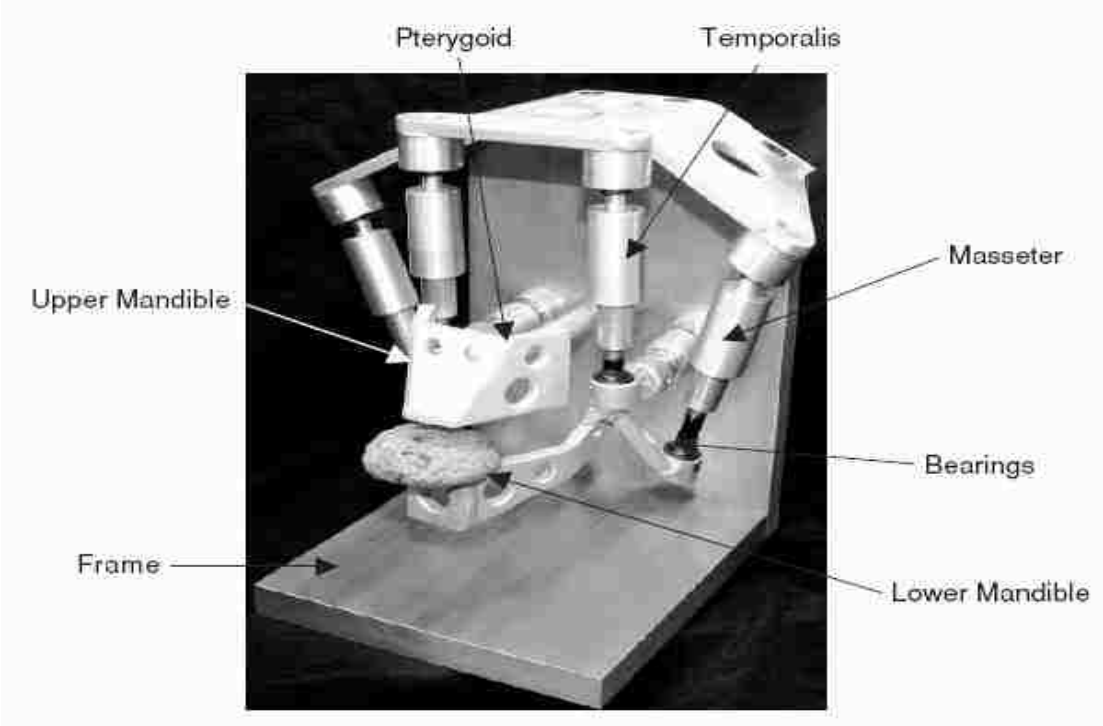

Figure 2.20: Chewing robot model, (c) kinematical model

2.3.1.2 Simulation results of robotic motion

The mastication motion of the robot was simulated by CosmosMotion which is embedded within Solidworks. Figure 2.21 [1] shows the moving range of the robot, while Figure 2.22 [1] shows the chewing trajectory.

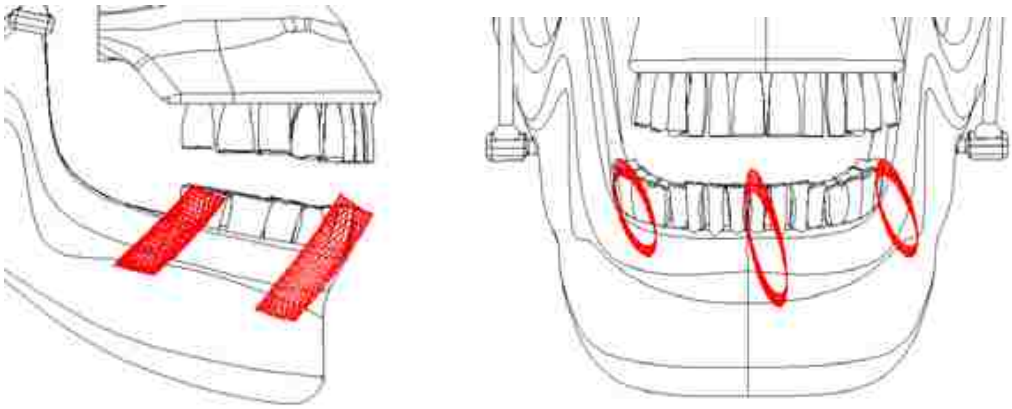

(a) (b)

Figure 2.21: Jaw chewing range, (a) side view and (b) frontal view

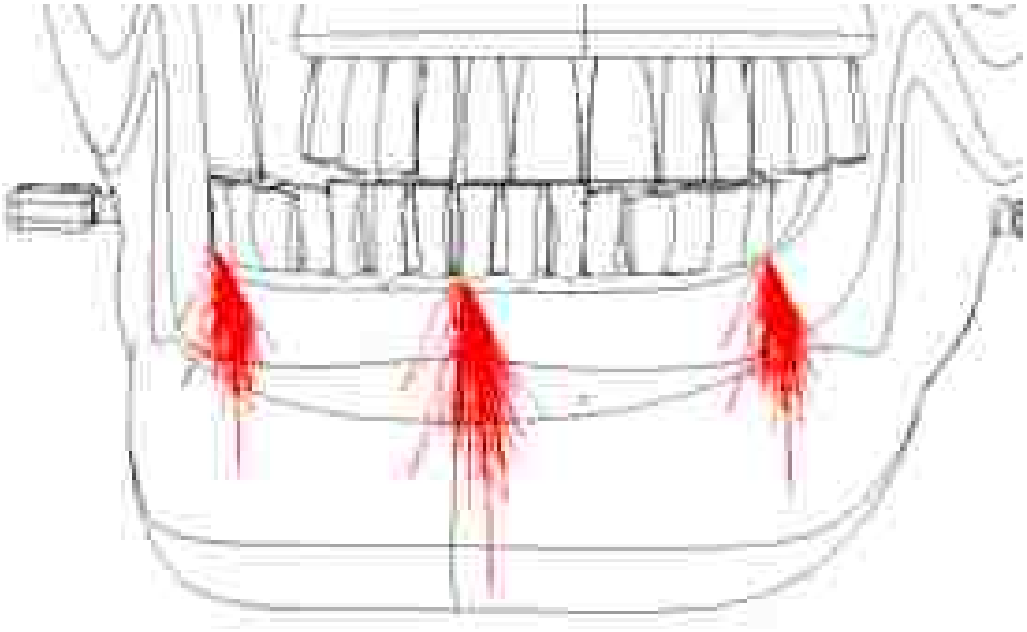

Figure 2.22: Jaw chewing trajectories in frontal view

2.3.2 Robotic Model of Crank Actuation

According to the robotic model for linear actuation, the robot can produce human –like chewing trajectory and biting force. However, problem of this robot is that linear actuators using existing technology could not produce a sufficiently force if the actuator has to fit within the skull [1]. Hence the second model. By using crank actuation to replace the linear actuation at the same reference points, a larger chewing force can be produced.

2.3.2.1 Mechanism model

The robot using a 6RSS parallel mechanism is developed at Massey University in

2005, and is shown in Figure 2.23 [1]. The mandible is actuated by six RSS linkages, and the connecting points on the mandible is the same as the mandible model together with the reference points which are introduced in 2.3.2.1. Each linkage is driven by a 60W dc motor with 66:1 gear box and consists of a crank and a coupler; the coupler is able to rotate around its connecting shaft and could move freely in a frontal angle direction. The RSS linkage is shown in Figure 2.24 [1].

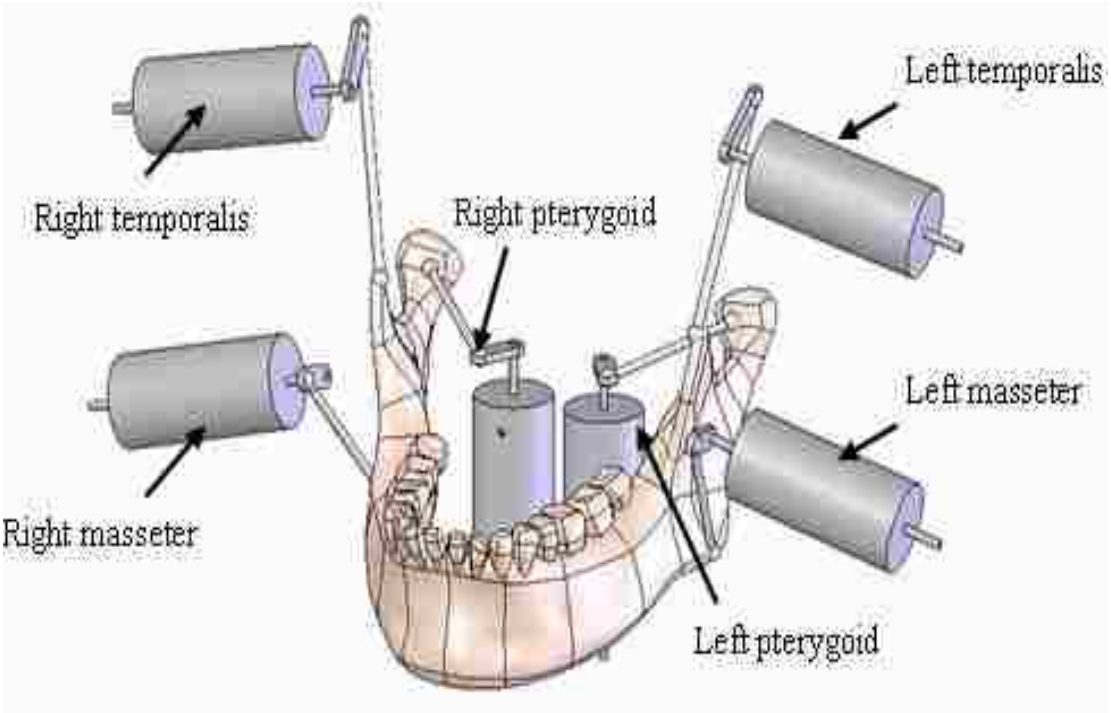

Figure 2.23: The 6RSS parallel mechanism, (a) CAD model

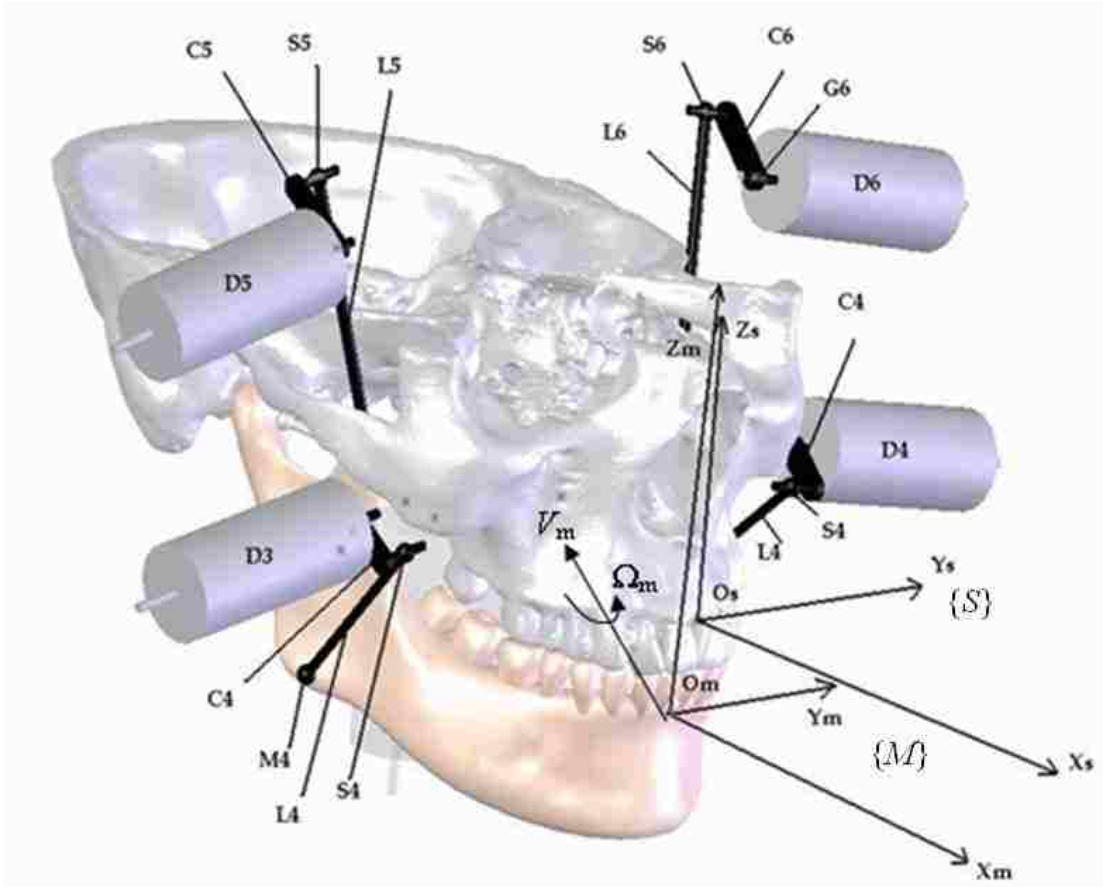

Figure 2.23 The 6RSS parallel mechanism, (b) Coordinate systems of the robot

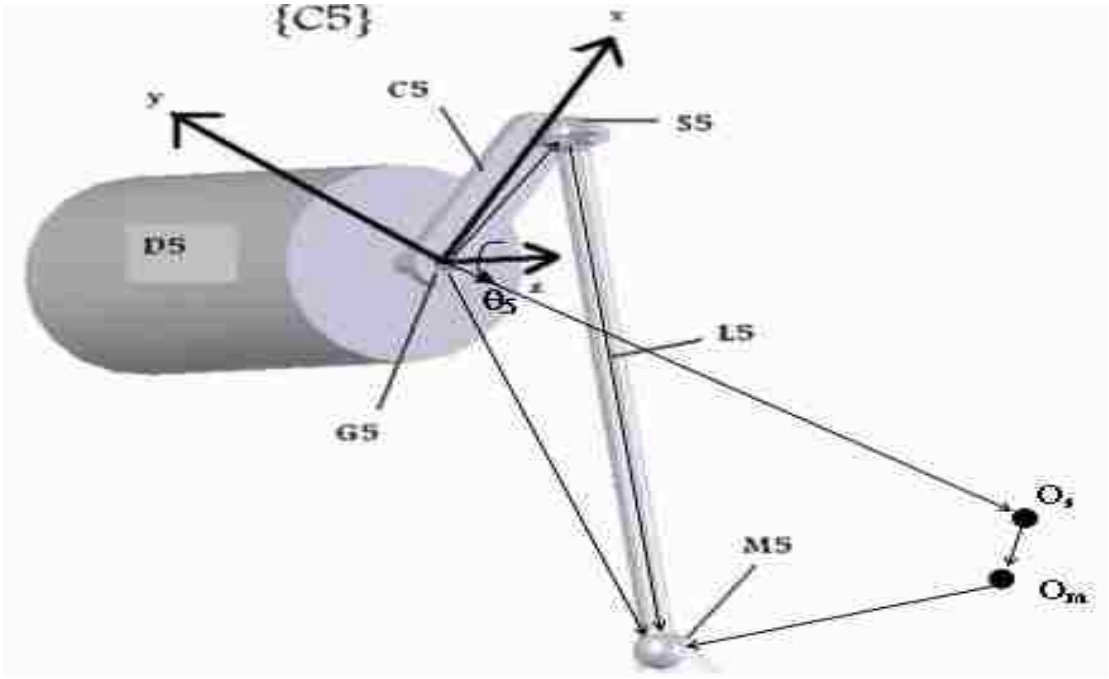

Figure 2.24: RSS linkage

2.3.2.2 Motion control and the actuation moving results

The motion control system consists of a six-axis motion control card (Galil DMC-1860), two amplifiers (each driving up to four motors), a power supplier, and a program (Galil DMC Smart Terminal) [1]. The designers used PID controllers to command the robot and reproduce the chewing motion. Figure 2.25 [1] shows an actuation moving trajectory and error. Figure 2.26 [1] shows a series of photos as the robot executes mastication steps under motion control.

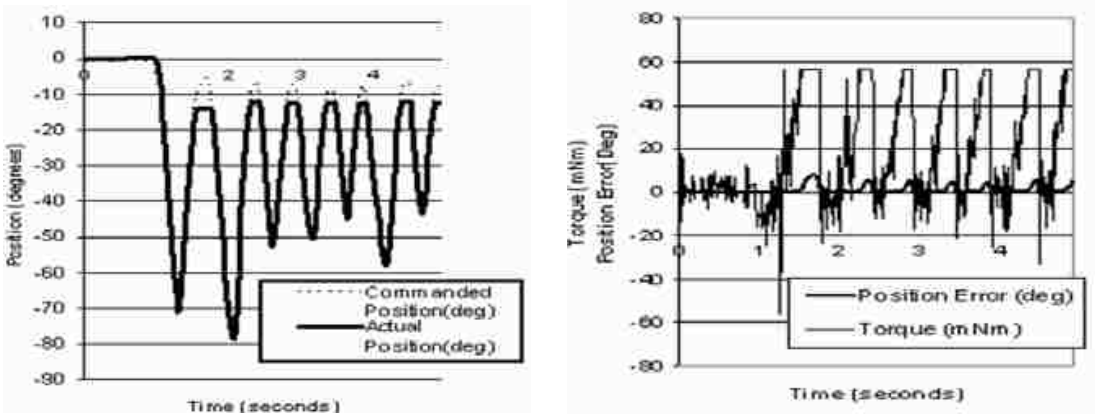

(a) (b)

Figure 2.25: An actuation example, (a) commanded and actual trajectory and (b) motor torque and position error

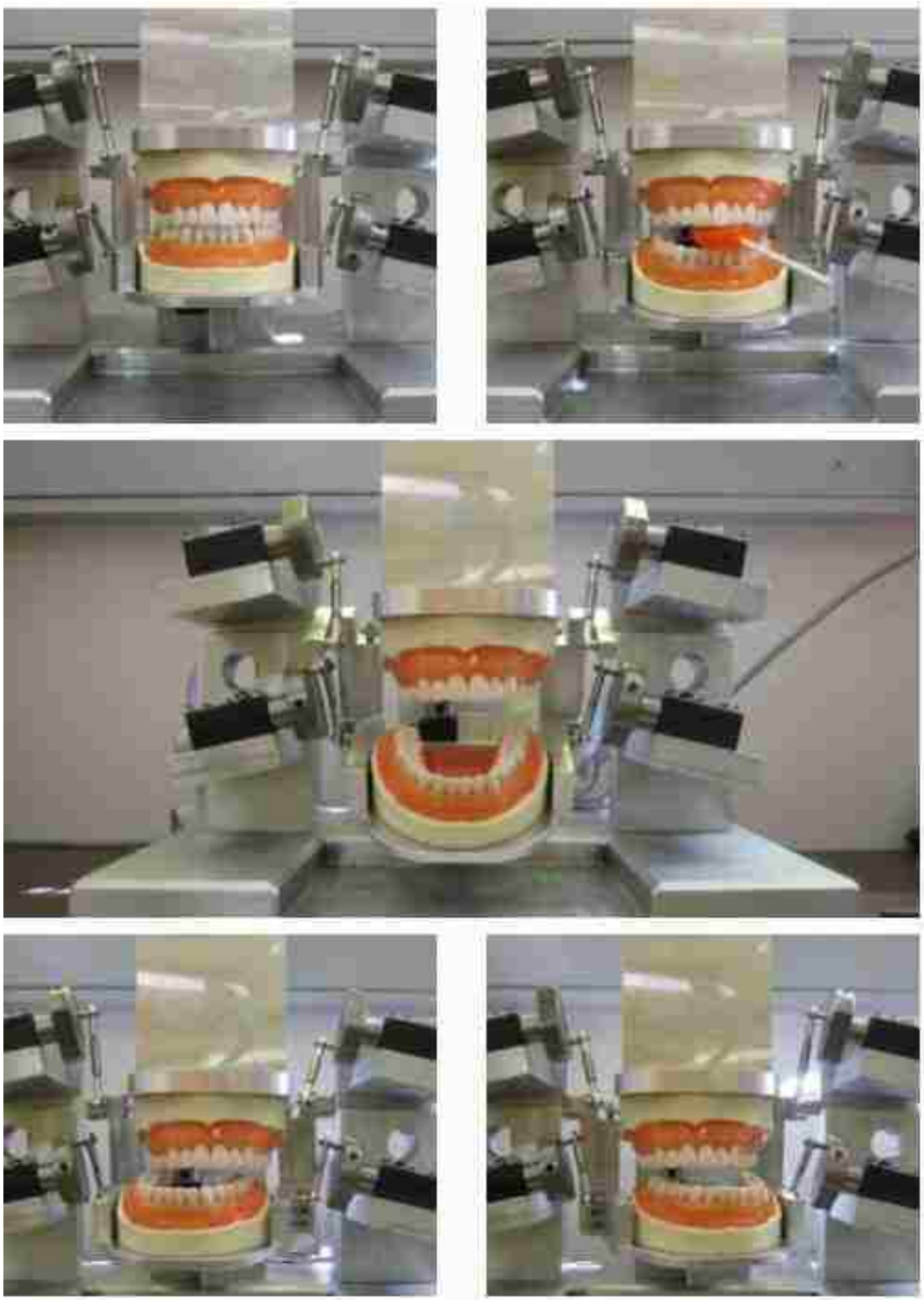

Figure 2.26: Close-up of the physical robot at various configurations

CHAPTER 3:

DESIGN DESCRIPTION OF A MASTICATION ROBOT

The design of a new mastication robot must satisfy the following requirements: (1) it must perform the basic jaw motion and help user in chewing food, (2) the operation speed of the device must be similar to normal chewing. (3) the operation force must conform to the average chewing force and (4) the device must be light. The first step is in realizing the jaw movement and chewing force details. Then, the mastication robot must be able to assist in chewing, so that the motion of the device must follow the actual chewing trajectory. According to jaw motion details presented in the Chapter 3.1, the design is seperated into two subsystems: clenching subsystem and grinding subsystem. The clenching subsystem performs a normal jaw clenching movement and assist the user to have a biting force for chewing. The grinding subsystem produces jaw lateral motion within the chewing cycle.

3.1 Concept of the Jaw Movement and Chewing force

3.1.1 Jaw Movement

From the discussion in Chapter 1.2, the maxilla is the fixed part and mandible is pivoted at condylar via the temporomandibular joint (TMJ) and works as the moving part. Figure 3.1 [14] shows a lateral view of the jaw joint region. The articular disc is

a unique feature of the TMJ that is composed of fibrocartilagenous tissue. It is positioned between the two bones that form the joint and enables the jaw to move along the mandibular fossa[16]. TMJ is a synovial joint (movable joint) in the human body with an articular disc, so that the TMJ functions by providing the jaw with rotation, translational and lateral movements. The jaw can only perform two basic chewing movements: clenching (opening and closing) and grinding (side by side). The following is discussed in two parts, jaw opening and closing (rotation and translation movement) and jaw grinding (lateral/medial movements).

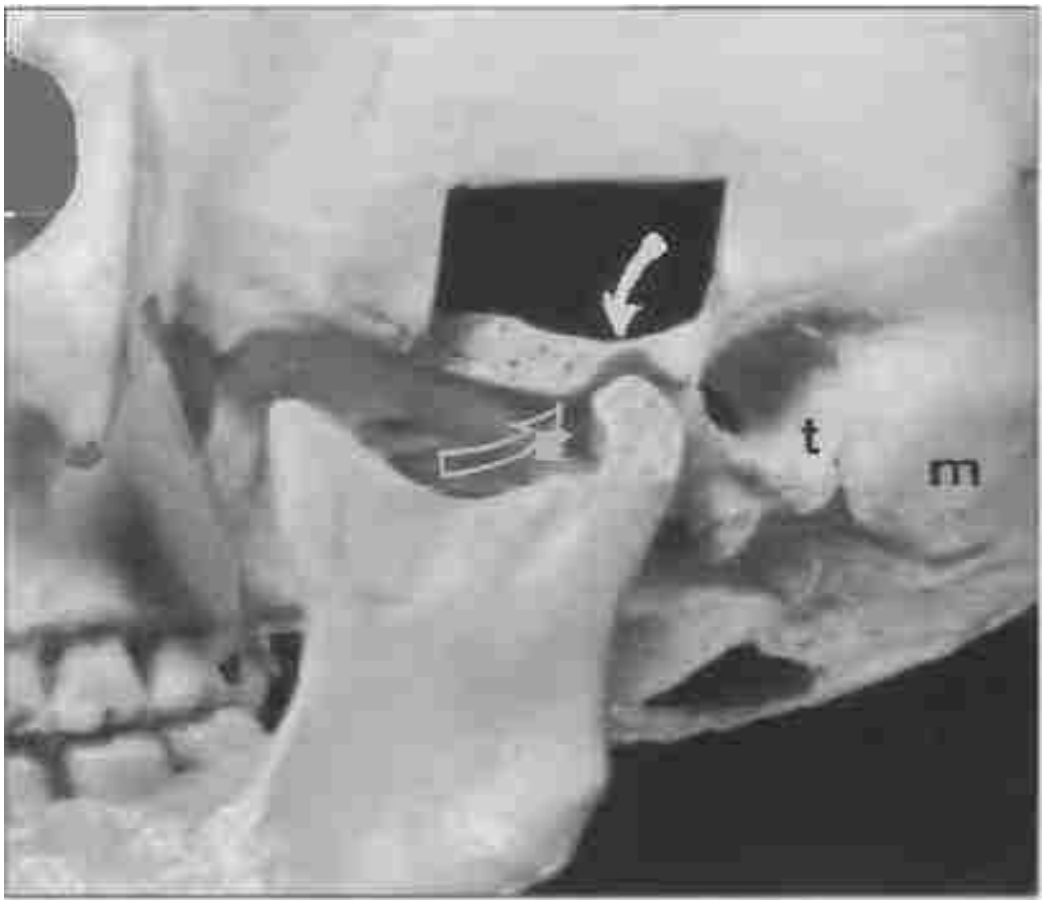

Figure 3.1: Lateral view of jaw joint region

3.1.1.1 The jaw of opening and closing motions

TMJ is the most movable type of joint in the body. Figure 3.2 [15] shows a sagittal view of the TMJ. The condyle and the lower part of articular disc act as a hinge and allows the jaw to rotate. The upper portion of the articular disc and the temporal bones act as a surface to allow the condyle to slide in an anterior/posterior and downward/upward manner. Figure 3.3[14] shows the vertical and horizontal displacement of the condyle in opening and closing motion. On average, the mandible rotates about 2 degrees for each millimeter of translation [14]. Figure 3.4 shows the jaw joint moving in translation and rotation.

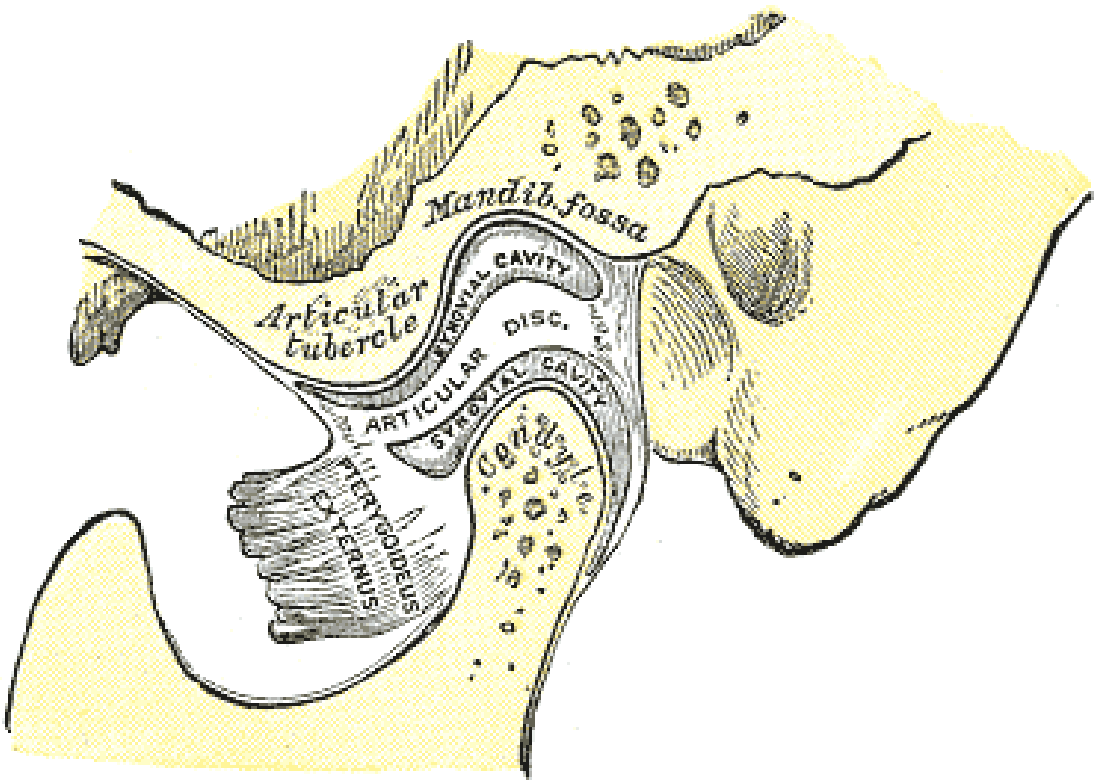

Figure 3.2: Sagittal view of the TMJ

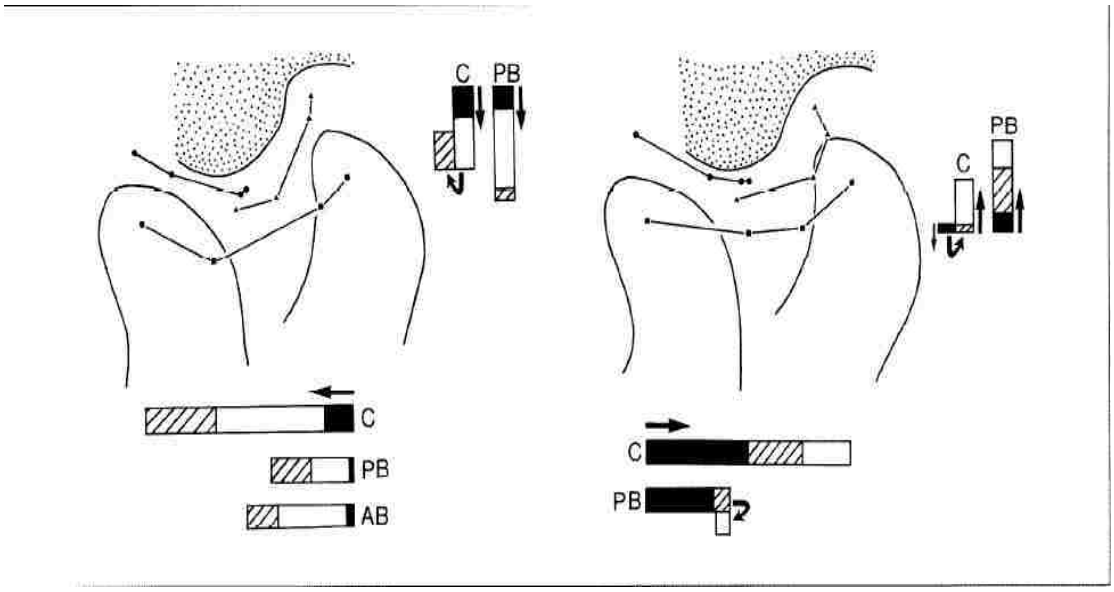

Figure 3.3: Vertical and horizontal displacement of the condyle in jaw opening and closing

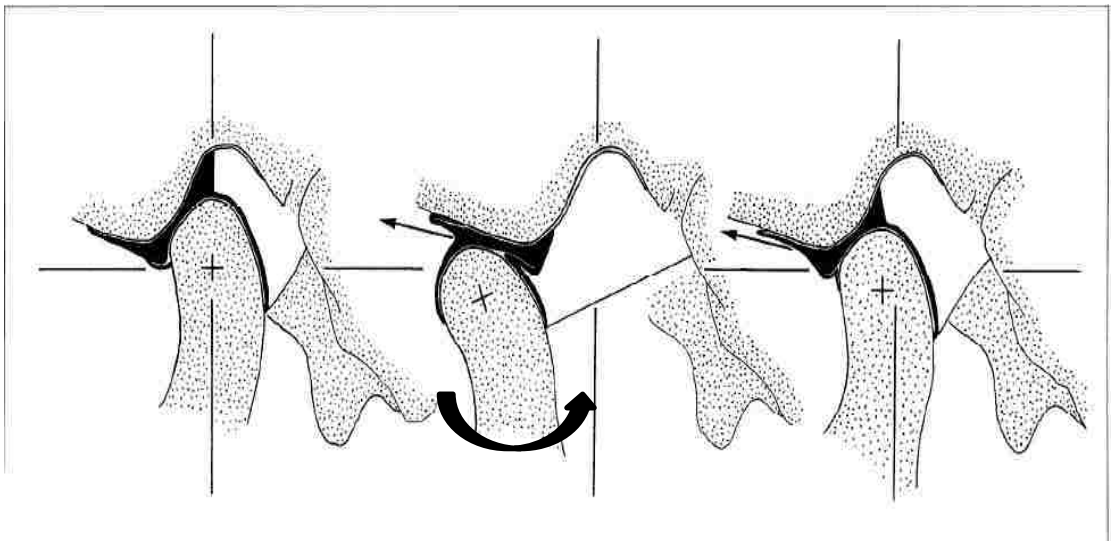

Figure 3.4: Jaw joint moving in translation and rotation, from left to right, jaw-closed, widely open and partly closed

Although the TMJ is the most movable joint in the human body, there are several ligaments which guide the TMJ and define the border movements of the mandible. The Collateral ligament guides the articular disc when moving in the anterior and posterior direction [2]. Capsular and temporomandibular ligaments resist any excessive movement in the inferior direction [2]. Besides, the temporomandibular ligament also guides the condyle when moving in the forward and downward direction [2]. The sphenomandibular ligament prevents the joint from an anterior and lateral dislocation [2]. Thus, the jaw has a maximum moving range and Figure 3.5 [14] illustrates the maximum moving path (Posselt envelope) in the sagittal plane. The extreme movement paths separate into two types: extreme-posterior opening, and extreme-anterior closing. Extreme-posterior opening (from points 1 to m.o.) is divided into two steps, the first step (points 1 to H) is the condyle only rotating 10 degrees around the TMJ as the hinge axis and the second step (points H to m.o.) is the condyle not only rotating but also moving forward following the upper portion of the articular disc [1]. Anterior-extreme closing (points m.o. to 5) is the pure hinge rotation movement after the condyle moves to the extreme forward position.

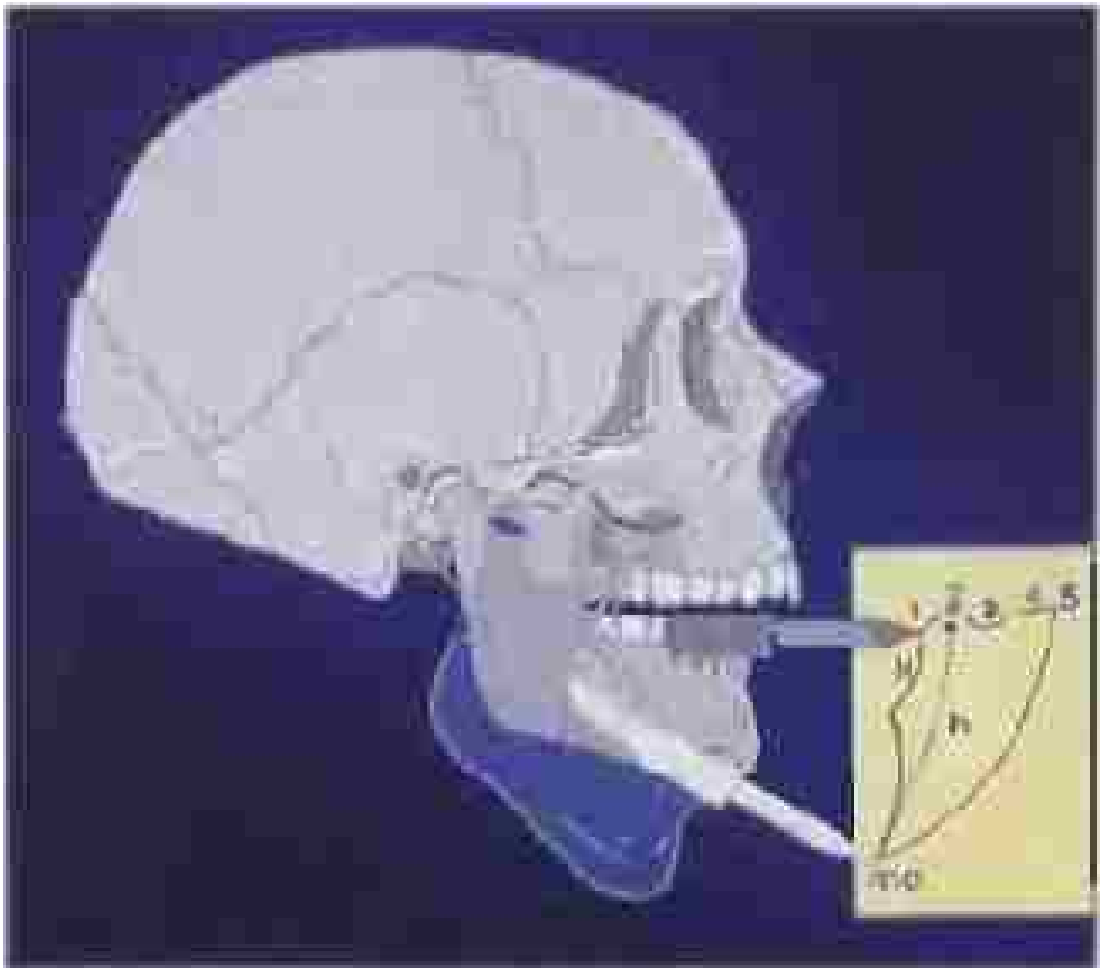

Figure 3.5: Posselt envelope in sagittal plane

3.1.1.2 Jaw grinding (lateral movements)

Capsular and sphenomandibular ligaments also resist excessive lateral movements of the mandible. Futhermore, the masseter and the medial muscle exert high forces and control the jaw motion in the lateral direction. Figure 3.6 [2] shows vector forces from the masseter and medial muscles. Based on the ligament and the muscle function, the condyle can therefore slide on the upper articular disc and side-by-side in the lateral direction. Figure 3.7 [14] shows the maximum jaw lateral movement paths (Posselt envelope) in the frontal plane and horizontal plane. When the jaw works in grinding, the condyle not only moves in the lateral direction but also performs a small forward movement.

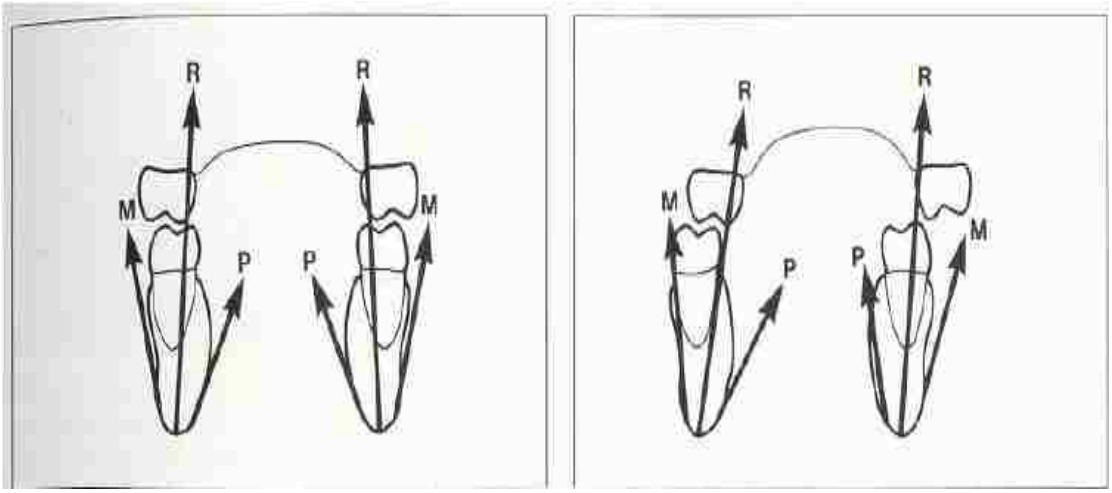

Figure 3.6: Vector forces from masseter and medial pterygoid muscles

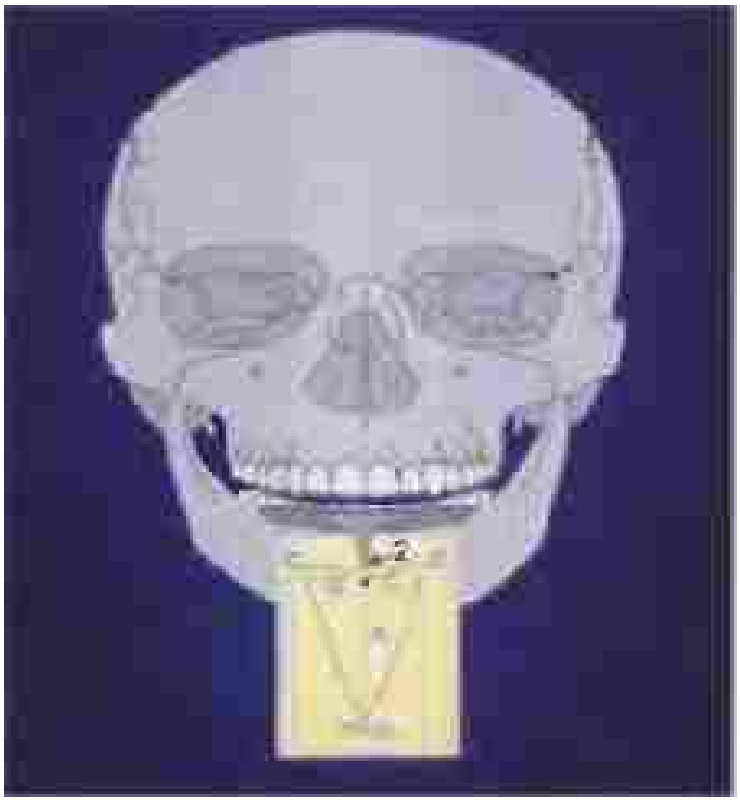

(a)

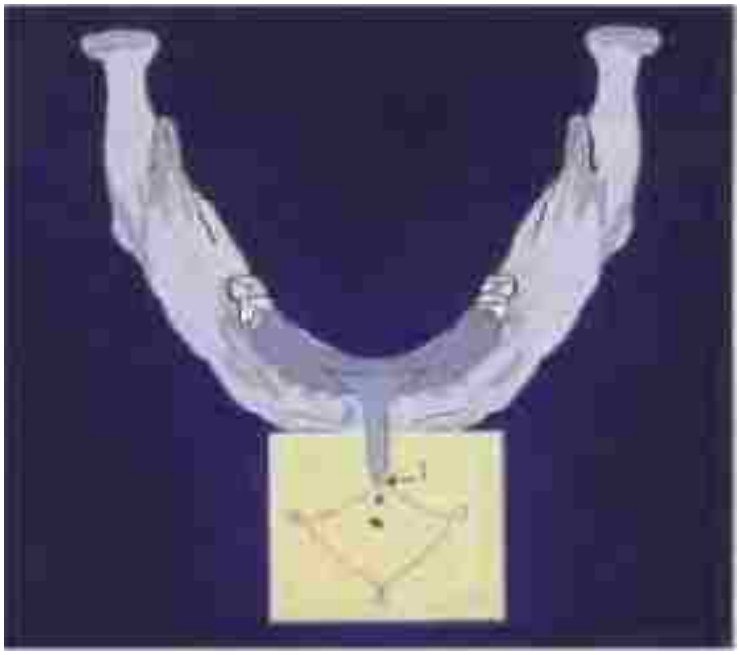

(b)

Figure 3.7: Posselt envelope in (a) the frontal plane, jaw opening/closing and grind situation and (b) the horizontal plane, jaw moving in lateral and anterior direction

3.1.2 Chewing force and jaw chewing trajectory

In order to perform mastication, the associated muscles not only control the motion of the mandible but also provide the chewing force. There are four main muscles for closing or elevating the jaw. The temporal muscle is a large, flat-shaped muscle which is separated into two parts, anterior fibres and posterior fibres. First, contraction of the anterior fibres elevates the mandible and closes the mouth [1]. Secondly, the function of posterior fibres is for moving the mandible in a lateral direction to create mouth grinding movements [1]. Figure 3.8 [2] shows the temporal muscle vector force and the muscle structure. The masseter muscle is the most powerful muscle of the mandible and it is the main power source for the chewing force. The vector force and masseter muscle structure can be seen in Figure 3.9 [2,15]. The medial pterygoid muscle drives the mandible in a lateral motion while closing and it can exert a high force though not as large as the masseter muscle [2]. The lateral pterygoid is the only muscle of mastication that assists in opening the jaw.

Since the masseter muscle generates most of the chewing force, the occlusal force increases as the bite point moves closer to the posterior molar teeth. There are two reasons: first is that the dental lever arm is getting shorter and second is that more muscle groups become active. On average, for the first molar, the maximum of chewing force is 300 to 400 N and the incisors are from 100 to 150 N [14].

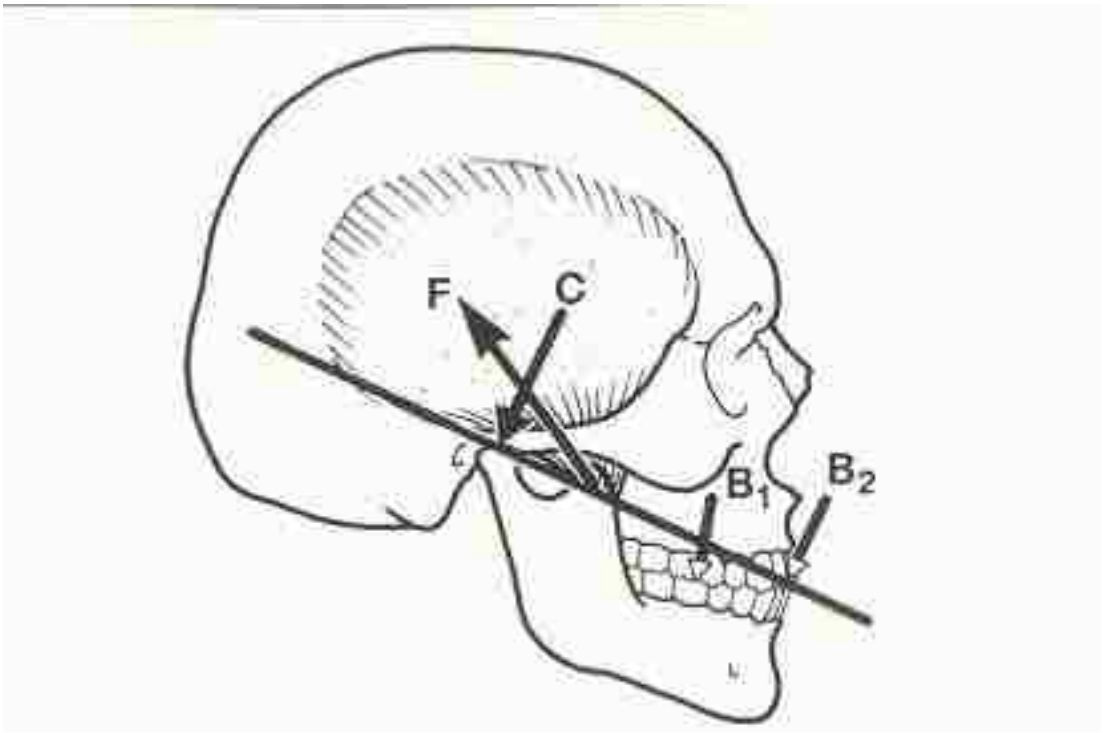

(a)

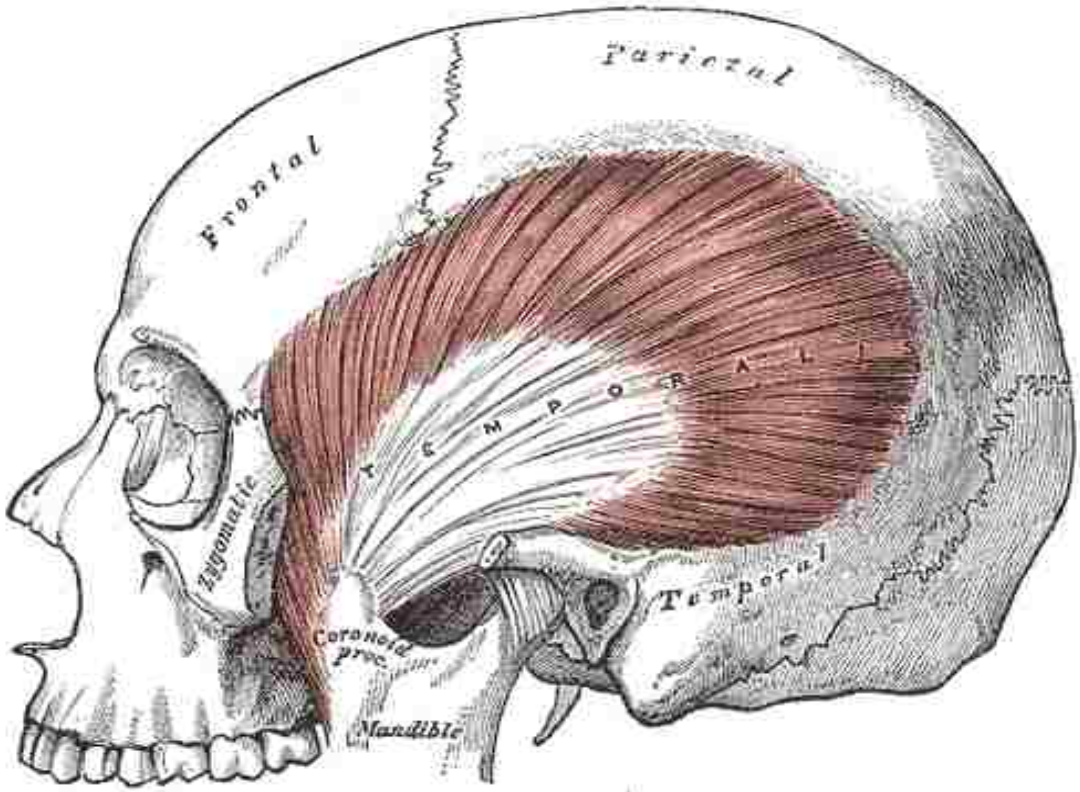

(b)

Figure 3.8: (a) Temporal muscle vector force and (b) muscle structure

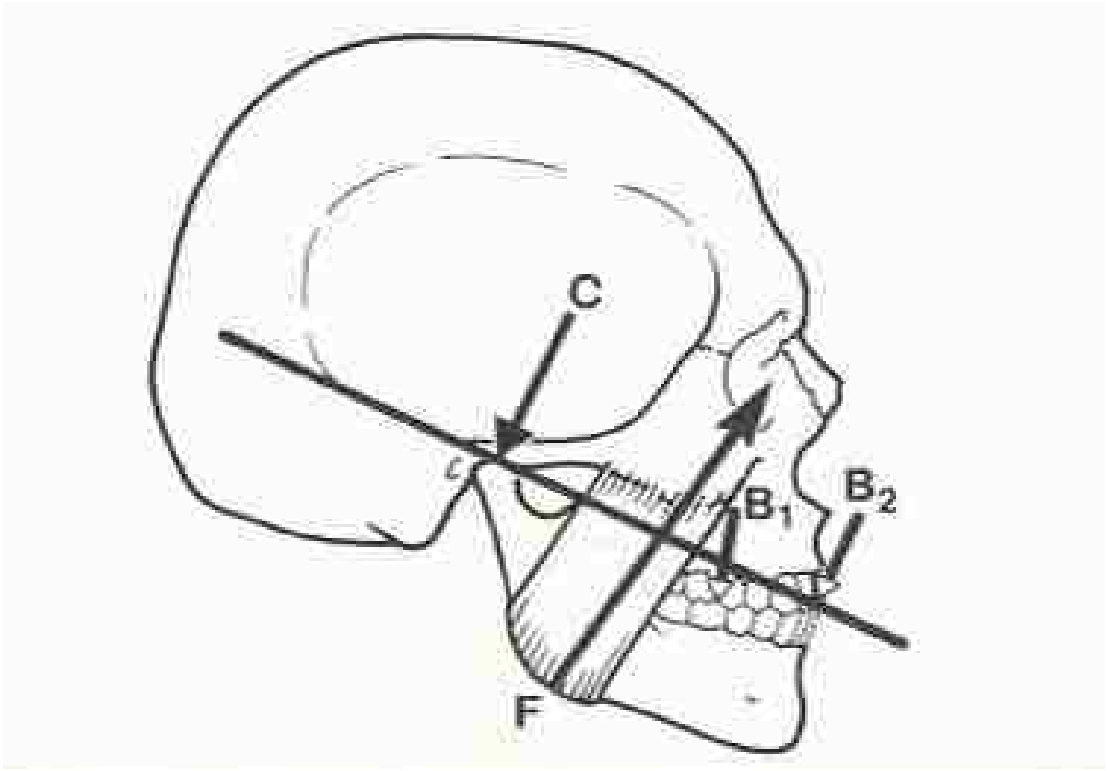

(a)

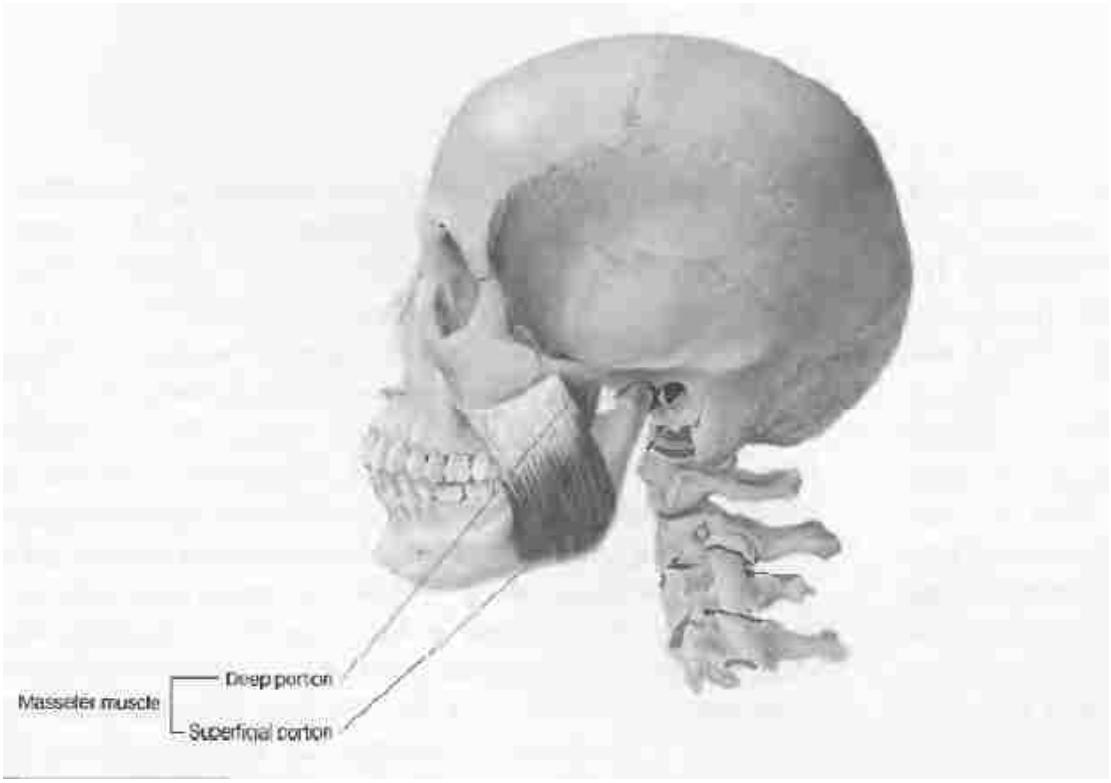

(b)

Figure 3.9: (a) masseter vector force and (b) muscle structure

Before starting on the design of a mastication robot, the chewing forces, trajectory and amplitudes are important information that has to determine. Even though the chewing trajectory varies with the type of food that is being chewed, a normal chewing cycle may be separated into opening, closing and occlusion [2]. At the first step, the mouth starts to open and depresses the mandible vertivcally downward. Then, the jaw moves laterally outward and elevate upward while mouth is closing. At the last step, occlusion, when the jaw is moving upward to the postion of upper and lower teeth contact, the mandible starts to move laterally inward to the original situation. Figure 3.10 [2] shows the chewing trajectory of the incisor point. On average, the jaw vertical amplitude is 15 to 20 mm and the lateral amplitude is 5 to 10 mm. The mandible opening velocity is 52 to 63 mm/s and closing velocity is 47 to 57 mm/s [16].

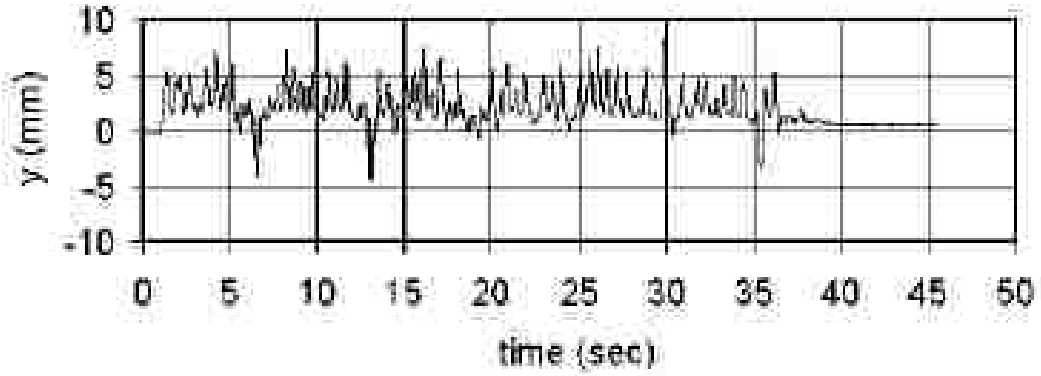

Figure 3.10: Chewing trajectory of the incisor point, (a) lateral movement

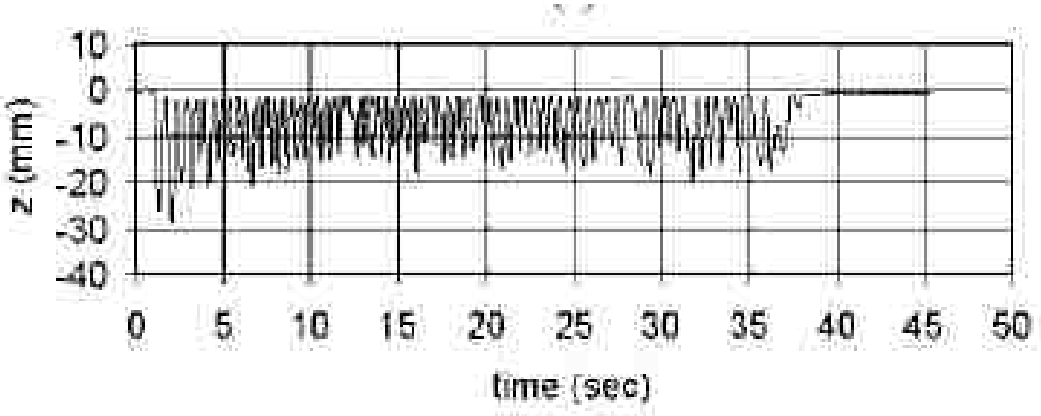

Figure 3.10: Chewing trajectory of the incisor point, (b) superior-inferior movement

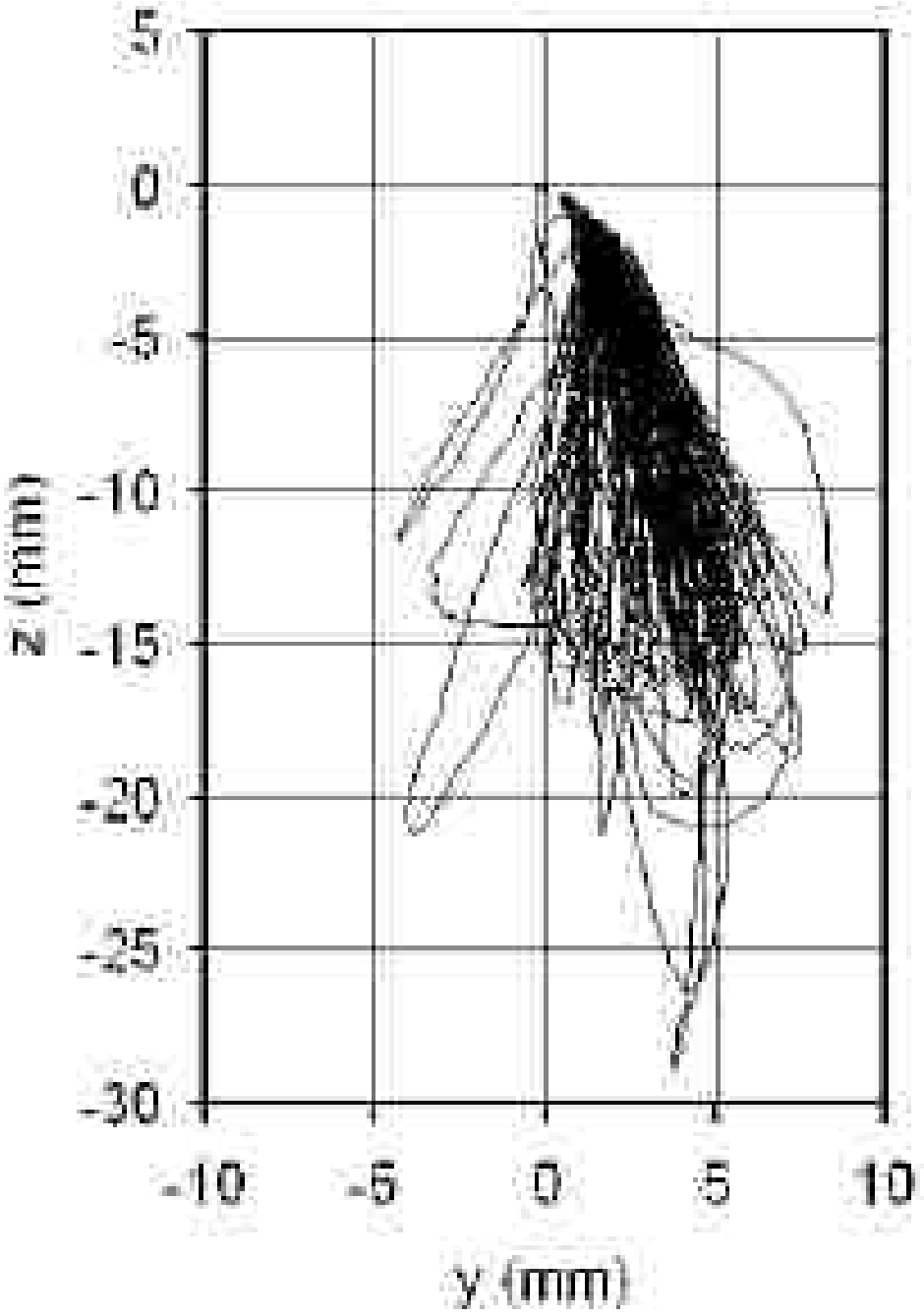

Figure 3.10: Chewing trajectory of the incisor point, (c) in frontal plane

3.2 Design of a Clenching Subsystem

3.2.1 The concept of a clenching subsystem

When a jaw is performing a clenching movement, the condyle moves by following the upper portion of the articular disc and the temporal bones which then act to slide in an anterior/posterior and a downward/upward. This action can be seem as a bar connecting with a roller which rolls along a mandible fossa and articular tubercle-shape surface. Also, the bar is pivoted at the roller. Thus, the jaw condyle movement is composed by single curvilinear translation and with a rotation. Figure 3.11 illustrates the relationship between mandible moving action with mouth opening to the roller bar mechanism.

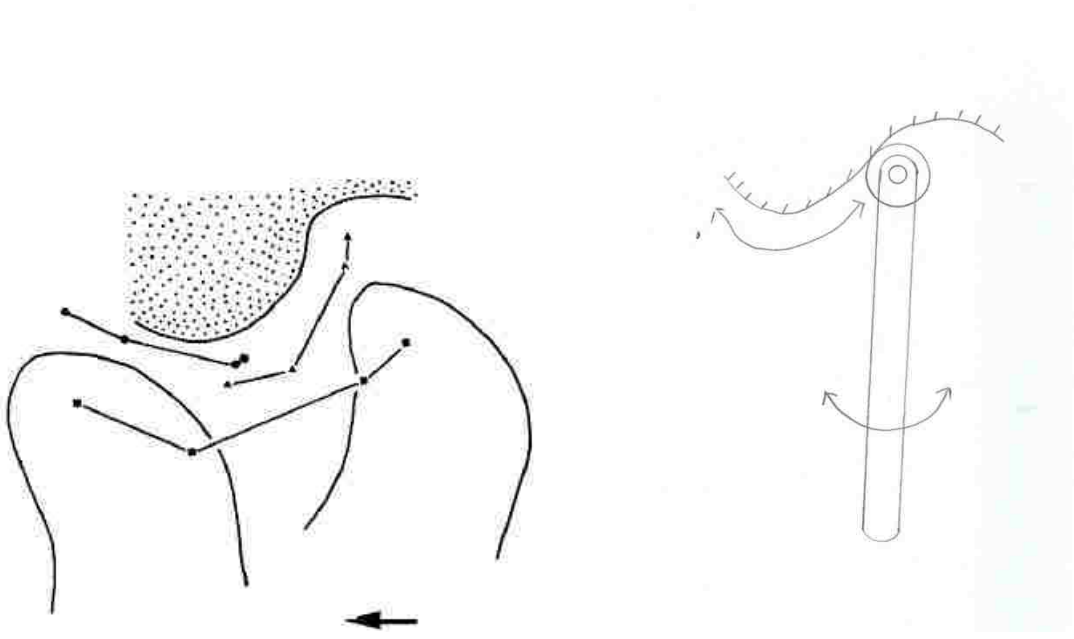

(a) (b)

Figure 3.11: (a) Vertical and horizontal displacement of the condyle in jaw opening and closing, and (b) roller bar mechanism

However, it’s unrealistic to build a mandible fossa and articular tubercle-shaped surface as a roller follower because everybody’s bone structure and shape is not the same. According to Chasle’s theorem, a rigid body displacement can be produced by one translation and one rotation, so it is then possible to design another mechanism which can perform a single translation and a rotation to drive the mandible motion. Figure 3.12 shows a simple concept of such a clenching system. The nut translates along the bar and the bar is pivoted at the hinge. Therefore, the shaded area gives the region where in the nut may be positioned. Due to the short concyle horizontal displacement (5mm [14]) and long verticle movement for normal chewing, this simple mechanism can get at any position while the jaw is moving.

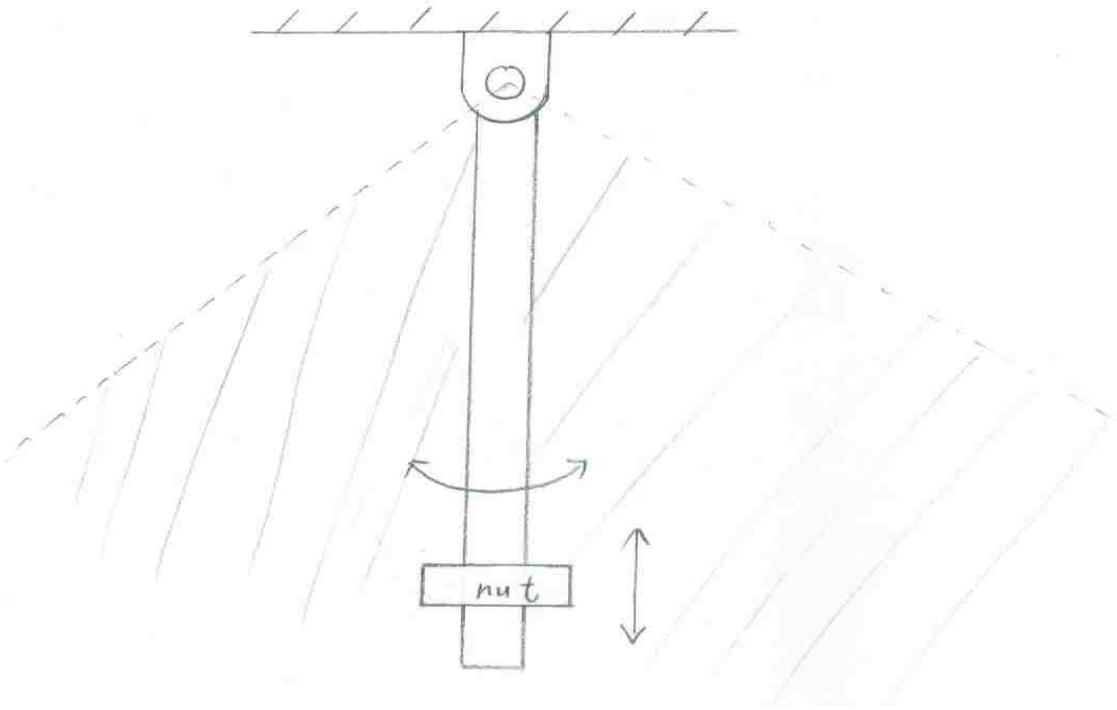

Figure 3.12: Simple mechanism concept of clenching system

3.2.2 Detailed design of clenching subsystem

The detailed design of the clenching subsystem will be based on the concept introduced in the previous subsection. Two lead screws are used to drive nuts moving vertically at the same time and the nuts are connected to the grinding subsystem to pull or push on the jaw. Pertaining to the rotating concept shown in the previous page, a hat with two aluminum support frames can be worn by the user. A box is attached to a round rod that hangs off each side hanging onto both of them. The two lead screws are held by the box. There is a double-shaft motor that drives the lead screws through a gear box. When the lead screws drive the clenching subsystem to push or pull on the mandible, they also push on the box because the condyle executes a rotating motion. The simulation model of dynamic systemis shown in Figure 3.13 and, Figure 3.14 illudtrstes a 3D CAD model of clenching subsystem. The components of design are discussed in greater detail in the following section. The CAD of each components is shown in Appendix A.

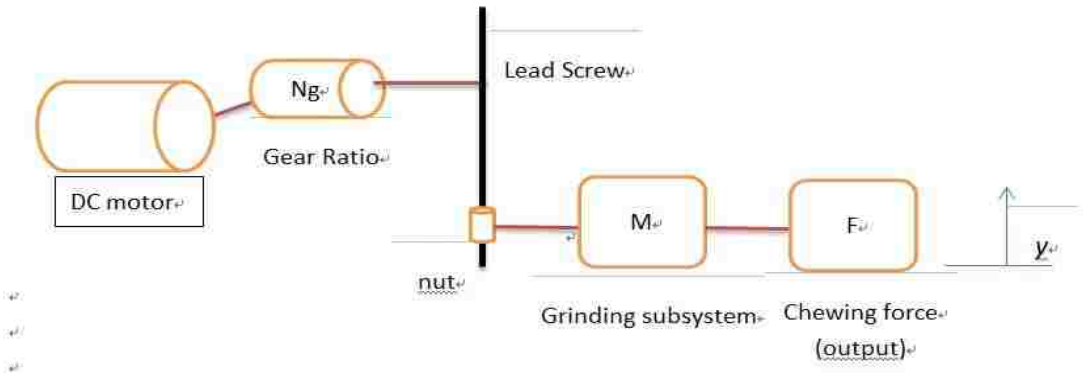

Figure 3.13: Simulation model of dynamic system

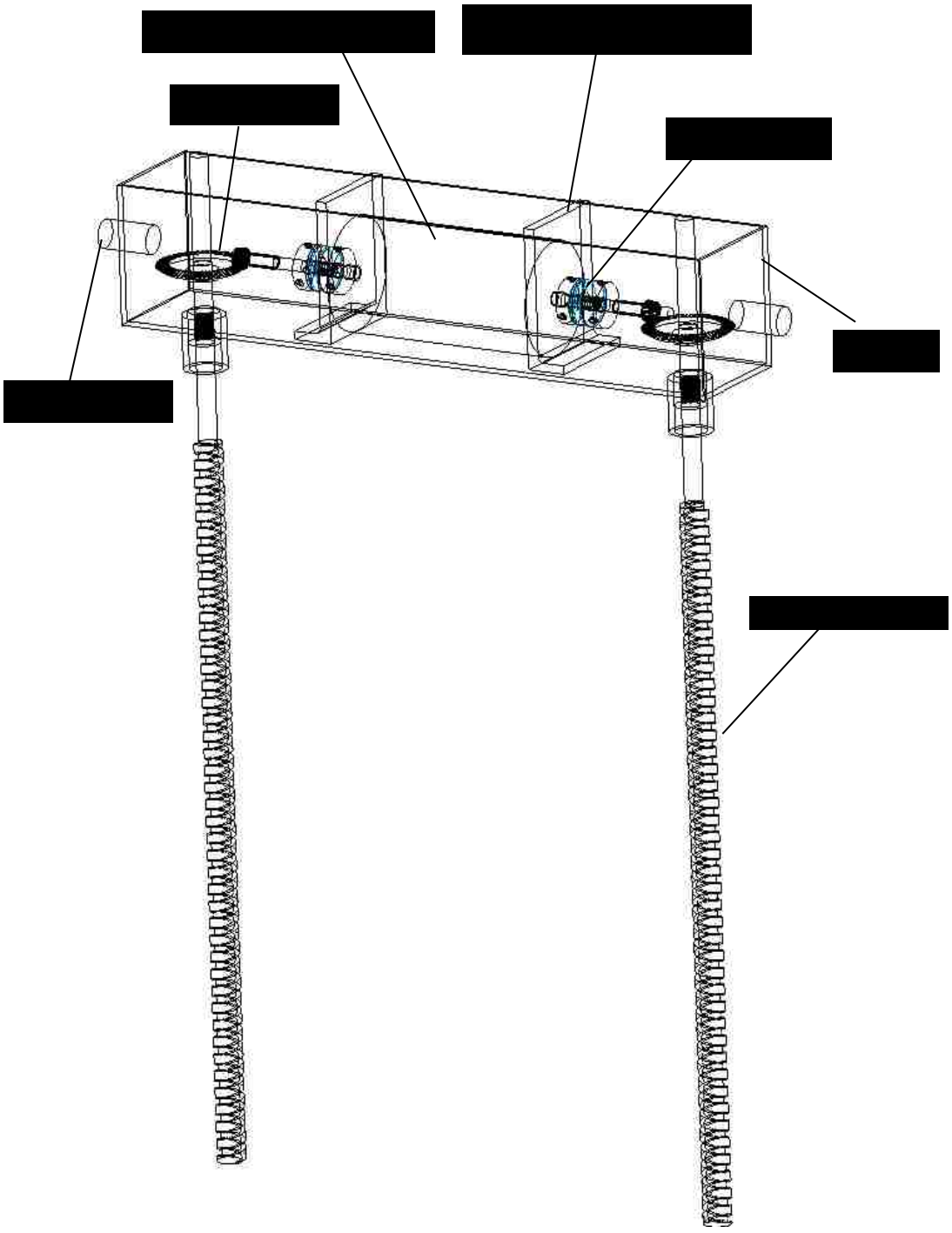

(a)

Figure 3.14: (a) Wirefram CAD model of clenching subsystem

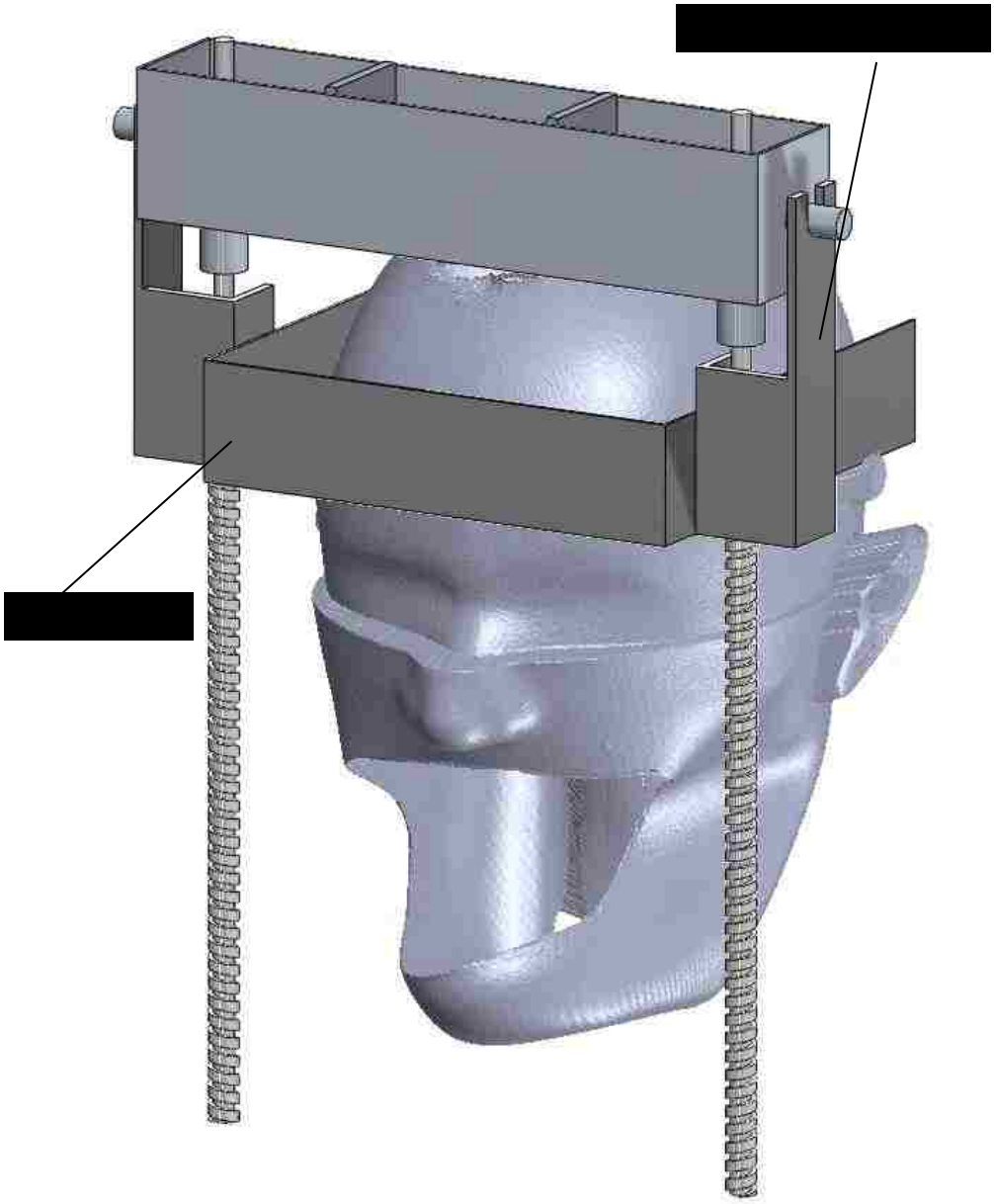

Figure 3.14: (b) CAD model of clenching subsystem with imitation user head

3.2.2.1 Lead screw

Lead screws can transform a rotary motion into a translational motion while generating large forces from the input motor torque. Such a design is economical in motor weight and size because the chewing force is very large. The concept is to use the motor to drive two different thread-handed lead screws (one is right-handed, and the other left-handed) through a series of bevel gears (1:5), so that, the lead screws can exert a large force to simulate the chewing force, as well as to suspend grinding subsystem. If the same handed threads are used (ie. RH), then the friction between the lead screw and nut will generate a torqueon the grinding subsystem resulting bending of the subsystem. Opposite handed-screw threads result in a cancellation of this undesirable torque.

The considerations when choosing lead screws are driven by the requirements of the chewing force and vertical moving speed. Normally, the maximum chewing force is about 300N to 400N and the mandible opening velocity is 52 to 63 mm/s and closing velocity is 47 to 57 mm/s [16]. The goal of this design is set to generate a 400N force with a nut moving speed of 50 mm/s. The resulting design of the lead screw systems are realized using: BFWFSR-0.37-0500-BY18 and BFWFSL-0.37-0500-BY18, HAYDON Co., USA.

The system consists of a set of two screws and nuts. The screw diameter is 0.375

inch with a 0.5 inch lead, and a total length of 14 inch. One end of the screw is fully milled down to become a 0.25 inch diameter round rod on which is mounted a bevel gear supported with a mounting unit within the box. The CAD drawing of the lead screw is shown in Appendix A. The lead screws system data requires the maximum input torque and rotation speed on the driven motor as inputs. These calculations are shown below.

1. Maximum input torque:

The maxumum input torque of the screw can be determined

$$T_L = \frac{Load \times Lead}{2\pi \times efficiency} \quad (3.1)$$

where load = 300 N, lead = 0.5 inch= 12.70 mm and the efficiency= 81%. Thus, input torque of the screw is equal to 0.7486 N-m. When driven through a bevel gear system (1:5), the required torque of motor is 0.1497 N-m

2. Require rotation speed:

The rotation speed (RPM) of the screw can be determined:

$$\text{RPM} = \frac{Linear\ speed(m/sec) \times 60(sec/min)}{Lead} \quad (3.2)$$

where linear speed = 50 mm/s, and lead = 0.5 inch= 12.70 mm. Therefore, the rotation speed of screw is 236 rpm and the required motor speed is 1180 rpm.

3.2.2.2 Rotating box

The rotating box shown in Figure 3.15 is made from an acrylic rectangular board for the bottom surface and sides along with two steel square panels. There are two round shafts at the steel panels so that the rotating shafts can be supported by the box support frame. Two round tubes place at the bottom board and two needle roller bearings are inserted into the tubes.

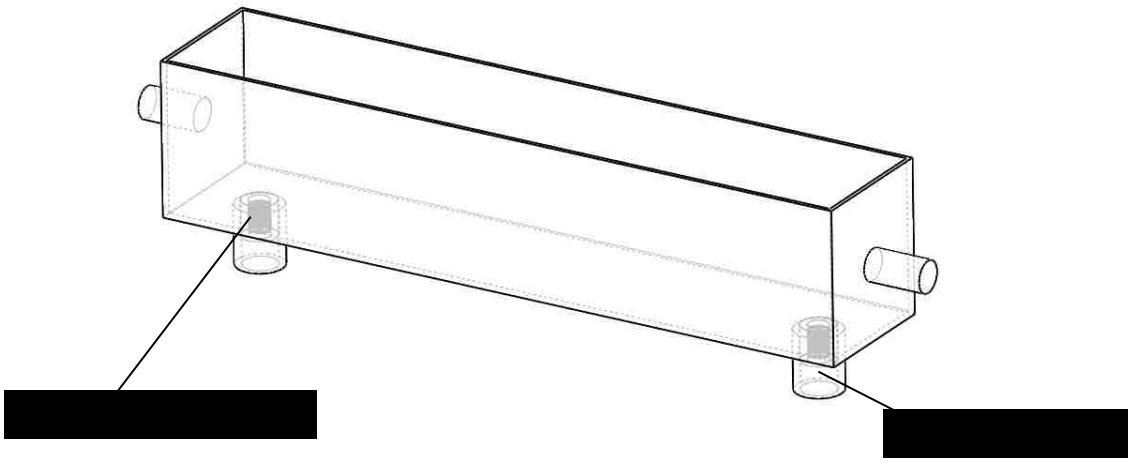

Figure3.15: Rotating box CAD model

3.3 Design of a Grinding Subsystem

3.3.1 Problem description

The objective is to design and construct a device that can perform the grinding motion in the chewing process. In this design, the maximum horizontal displacement of jaw is set at 5 mm.

3.3.2 Design description

In the grinding motion, the jaw moves from the center position to the right or left and then returns. In order to avoid early motor failure in changing direction within a short horizontal displacement (5mm), a scotch yoke mechanism is used to convert the rotational motion into a linear motion of the slider.

Figure 3.16 shows the grinding subsystem model. The scotch yoke in this design is a circular disk engaging the crank. There is a motor driving the circular disk through a spur gear box and the distance between rotating shaft and the center point of circle panel is 5 mm. The function of the gear box is to reduce the motor speed to the required rotational velocity of circular disk (30 rpm). The yoke system is fixed on a 0.6-inch thick board which connects to the two nuts. A cap held up by two aluminum rectangular bars is connected to the crank via the scotch yoke. When the crank is moving horizontally, the cap pushes user’s jaw to perform the required lateral motion.

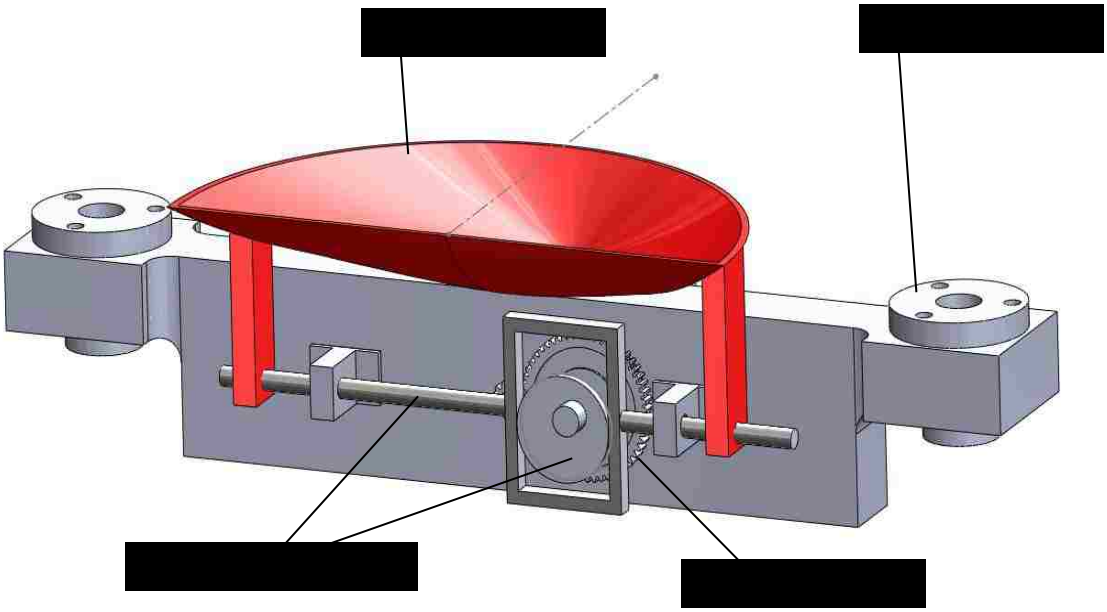

(a)

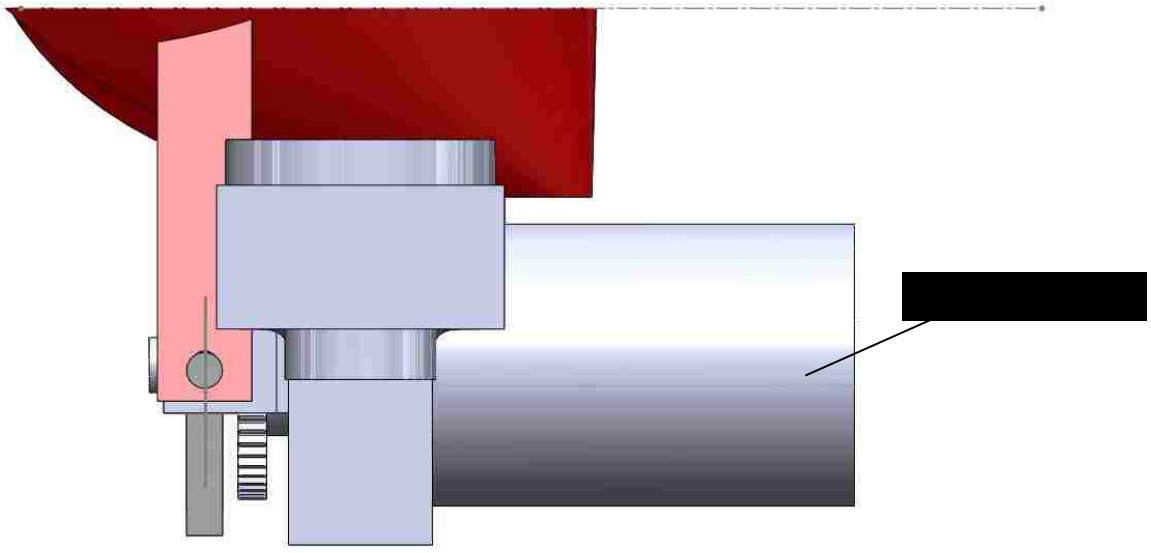

(b)

Figure 3.16: Grinding subsystem CAD model, (a) dimetric view, and (b) right side view

3.4 Final Design of a Mastication Robot

The mastication robot is composed of a clenching subsystem and a grinding subsystem. Figure 3.17 is a CAD model of the entire system. When the lead screws of clenching subsystem rotate, the grinding subsystem move in vertically and the cap moves the mandible executing an opening or closing motion. The grinding subsystem on the other hand, pushes the jaw laterally. From this combination of motions, this device duplicates the basic jaw movement and assists in the chewing process subjected to the required forces and moving speeds. In this way, this mastication robot satisfies the requirements set for the earlier. Different chewing trajectories can be achieved by controlling and coordinating these two subsystems and the results are shown in the next section.

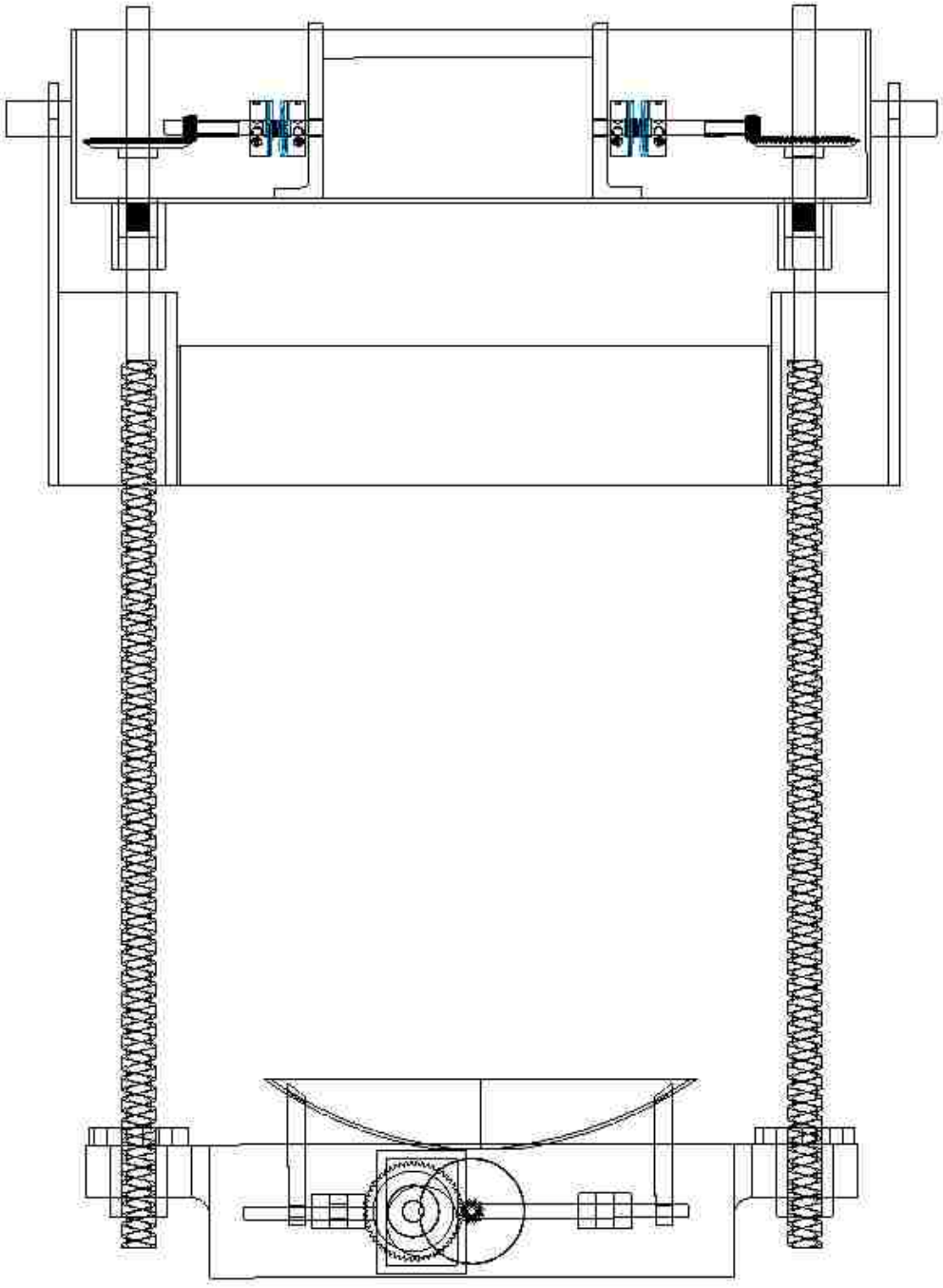

Figure 3.17: (a) Frontal view of mastication robot CAD model

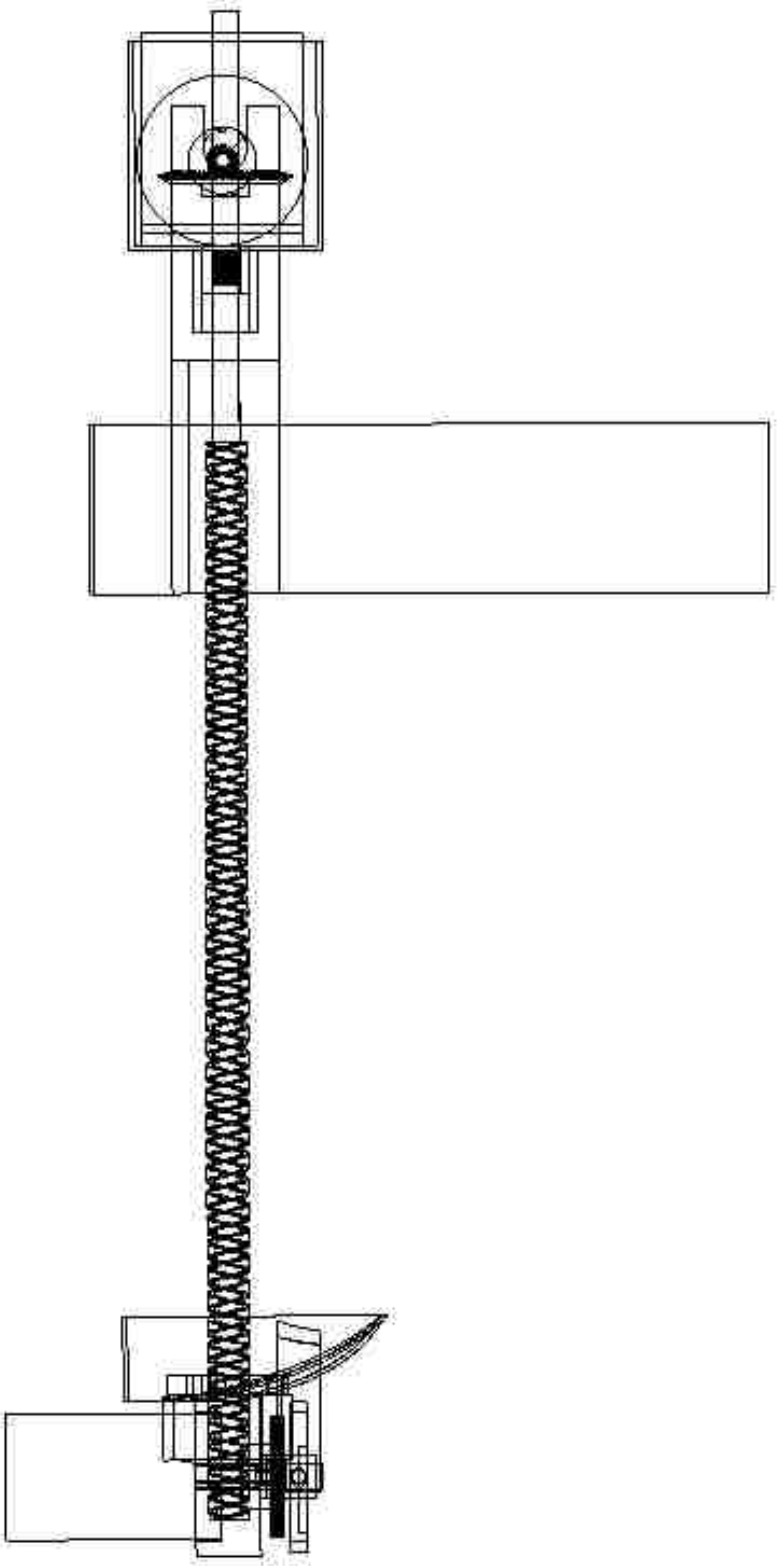

Figure 3.17: (b) Side view of mastication robot CAD model

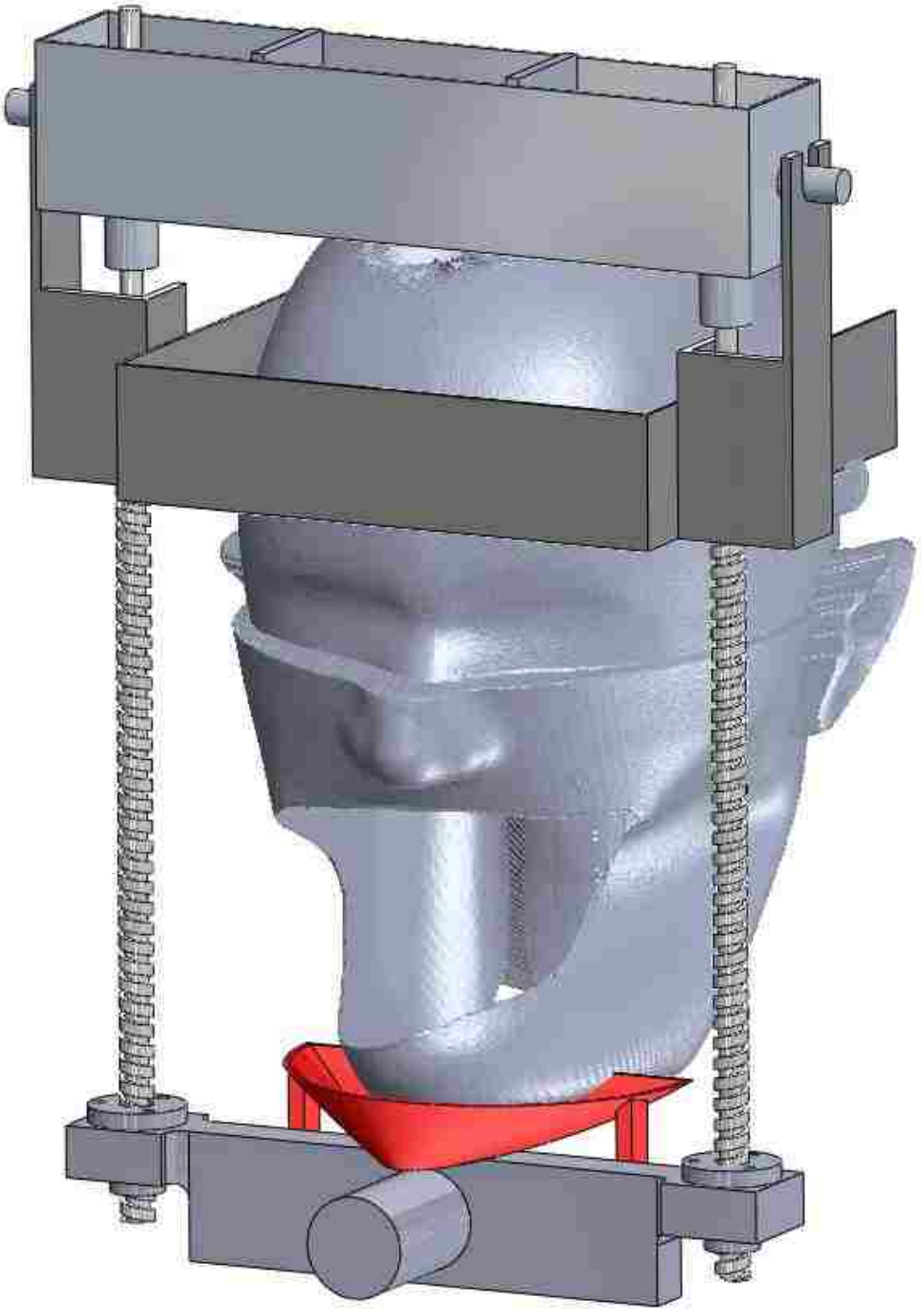

Figure 3.17 (c) Mastication robot CAD model in Dimetric view with imitation user head

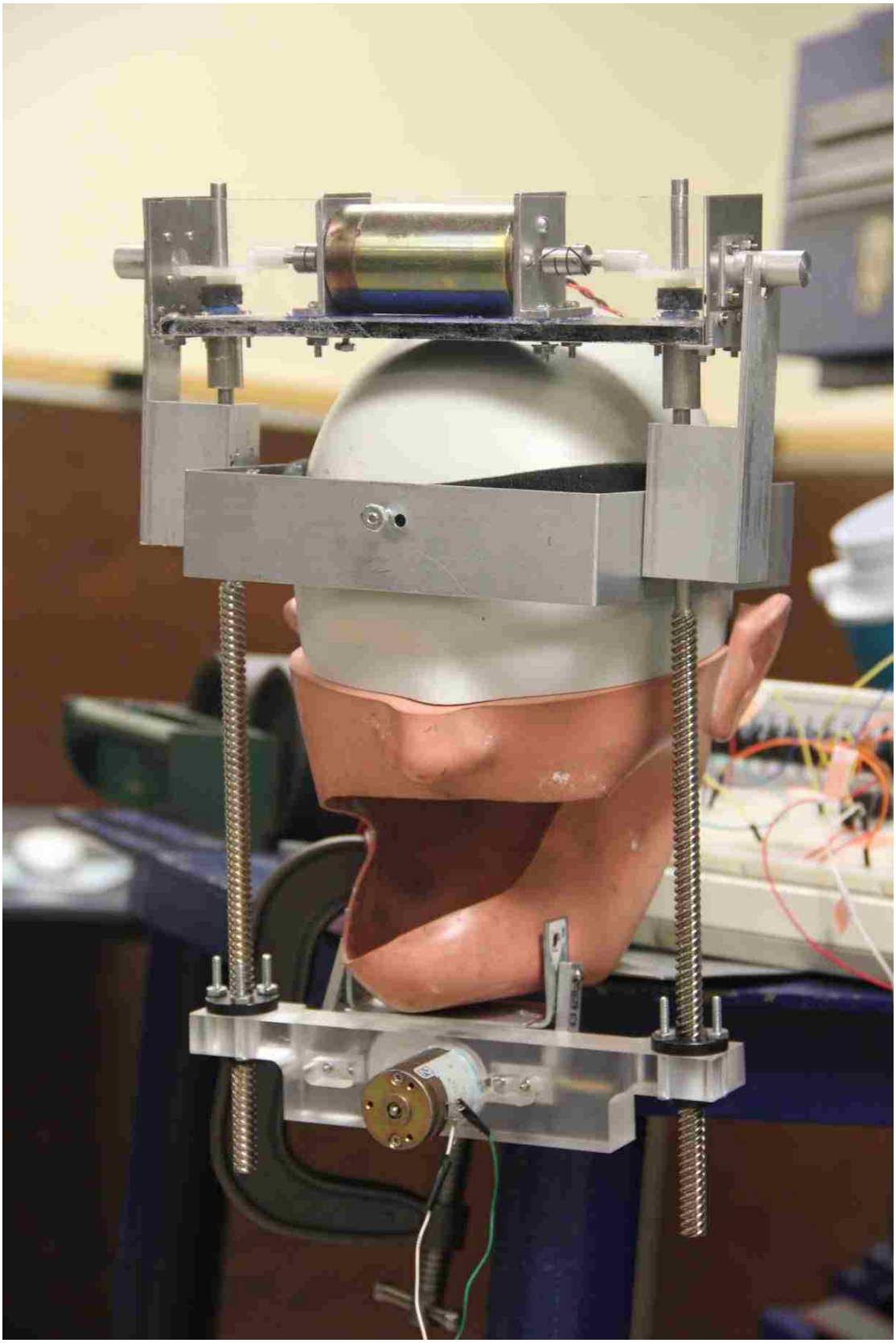

Fig 3.17 (d) Prototype of mastication robot

3.5 Results of Mastication Robot Moving Trajectory Measurements

A masticatory robot is comprised of a set of lead screws and a scotch-yoke mechanism and this mechanical system supports and moves the mandible. The mastication robot motors are controlled by the Anduino Duemilanove microcontroller board and PWM is used to adjust the output voltage for the motor. A series of experiments have been carried out on the model to verify the performance of this mastication robot.

In order to measure working displacements in this robot and to help record data in real time, a digital data acquisition system (LabVIEW) in conjunction with a standard 16-bit A/D converter has been used in conjunction with an LVDT. An LVDT is a transducer that produces a voltage that is linearly proportional to the displacement of a rod running through its core. To calibrate this LVDT, the rod through the LVDT is moved through several specific displacements, and the corresponding voltages are then recorded. Then, a linear, least-squares fit is applied to those points on the displacement-voltage space. The linear, least-squares fit produces an equation of the form:

$$D = aV + b \tag{3.3}$$

from which the slope and the intercept can then be determined for use in calculating the displacement for any given measured voltage. After getting the slope and intercept

in calibrating, the parameters can be used in the LabView program which shown in Appendix B. While the LVDT using, the voltages are recorded and then calculate the corresponding displacement through Eq. 3.3. Figure 3.18 below shows the displacement measuring experiment of mastication robot using LVDT.

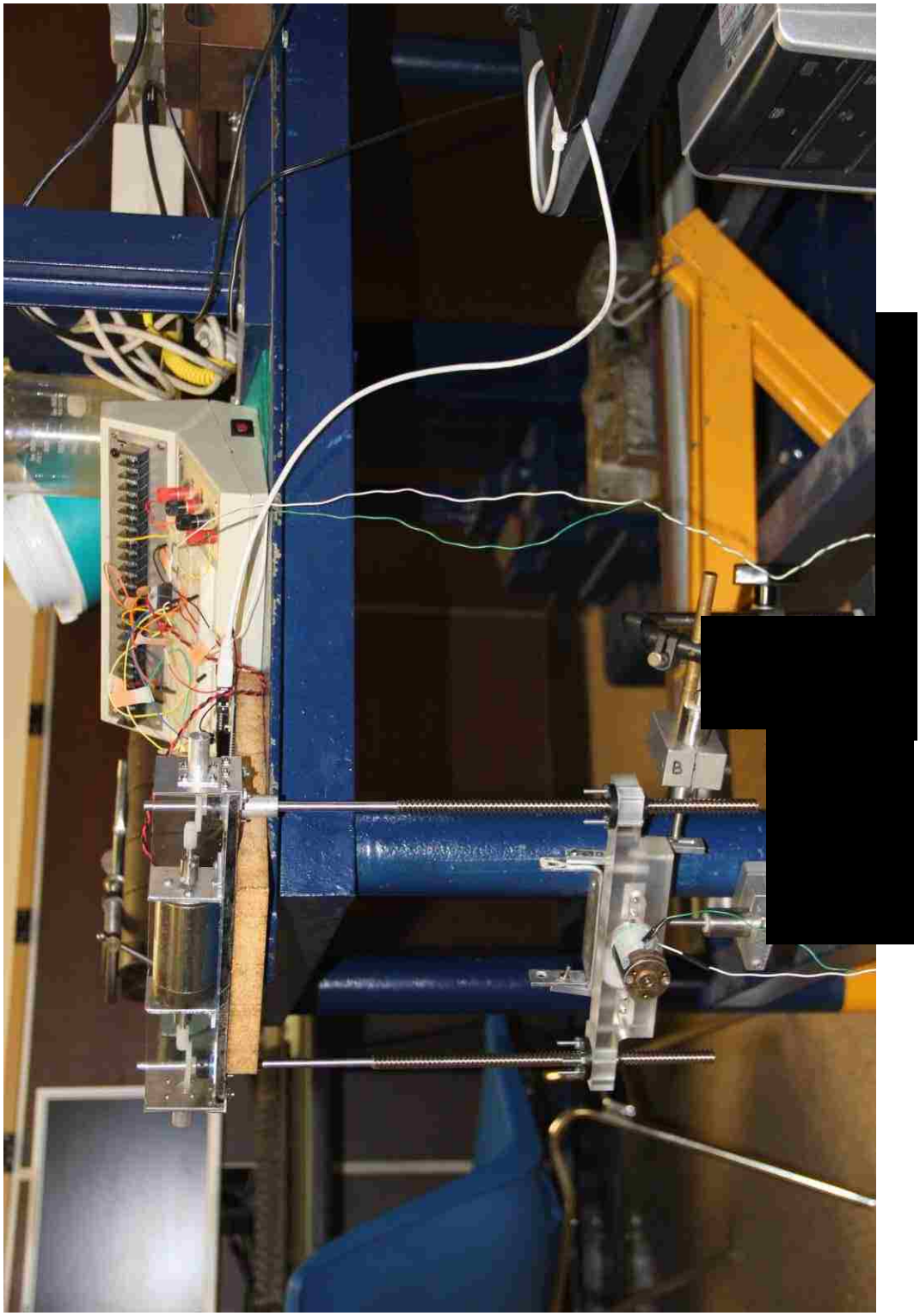

Fig. 3.18: Displacement measuring experiment of mastication robot using LVDT

In this section, several jaw trajectories have been recorded from the robot using LabVIEW with a LVDT transducer to verify the feasibility of this robot in comparison to the motion of a real human jaw. Since the maximum permissible displacement of the LVDT is 17 mm, the vertical motion of chewing cycle is therefore limited to this range. Shown in Figure 3.19 is 2DOF plot of the chewing trajectory for one chewing cycle in the frontal plane. It shows that motion trajectory produced by the coordinated controlled motion of the two subsystems is similar to the mandible chewing motion shown in Figure 3.20 and reported in [14].

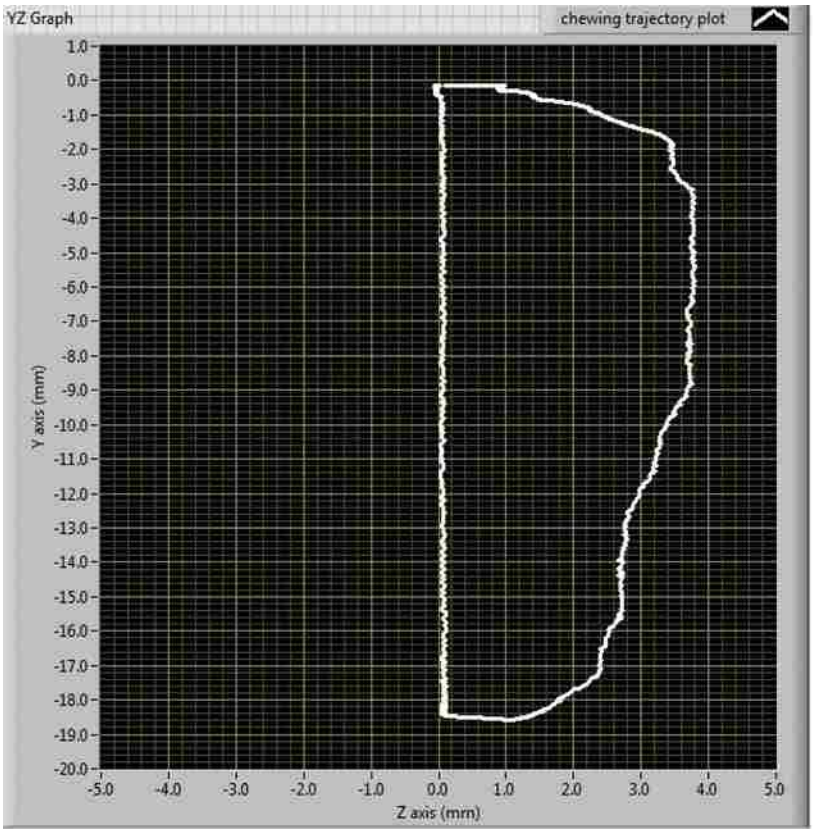

Figure 3.19: Mastication robot 2DOF trajectory for one cycle in frontal view

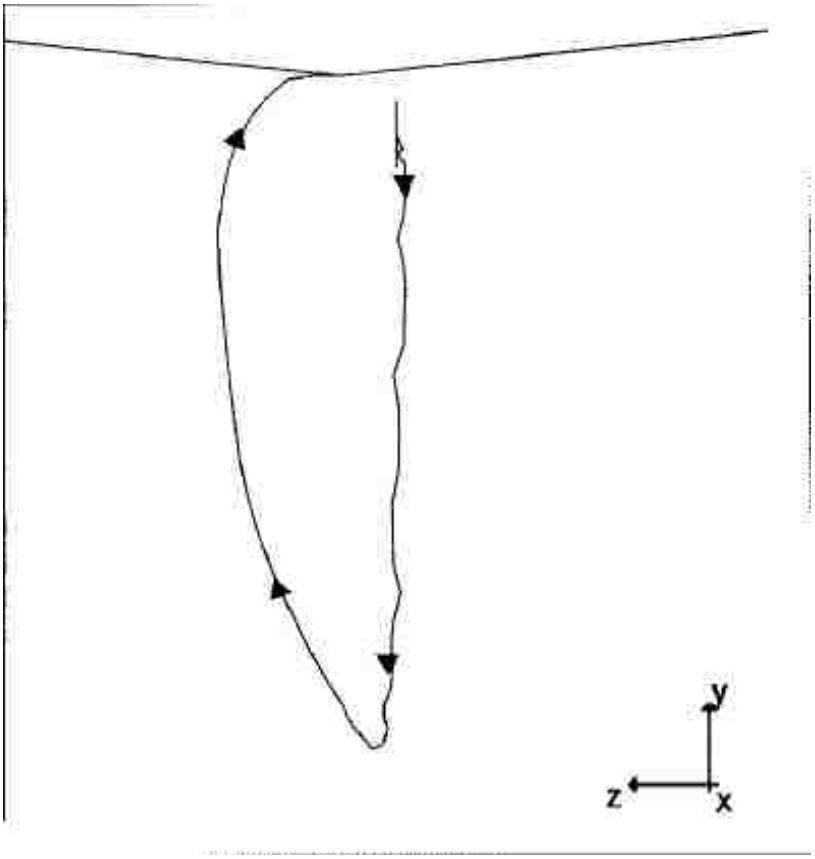

Figure 3.20: Human jaw 2DOF trajectory for one cycle in frontal view

The second experimental result is for several chewing cycles in continuous time. In this case, the same code in Anduino is used but the robot is run twice to get two different plots. Figure 3.21 shows that 1DOF chewing trajectory plots (horizontal displacement versus time and vertical displacement versus time) which confirms the robot feasibility as a function of time. These two results shows that mastication robot working for several chewing cycle in continuous time, compares favorably with Figure 3.22 (a) and (b) [1] for a real human jaw.

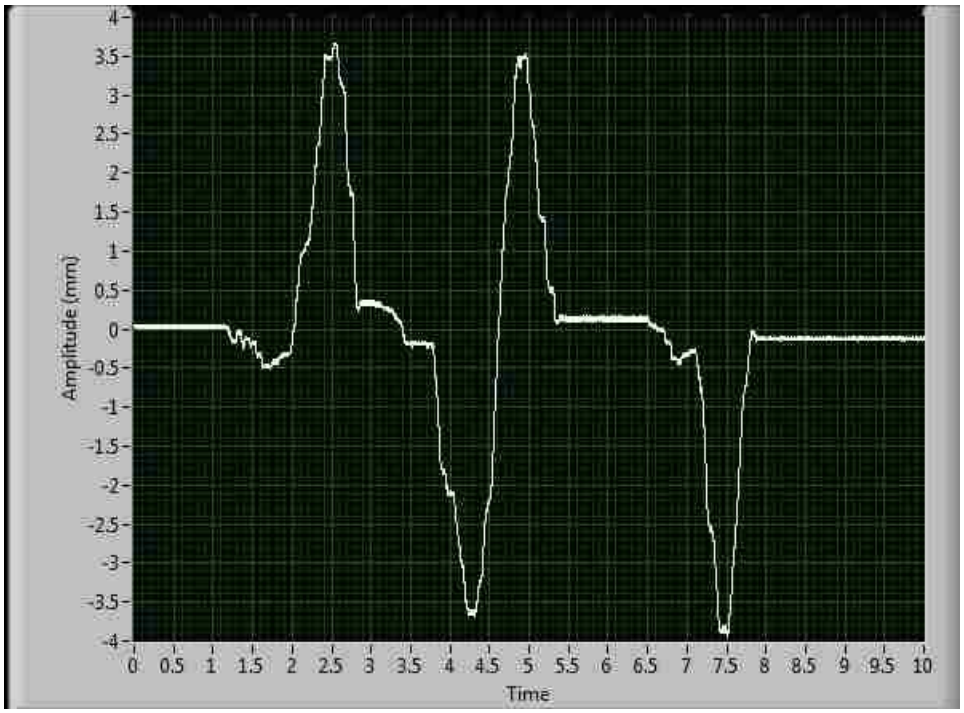

(a)

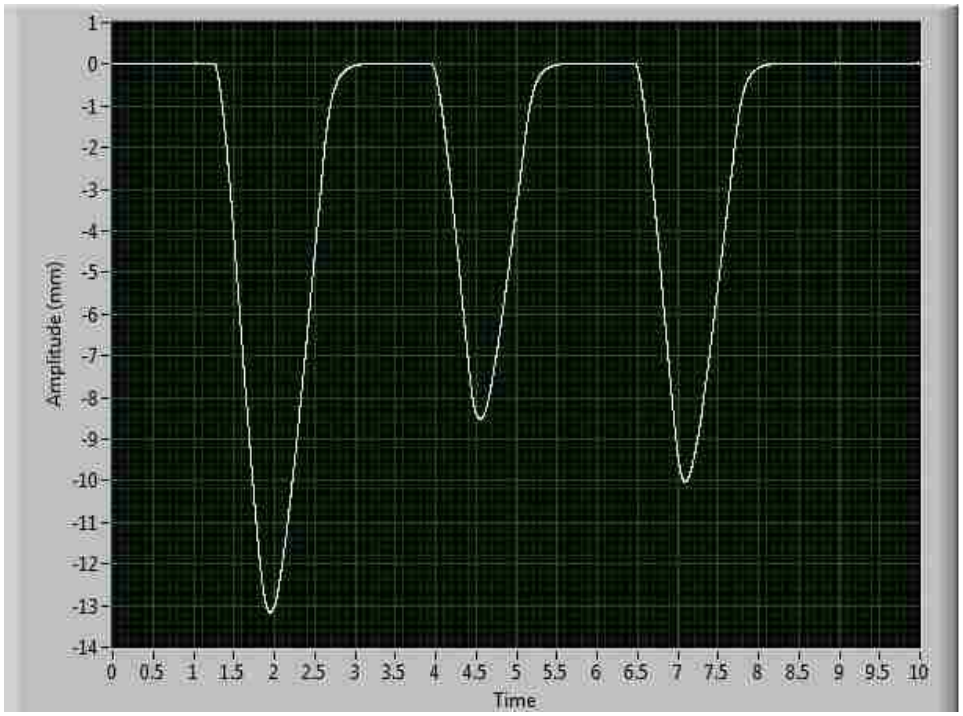

(b)

Figure 3.21: Mastication robot moving trajectory in time, (a) vertical displacement, and (b) lateral displacement (the zero point of y-axis in (a) denotes a closed mandible with a positive value representing motion to the right, the zero point of y-axis in (b) represents a closed position jaw and negative value represents downward motion)

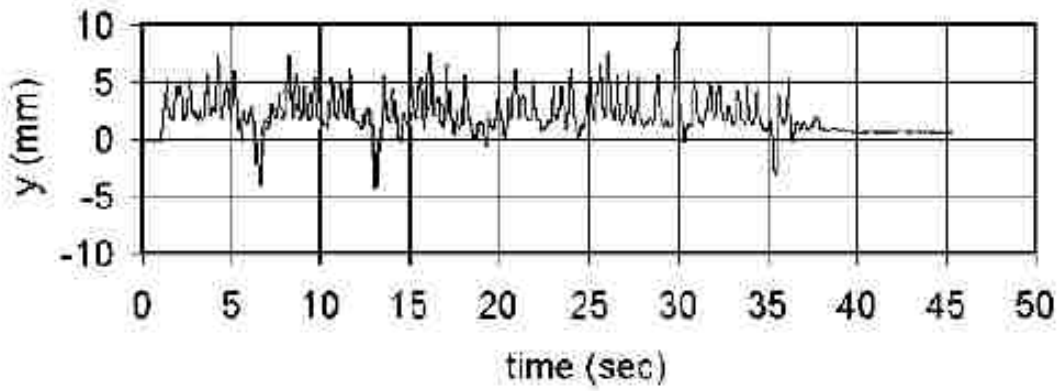

(a)

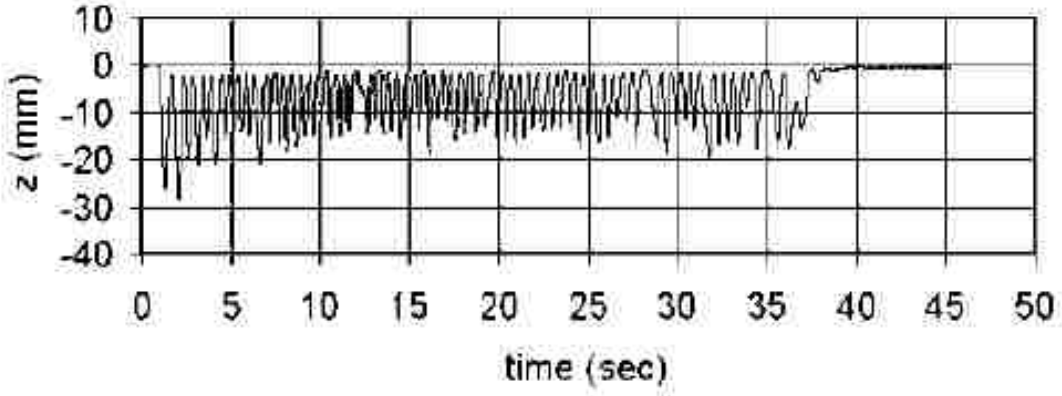

(b)

Figure 3.22: Human jaw moving trajectory in time, (a) vertical displacement, and (b) lateral displacement

A 2DOF trajectory is reproduced by the mastication robot. Figure 3.23 below shows that the actual trajectory in frontal plane. The y-axis represents vertical displacement and z-axis, the lateral displacement. This result compared favorably with Figure 3.24 [1] for a real human mandible trajectory.

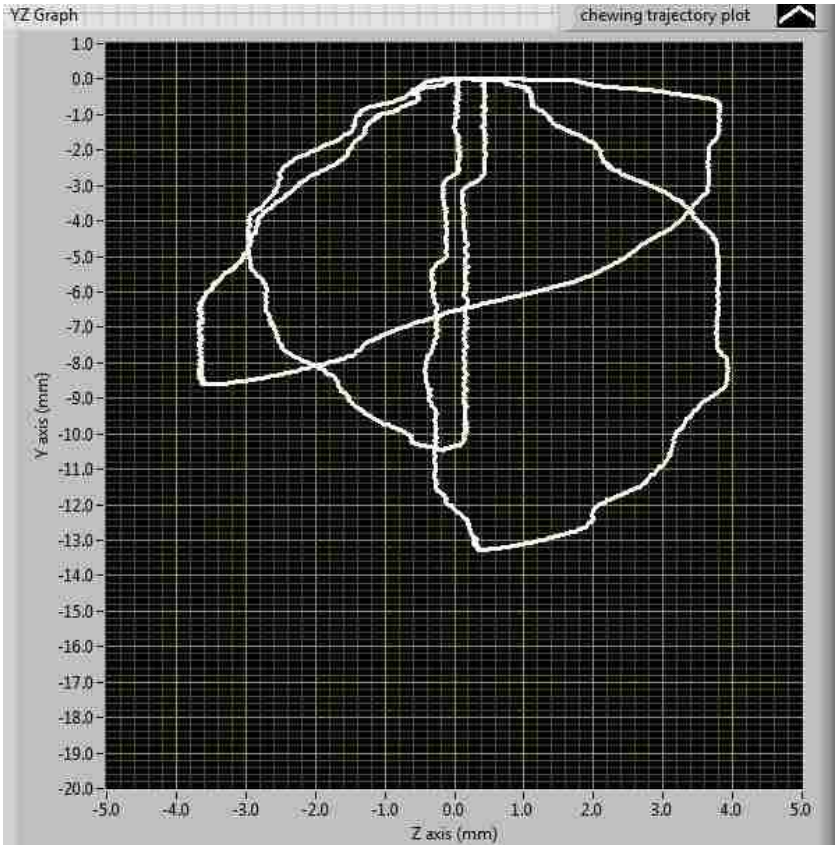

Figure 3.23 Recorded moving trajectory of the mastication robot in frontal plane

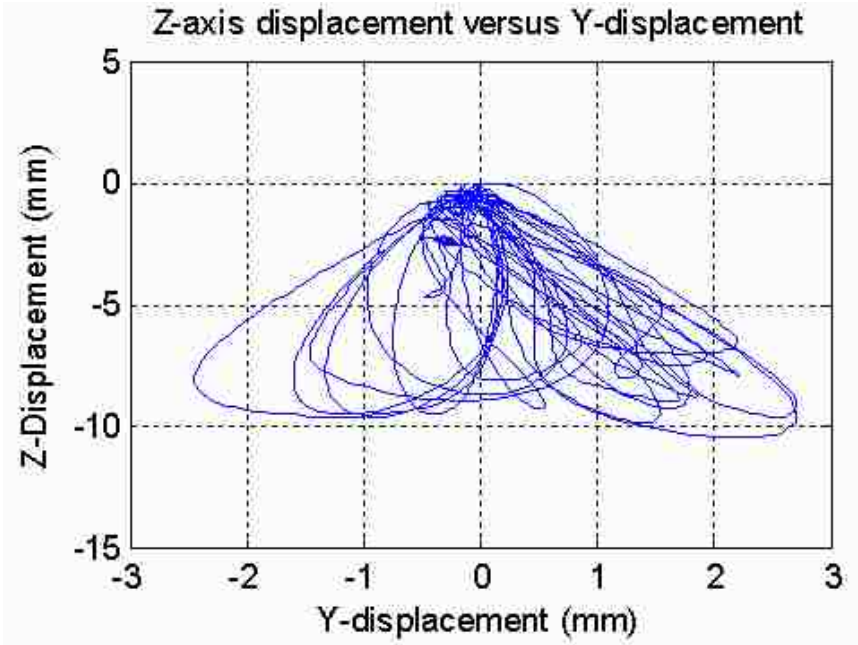

Figure 3.24 Human jaw moving trajectory in frontal plane (y-displacement is lateral movement, and z-displacement is vertical movement)

From the experimental results on the robotic prototype, it is found that the mastication robot can indeed perform human-like motion. However, there is some jerkiness in the plot of the motion, and that is due to the following problems. In the first half of the rotation of the scotch yoke during the lateral movement in the clenching cycle, the motor rotated at too low a speed (20 rpm) due to the low gear ratio. Friction becomes a major factor and so it is difficult to maintain a smooth rotational speed. Moreover, the presence of backlash between the two nuts (shown in Figure 3.25) permitted the yoke to be able to move vertically. It seems that the scotch yoke does not work well during the vertical straight line parts in the above plots. Even though the scotch moved, the backlash causes the yoke to have same free play at the interface with the LVDT.

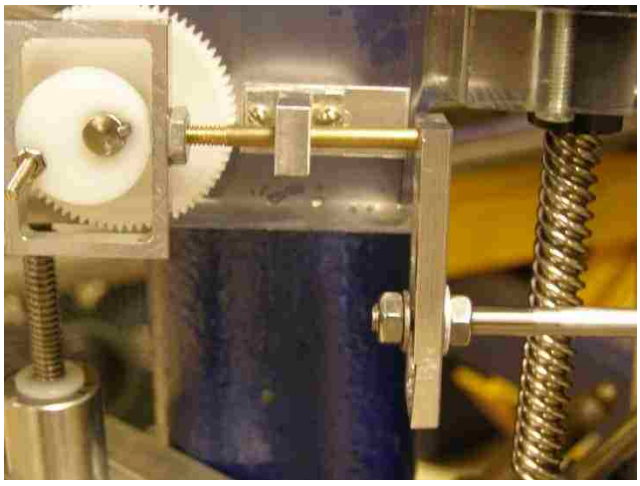

Figure 3.25: Backlash between two nuts

CHAPTER 4:

APPLIED OPTIMIZATION OF THE ROBOT

The chewing support system provides patients with the assistance needed in chewing and the details of which have been introduced in prior chapters. In this chapter, an optimization method is used to calculate the least energy expended at the clenching subsystem motor when the robotic mandible is functioning.

In this chapter, the contents are separated into three sections. In the first section, the dynamic equations for the mastication robot are derived and serve as the simulation model. In the second section, Sequential Quadratic Programming (SQP) technique will be used to calculate the least energy consumed at clenching subsystem motor. The final section provides the optimization settings and results. Since the chewing force is complicated by the kinds of foods chewed, several simple chewing force assumptions will be made to arrive at some reasonable and clearer understanding of the optimal system.

4.1 Simulation model and govern equations

Before optimizing for energy consumption of the system, the simulation model shown in Figure 3.13 is used to represent the dynamics of the system. Based on the equations for the model, the system can be optimized for a given speed trajectory.

In this section, a total of five equations are presented to describe this model. First, the output torque from the DC motor, drives the lead screw through bevel gears, so that

$$k_m i = (J_m + J_c N_g{}^2)\ddot{\theta}_m + T_c N_g \tag{4.1}$$

where k_m is motor torque constant , i is current, J_m is armature & pinion gear inertia, J_c is bevel gear & ball screw inertia, $\ddot{\theta_m}$ is the motor output angular velocity, T_c is the screw torque and the N_g is the bevel gear ratio. The screw torque drives the grinding subsystem load and chewing force so that:

$$T_c = f \times \frac{l}{2\pi e} \tag{4.2}$$

where l is the screw lead and e is screw efficiency, and, f is the total force which is sum of the grinding subsystem load and chewing force. This total force f can be separated into two loads depending on the upward and downward motion of the jaw:

$$\begin{cases} f_u = W(g + \ddot{y}_m) + f_c \text{.....}(upward) & (4.3) \\ f_d = W(g - \ddot{y}_m) \text{.....}(downward) & (4.4) \end{cases}$$

where f_u is required force when the jaw closes, f_d is the force in mandible opening, $\ddot{y}_m$ is the grinding subsystem vertical moving acceleration which followed the lead screw nuts and W is the clenching subsystem load and f_c is chewing force. Therefore, the relationship between motor angular acceleration and the grinding subsystem vertical acceleration becomes:

$$\ddot{y}_m = \ddot{\theta}_m \times \frac{N_g l}{2\pi} \tag{4.5}$$

These five equations govern the dynamics of the motor in the clenching subsystem and will be used in the optimization.

4.2 Optimization Method

An optimization procedure will be used to minimize an objective function when operating within a set of constraints [17]. In order to apply optimization, a verbal description of the problem formulation has to be translated to a well-defined mathematical expansion. The mathematical model for the optimization includes design variables, design parameters, and design functions. The design variables serve as the unknowns within the problem being solved, and they need to be linearly independent [17]. Design parameters are constants which will not change in the problem. Design functions, on the other hand, can be separated into object functions and constraint functions the provided meaningful information about the problem and establish the mathematical model for the design [17]. Object function (cost function) is an expression to present one design against another, and normally, it is to be minimized. The functions are limitations or performance requirements and there can be classified into equality or inequality constraints.

For this specific design problem, the purpose of applying optimization is to find

a design that achieves the objective of minimum motor energy used in activating the clenching subsystem. According to the Eqs. 4.1 and 4.4, the current input depends on the angular acceleration of the DC motor and the lead screw torque. Since there are many different kinds of curve functions, some simple ones such as: cubic equation $(a+bt+ct^2+dt^3)$, quadratic $(a+bt+ct^2)$ and Trigonometric $(a*sin\ (bt+c))$ function for angular velocity of the DC motor will be used. Starting and ending velocity is set at zero. The support package moving distance is equal to 5.0 cm and the time duration is set to be between one second and two seconds. According to Eqs.4.3 and 4.4, the lead screw torque has been separated into two parts, upward and downward. This will be discussed separately. Besides, there is one extra design parameter using in moving upward case because of 300N chewing force applied over the second half of the upward jaw motion. These verbal descriptions will now be translated into a mathematical model.

The standard format of mathematical model (using cubic equation):

Design Parameters: All design parameters are shown in Appendix Table C.1

Design Variables: *a, b, c, d* (cubic equation parameter), *T* (cost of time)

Objective Function:

Minimize E (a, b, c, d, T) = $\int_0^T i^2 R_m\, dt$

$$= \left\{ \int_0^T \frac{1}{k_m} \left[(J_m + J_c N_g^2)(b + 2ct + 3dt^2) + T_c N_g \right] \right\}^2 R_m dt$$

Downward:

$$\left\{ \int_0^T \frac{1}{k_m} \left[(J_m + J_c N_g^2)(b + 2ct + 3dt^2) + \frac{WlN_g}{2\pi e}(g - \frac{N_g l}{2\pi}(b + 2ct + 3dt^2)) \right] \right\}^2 R_m dt \quad (4.6)$$

Upward:

$$\left\{ \int_0^T \frac{1}{k_m} \left[\begin{array}{l} (J_m + J_c N_g^2)(b + 2ct + 3dt^2) + \frac{N_g l}{2\pi e}(W(g + \frac{N_g l}{2\pi}(b + 2ct + 3dt^2)) \\ +300u(t - \frac{T}{2})) \end{array} \right] \right\}^2 R_m dt \quad (4.7)$$

Constraint Functions:

1. The distance equality constraint is expressed as

$$\int_0^T (a + bt + ct^2 + dt^3) dt = aT + \frac{1}{2} bT^2 + \frac{1}{3} cT^3 + \frac{1}{4} dT^4 = \frac{2\pi D}{Ng \times l} \quad (4.8)$$

where D is the nut vertical moving distance.

2. The angular velocity equality constraint is set up as

$$a = 0 \quad (4.9)$$

$$aT + \frac{1}{2} bT^2 + \frac{1}{3} cT^3 + \frac{1}{4} dT^4 = 0 \quad (4.10)$$

The cost of time inequality constraint is written as

$$1 \le T \le 2 \quad (4.11)$$

Since this is a nonlinear optimization problem with equality and inequality constraints, Sequential Quadratic Programming (SQP) will be applied. SQP is an iterative method solve a problem at the current point x_k using Quadratic Programming (QP) as a subproblem. Based on the solution of this subproblem, a new point x_{k+1} can be found [19]. This process is iterated to create a sequence of approximations that will converge to a solution x^*. A quadratic subproblem optimization will have the form [17]:

Minimize:

$$\tilde{f}(\mathbf{S}) = f(\mathbf{X}_i) + \nabla f(\mathbf{X}_i)^T \mathbf{S} + \tfrac{1}{2}\mathbf{S}^T [\mathbf{H}]\mathbf{S} \tag{4.12}$$

Subject to:

$$\tilde{h}(\mathbf{S}): \quad ch_z(\mathbf{X}_i) + \nabla h_z(\mathbf{X}_i)^T \mathbf{S} = 0; \qquad k = 1, 2, \ldots, l \tag{4.13}$$

$$\tilde{g}(\mathbf{S}): \quad cg_j(\mathbf{X}_i) + \nabla g_j(\mathbf{X}_i)^T \mathbf{S} \leq 0; \qquad j = 1, 2, \ldots, m \tag{4.14}$$

$$s_i^l \leq s_i \leq s_i^u \qquad i = 1, 2, \ldots, n \tag{4.15}$$

where **S** is the search direction with respect to the active constraints and **H** is Hessian matrix *equal to* $\nabla^2 f(\mathbf{X}_i)$. In SQP, QP is used to optimize Eqs.4.12 to 4.15. Then the Kuhn-Tucker conditions are checked to see if they are satisfied. If it is, the optimum is the current solution, otherwise, next point (x_{k+1}) is applied and substitute into Eqs.4.12 to 4.15 and the process is repeated. The new point x_{k+1} is determined from $x_k + \alpha S$, where α is the stepsize which is based on minimizing an

unconstrained descent function, **descent function** [17]. This is described below:

Descent function:

Minimize:

$$\emptyset(x_{k+1}) = \mathrm{f}(x_{k+1}) + \mathrm{r}\sum_{z=1}^{l} h_z(x_{k+1})^2 + r\sum_{j=1}^{m} \beta_j max[g_j(x_{k+1}), 0]^2 \qquad (4.16)$$

4.3 Optimization Setting and Results

4.3.1 System Mathematical Model Using Cubic Equation Velocity *($a+bt+ct^2+dt^3$)*

To optimize this model, a single nonlinear objective function, a linear inequality constraint, three equality constraints are presented. The design variables are cubic equation parameters and the final time. Assuming cubic equation $\dot{\theta}$ is $a+bt+ct^2+dt^3$, and then $\ddot{\theta} = b + 2ct + 3dt^2$. There are two different objective functions because of chewing force occurring only in upward motion of the jaw. A 300N force is assumed from T/2 to T.

Design Parameters: All design parameters are shown in Appendix Table C.1

Design Variables: *a, b, c, d* (cubic equation parameter), *T* (cost of time)

Objective Function:

Minimize E (*a, b, c, d, T*) = $\int_0^T i^2 R_m \, dt$

$$= \left\{ \int_0^T \frac{1}{k_m} \left[(J_m + J_c N_g^2)(b + 2ct + 3dt^2) + T_c N_g \right] \right\}^2 R_m dt$$

Downward:

$$\left\{\int_0^T \frac{1}{k_m}\left[(J_m + J_c N_g^2)(b + 2ct + 3dt^2) + \frac{WlN_g}{2\pi e}(g - \frac{N_g l}{2\pi}(b + 2ct + 3dt^2))\right]\right\}^2 R_m dt \quad (4.17)$$

Upward:

$$\left\{\int_0^T \frac{1}{k_m}\left[\begin{array}{l}(J_m + J_c N_g^2)(b + 2ct + 3dt^2) + \frac{N_g l}{2\pi e}(W(g + \frac{N_g l}{2\pi} \\ (b + 2ct + 3dt^2)) + 300u(t - \frac{T}{2}))\end{array}\right]\right\}^2 R_m dt \quad (4.18)$$

The distance equality constraint is expressed as

$$\int_0^T (a + bt + ct^2 + dt^3)dt = aT + \frac{1}{2}bT^2 + \frac{1}{3}cT^3 + \frac{1}{4}dT^4 = \frac{2\pi D}{Ng \times l} \quad (4.19)$$

where *D* is the nut vertical moving distance.

The angular velocity equality constraint is set up as

$$a = 0 \quad (4.20)$$

$$aT + \frac{1}{2}bT^2 + \frac{1}{3}cT^3 + \frac{1}{4}dT^4 = 0 \quad (4.21)$$

The cost of time inequality constraint is written as

$$1 \le T \le 2 \quad (4.22)$$

Results:

i. Moving downward situation:

Clenching subsystem moving downward situation: optimization results by SQP using MATLAB

****

Design Variables [a,b,c,d,T] : 0.0000 237.1452 -121.0162 -9.9817 1.7166

objective function value E: 0.0015

motor angular velocity= 0.0000+237.1452*t+-121.0162*t^2 -9.9817*t^3

cost time = 1.7166 sec

energy consumption = 0.0015 J

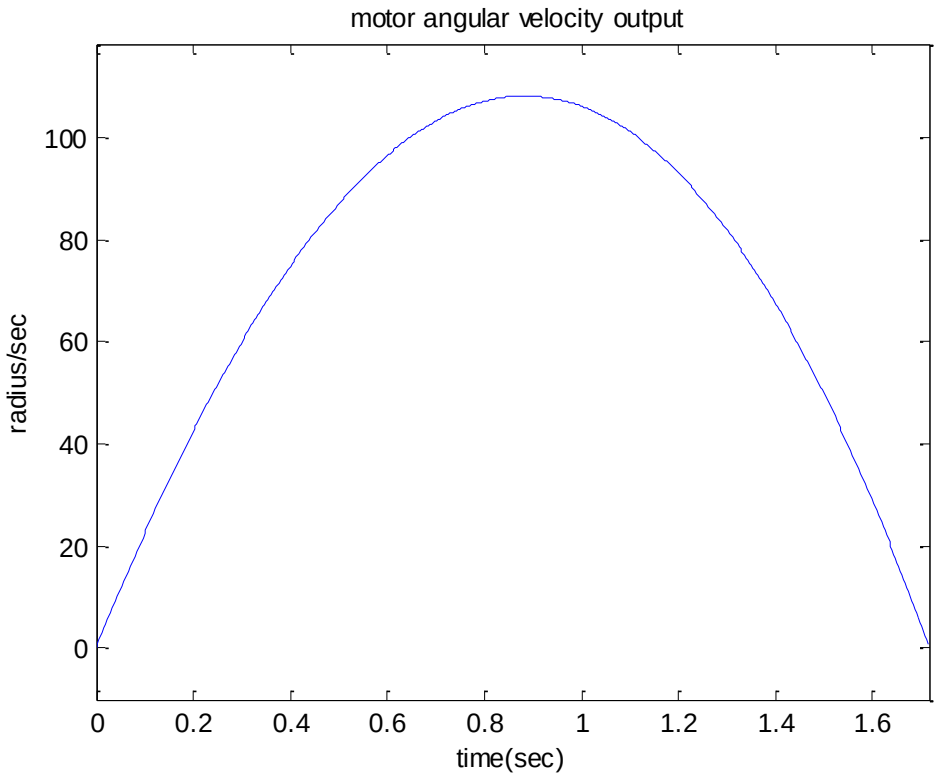

Figure 4.1: Cubic velocity function for clenching subsystem moving downward (a) motor angular velocity

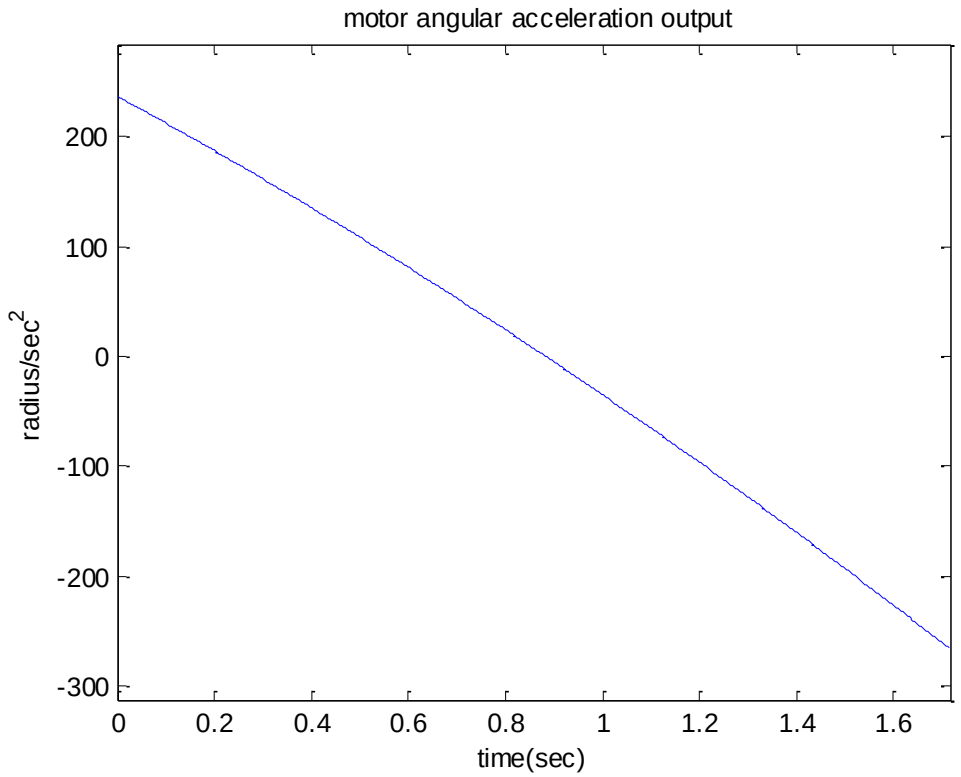

Figure 4.1: Cubic velocity for clenching subsystem moving downward (b) motor angular acceleration

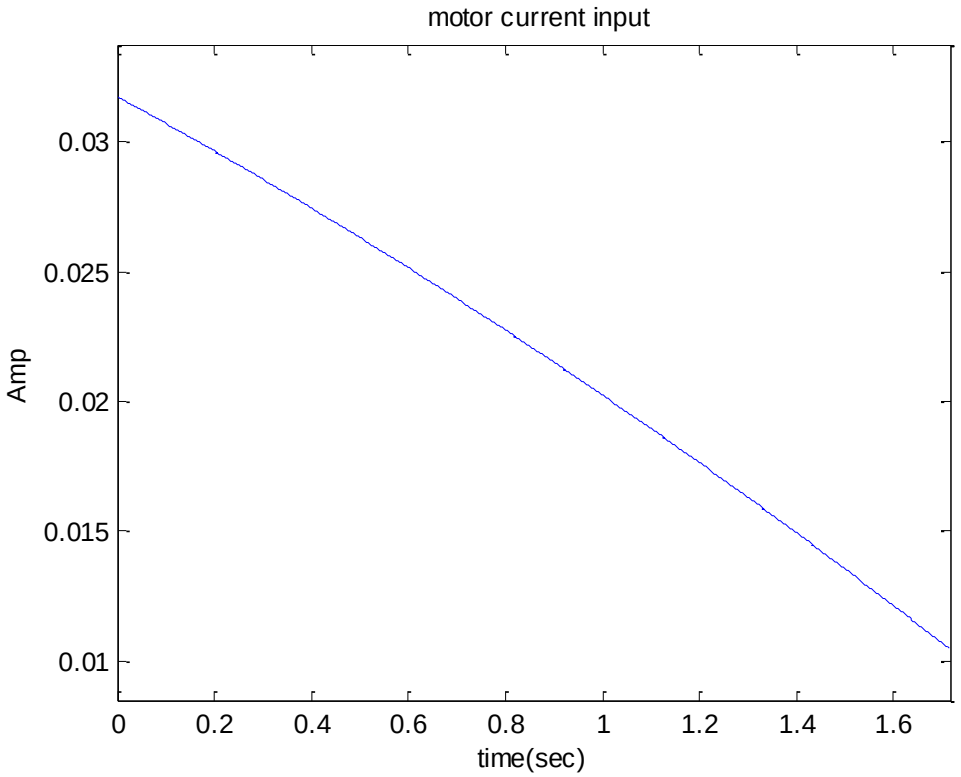

Figure 4.1: Cubic velocity function for clenching subsystem moving downward (c) motor currents using

ii. Moving upward situation

Clenching subsystem moving upward situation: optimization results by SQP using MATLAB

****

Design Variables [a,b,c,d,T] : 0.0000 507.0005 -36.7845 -470.2160 1.0000

objective function value E: 34.6861

motor angular velocity= -0.0000+507.0005*t+-36.7845*t^2 -470.2160*t^3

cost time = 1.0000 sec

energy consumption = 34.6861 J

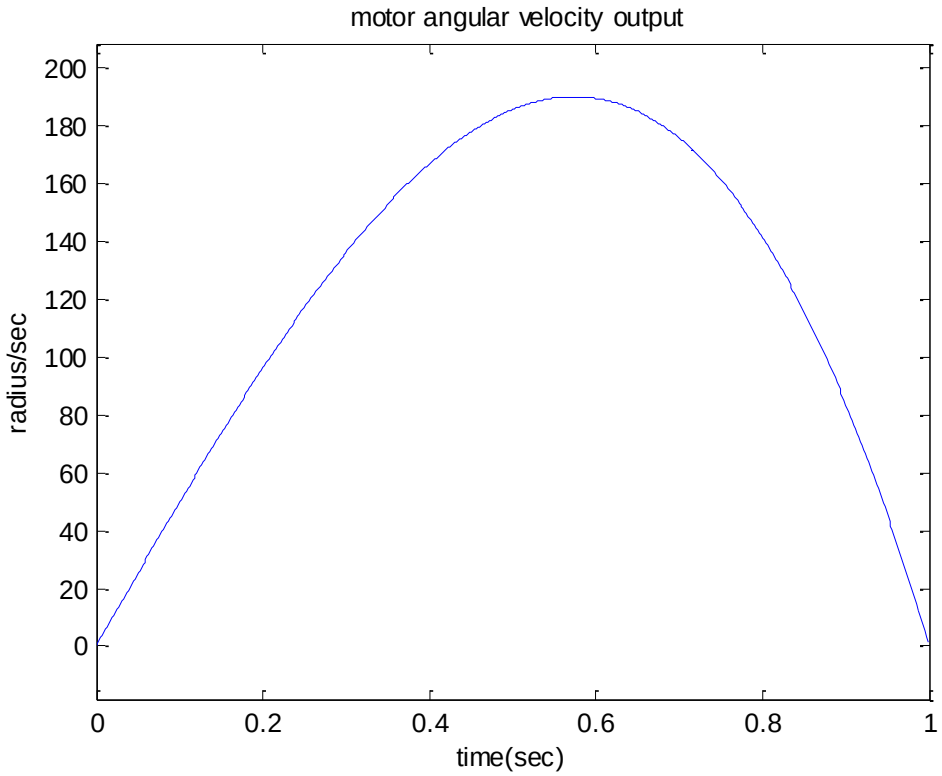

Figure 4.2: Cubic velocity for clenching subsystem moving upward (a) motor angular velocity

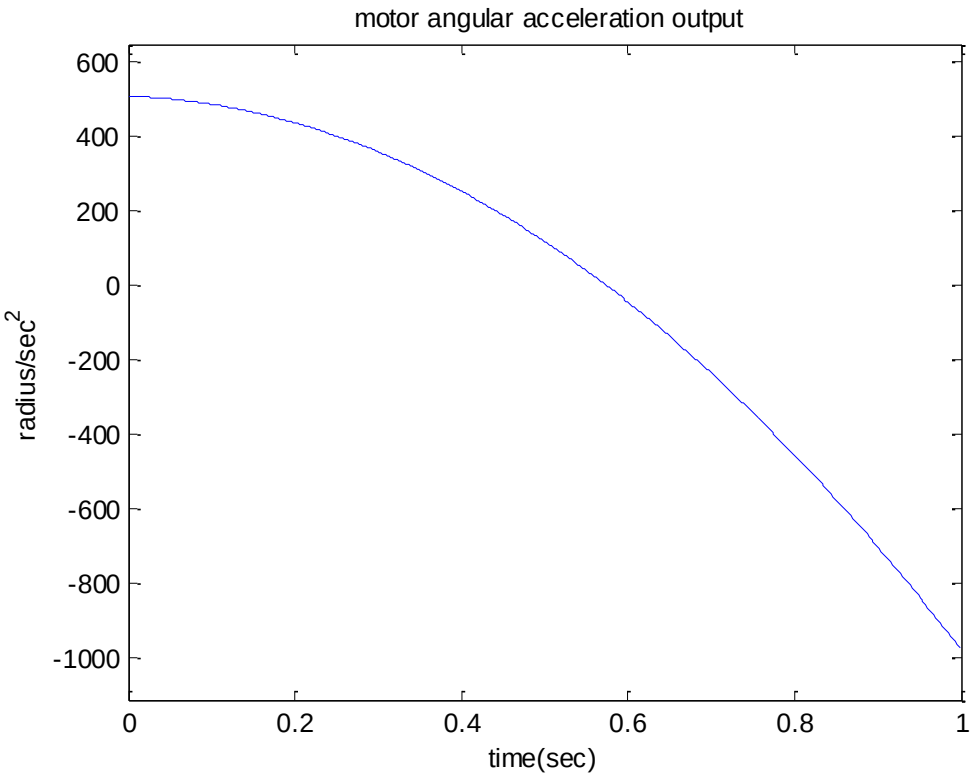

Figure 4.2: Cubic velocity function for clenching subsystem moving upward (b) motor angular acceleration

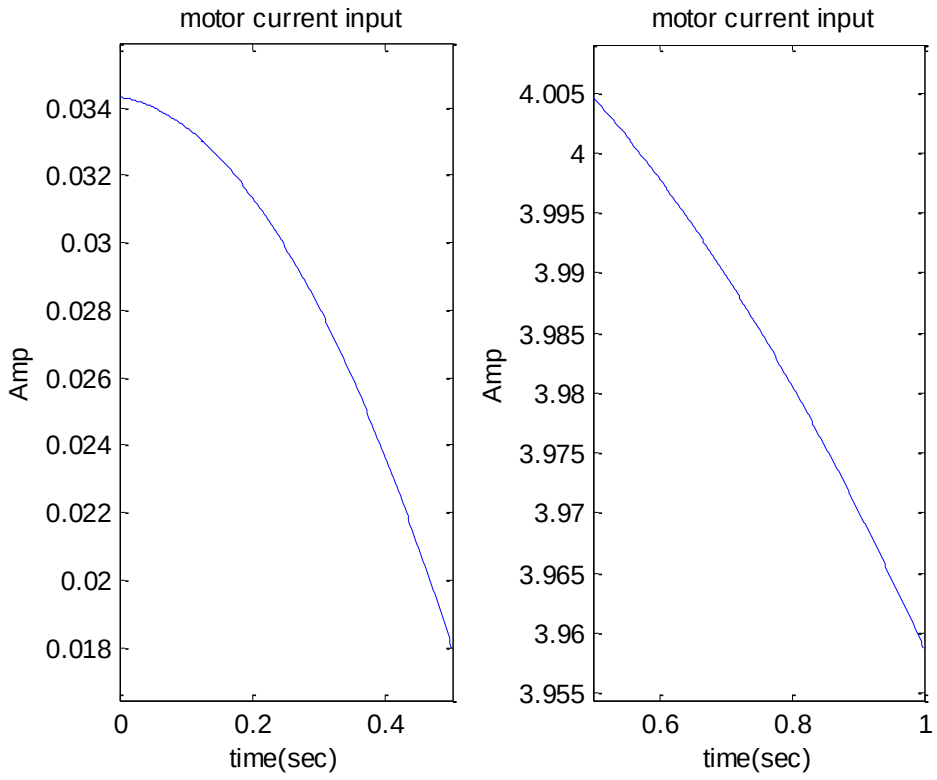

Figure 4.2: Cubic velocity function for clenching subsystem moving upward (c) motor current using

4.3.2 System Mathematical Model using Quadratic Equation Velocity($a+bt+ct^2$)

As in section 4.3.1, a quadratic function will be used for the motor output angular velocity. The number of design variables is one less than that for the cubic equation.

Design Variables: *a, b, c,* (quadratic equation parameter), *T* (cost of time)

Objective Function:

Minimize E (*a, b, c, d, T*) = $\int_0^T i^2 R_m \, dt$

$$= \left\{ \int_0^T \frac{1}{k_m} \left[(J_m + J_c N_g^2)(b + 2ct) + T_c N_g \right] \right\}^2 R_m dt$$

Downward:

$$\left\{ \int_0^T \frac{1}{k_m} \left[(J_m + J_c N_g^2)(b + 2ct) + \frac{WlN_g}{2\pi e} (g - \frac{N_g l}{2\pi} (b + 2ct)) \right] \right\}^2 R_m dt \qquad (4.22)$$

Upward:

$$\left\{ \int_0^T \frac{1}{k_m} \left[\begin{array}{l} (J_m + J_c N_g^2)(b + 2ct) + \frac{N_g l}{2\pi e} (W(g + \frac{N_g l}{2\pi} (b + 2ct)) \\ +300u(t - \frac{T}{2})) \end{array} \right] \right\}^2 R_m dt \qquad (4.23)$$

Constraint Functions:

The distance equality constraint is expressed as

$$\int_0^T (a + bt + ct^2) dt = aT + \frac{1}{2} bT^2 + \frac{1}{3} cT^3 = \frac{2\pi D}{Ng \times l} \qquad (4.24)$$

where *D* is the nut vertical moving distance.

The angular velocity equality constraint is set up as

$$a = 0 \tag{4.25}$$

$$aT + \frac{1}{2}bT^2 + \frac{1}{3}cT^3 = 0 \tag{4.26}$$

The cost of time inequality constraint is written as

$$1 \le T \le 2 \tag{4.27}$$

Results:

i. Moving downward situation:

Clenching subsystem moving downward situation: optimization results by SQP in MATLAB

****

Design Variables [a,b,c,T] : 0.0000 266.4277 -159.6377 1.6690

objective function value E: 0.0015

motor angular velocity= 0.0000+266.4277*t+-159.6377*t^2

cost time = 1.6690 sec

energy consumption = 0.0015 J

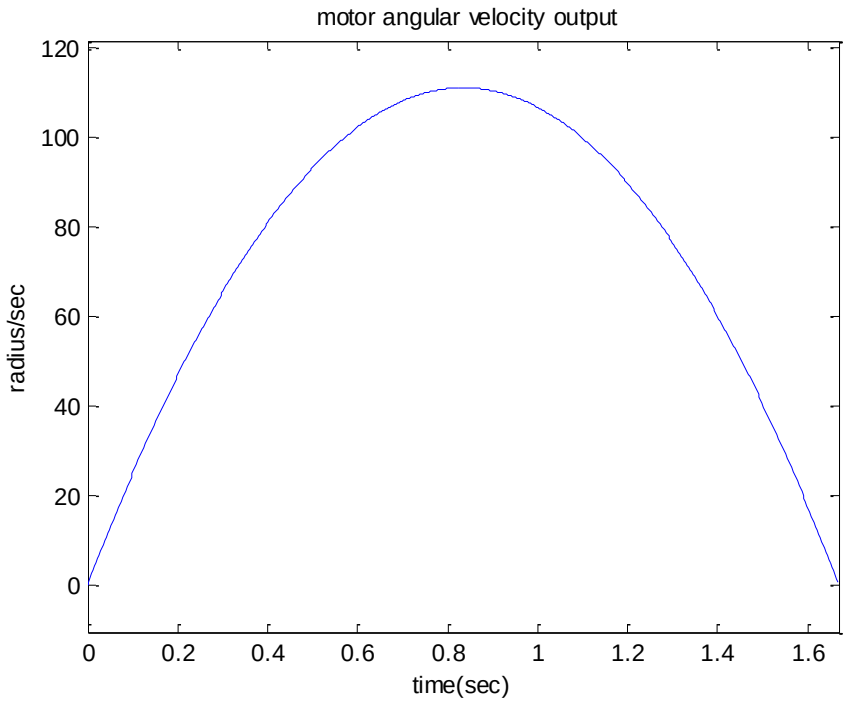

Figure 4.3 Quadratic velocity function for clenching subsystem moving downward (a) motor angular velocity

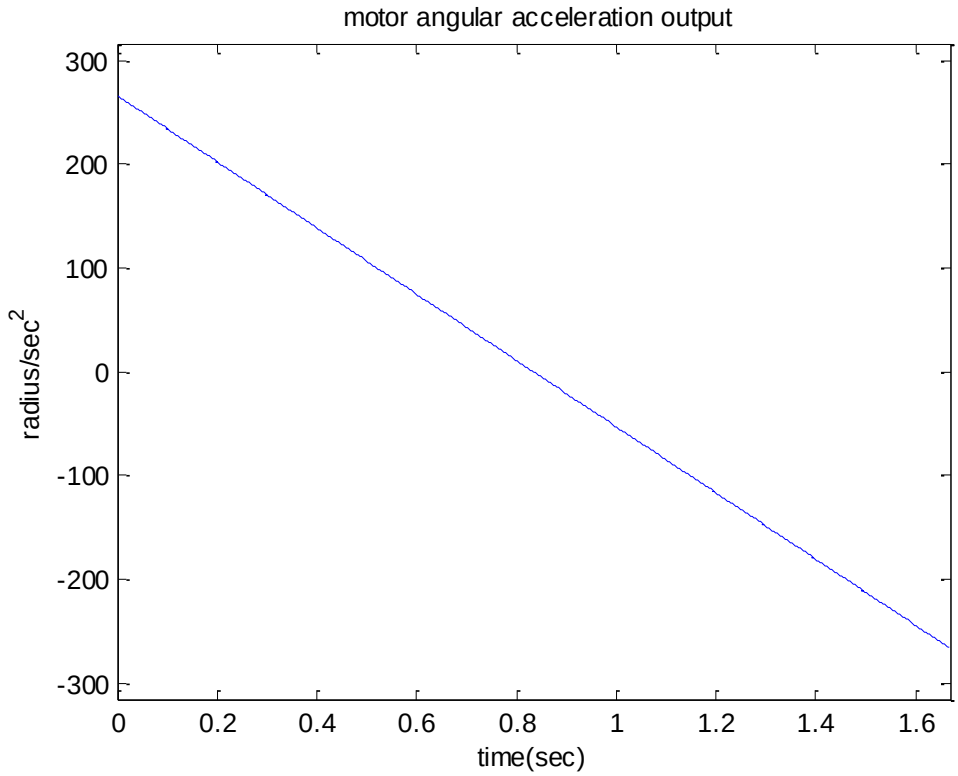

Figure 4.3 Quadratic velocity function for clenching subsystem moving downward (b) motor angular acceleration

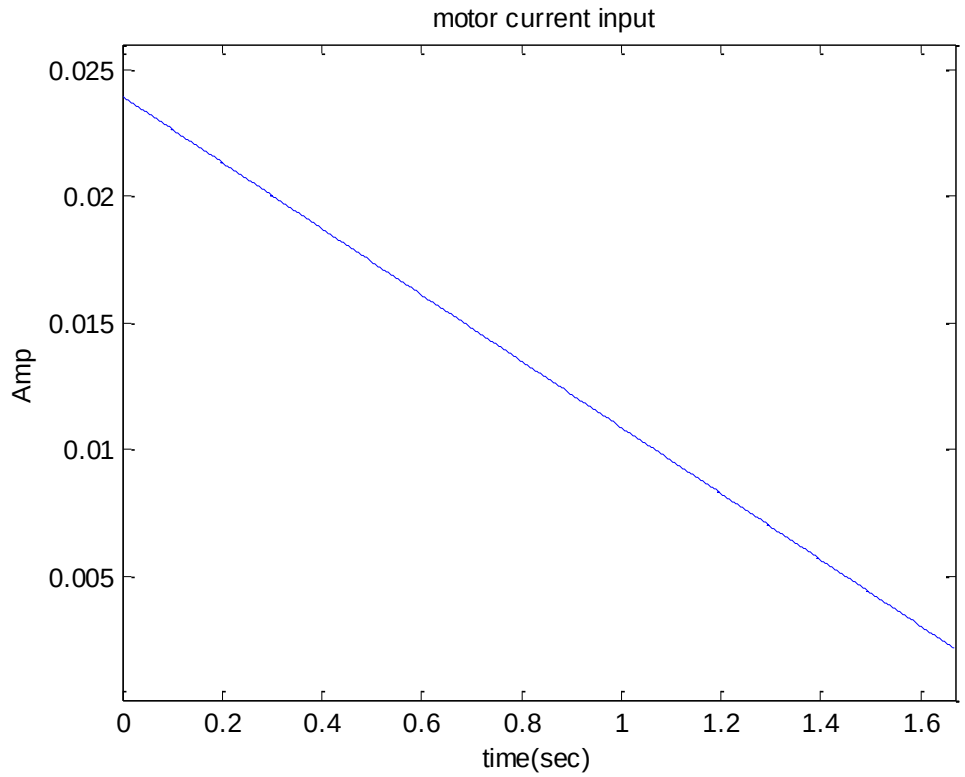

Figure 4.3: Quadratic velocity function for clenching subsystem moving downward

(c) motor angular currents using

ii. Moving upward situation

Since there is a 300N force from time T/2 to T, current input is large and is different at the T/2 time point.

Clenching subsystem moving upward situation: optimization results by SQP in MATLAB

****

Design Variables [a,b,c,T] : 0.0000 742.1085 -742.1085 1.0000

objective function value E: 34.6861

motor angular velocity= 0.0000+742.1085*t+-742.1085*t^2

cost time = 1.0000 sec

energy consumption = 34.6861 J

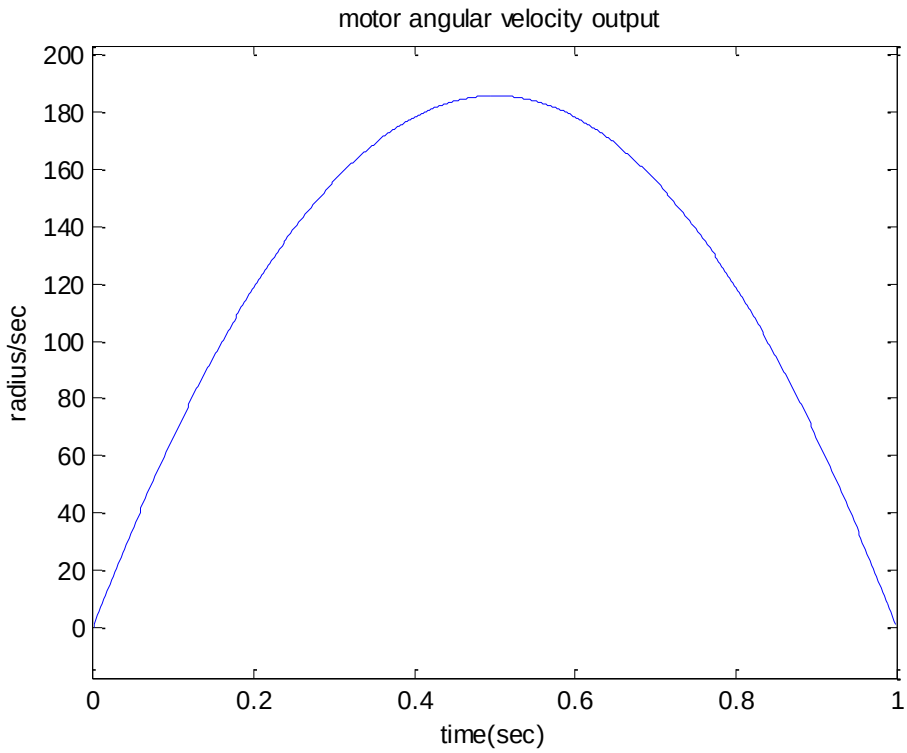

Figure 4.4 Quadratic velocity function for clenching subsystem moving upward (a) motor angular velocity

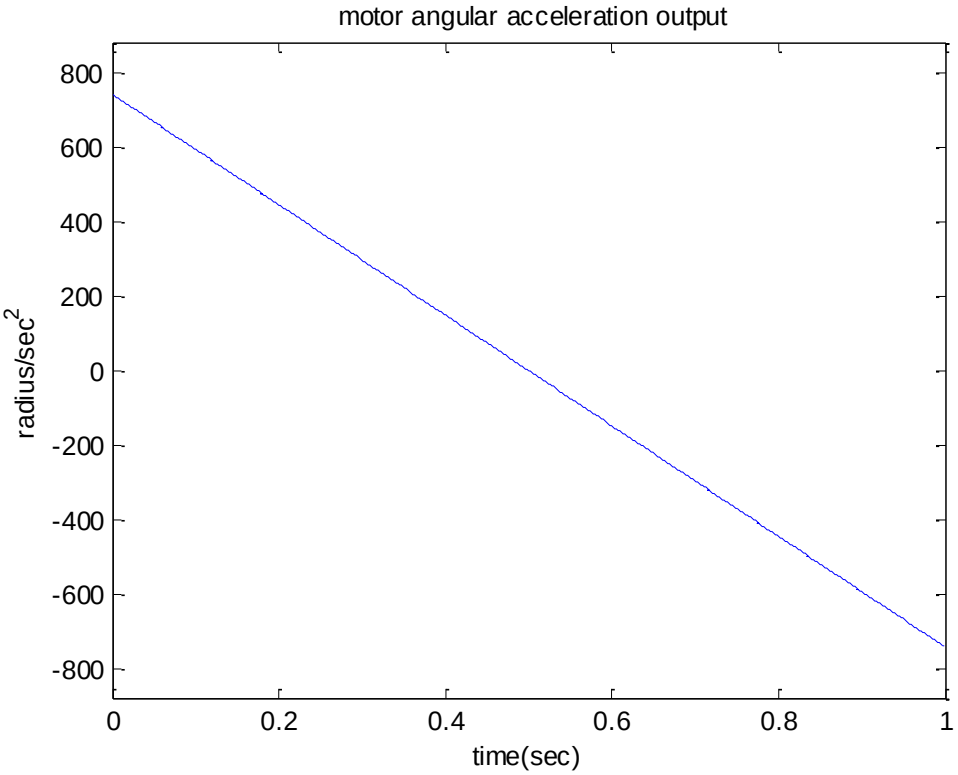

Figure 4.4 Quadratic velocity function for clenching subsystem moving upward (b) motor angular acceleration

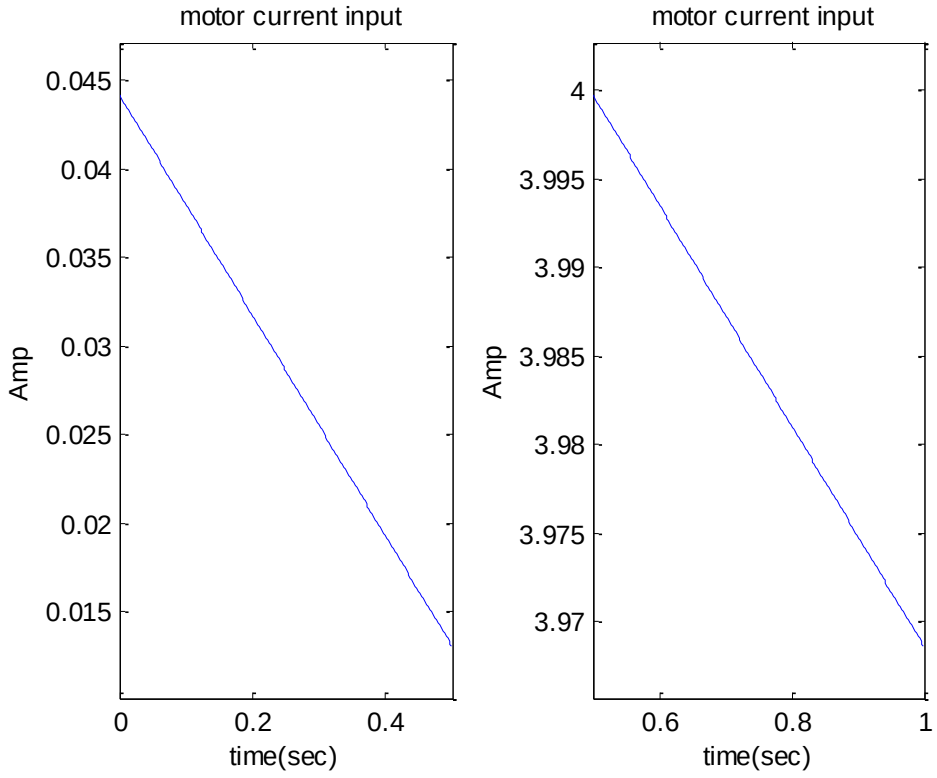

Figure 4.4 Quadratic velocity function for clenching subsystem moving upward (c) motor currents using

4.3.3 System Mathematical Model Using Sine Function Velocity *(a*sin(bt+c))*

This section, as in previous two sections are the same example for sine function that is applied to the motor output angular velocity. Therefore, angular acceleration set as $a \times sin(bt + c)$

Design Variables: *a, b, c,* (sine function parameter), *T* (cost of time)

Objective Function:

Minimize E (*a, b, c, d, T*) = $\int_0^T i^2 R_m \, dt$

$$= \left\{ \int_0^T \frac{1}{k_m} \left[(J_m + J_c N_g^2)(b + 2ct) + T_c N_g \right] \right\}^2 R_m dt$$

Downward:

$$\left\{ \int_0^T \frac{1}{k_m} \left[(J_m + J_c N_g^2)(b + 2ct) + \frac{WlN_g}{2\pi e} g - \left(\frac{N_g l}{2\pi} b + (ct)^2 \right) \right] \right\}^2 R_m dt \qquad (4.28)$$

Upward:

$$\left\{ \int_0^T \frac{1}{k_m} \left[\begin{array}{l} (J_m + J_c N_g^2)(b + 2ct) + \frac{N_g l}{2\pi e} W(g + \left(\frac{N_g l}{2\pi} b + (ct)^2 \right) \\ +300u(t - \frac{T}{2}) \end{array} \right] \right\}^2 R_m dt \qquad (4.29)$$

Constraint Functions:

The distance equality constraint is expressed as

$$\int_0^T a \sin(bt + c) dt = \frac{2\pi D}{l} \qquad (4.30)$$

where *D* is the nut vertical moving distance.

The angular velocity equality constraint is set up as

$$a\sin(c) = 0 \tag{4.31}$$

$$a\sin(bT + c) = 0 \tag{4.32}$$

The cost of time inequality constraint is written as

$$1 \le T \le 2 \tag{4.33}$$

Results:

i. Moving downward situation:

Clenching subsystem moving downward situation: optimization results by SQP using MATLAB

****

Design Variables [a,b,c,T] : -131.0279 -2.1187 -364.4247 1.4828

objective function value E: 0.0015

motor angular velocity= -131.0279*sin(-2.1187*t-364.4247)

cost time = 1.4828 sec

energy consumption = 0.0015 J

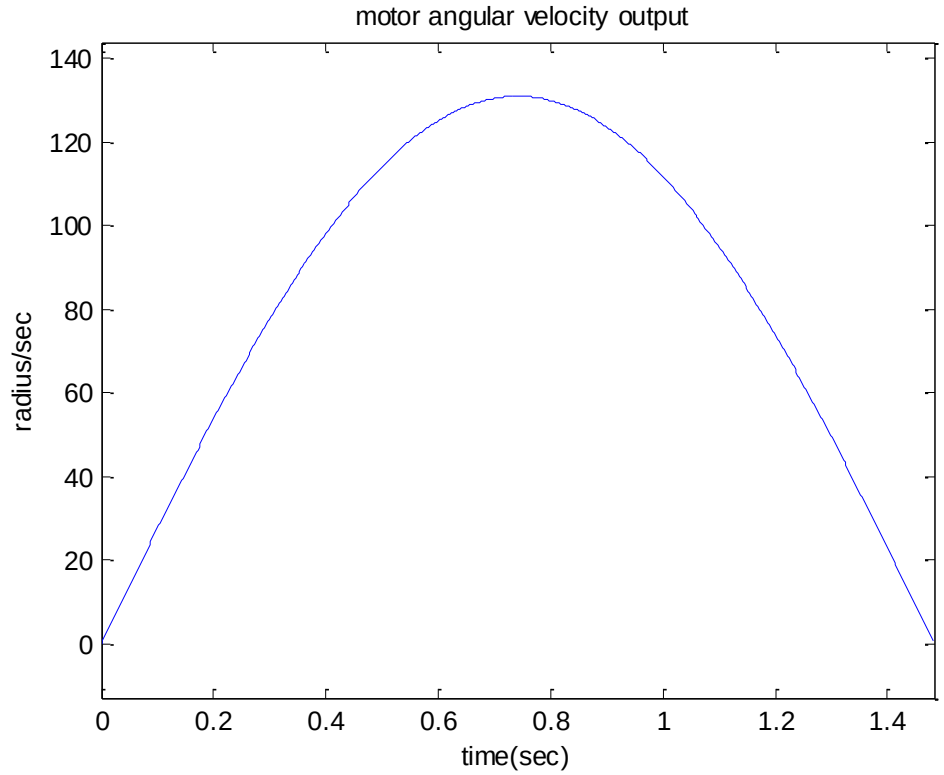

Figure 4.5 Sine velocity function for clenching subsystem moving downward (a) motor angular velocity

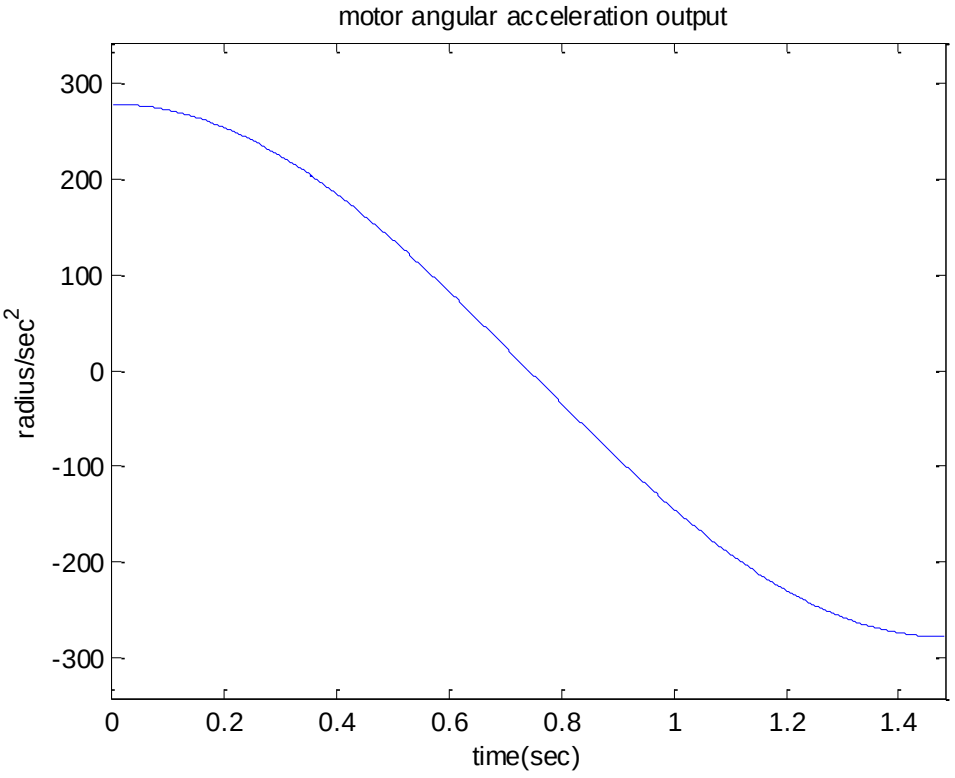

Figure 4.5 Sine velocity function for clenching subsystem moving downward (b) motor angular acceleration

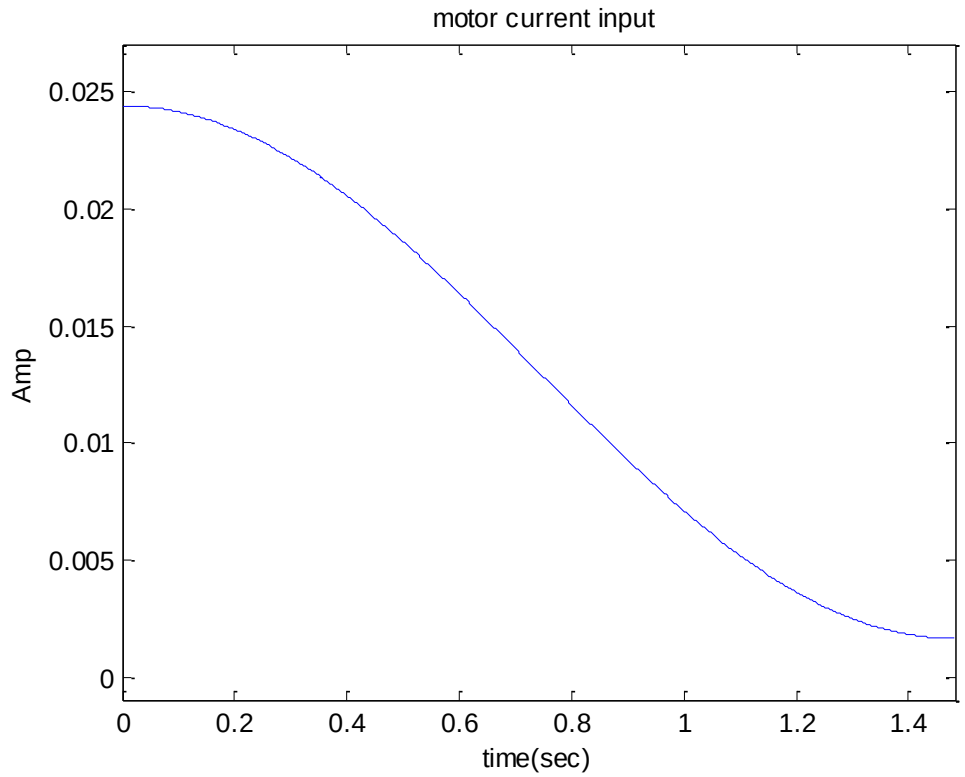

Figure 4.5 Sine velocity function for clenching subsystem moving downward

(c) motor angular currents using

ii. Moving upward situation

Clenching subsystem moving downward situation: optimization results by SQP using MATLAB

****

Design Variables [a,b,c,T] : 194.2836 -3.1416 3.1416 1.0000

objective function value E: 34.6733

motor angular velocity= 194.2836*sin(-3.1416*t+3.1416)

cost time = 1.0000 sec

energy consumption = 34.6733 J

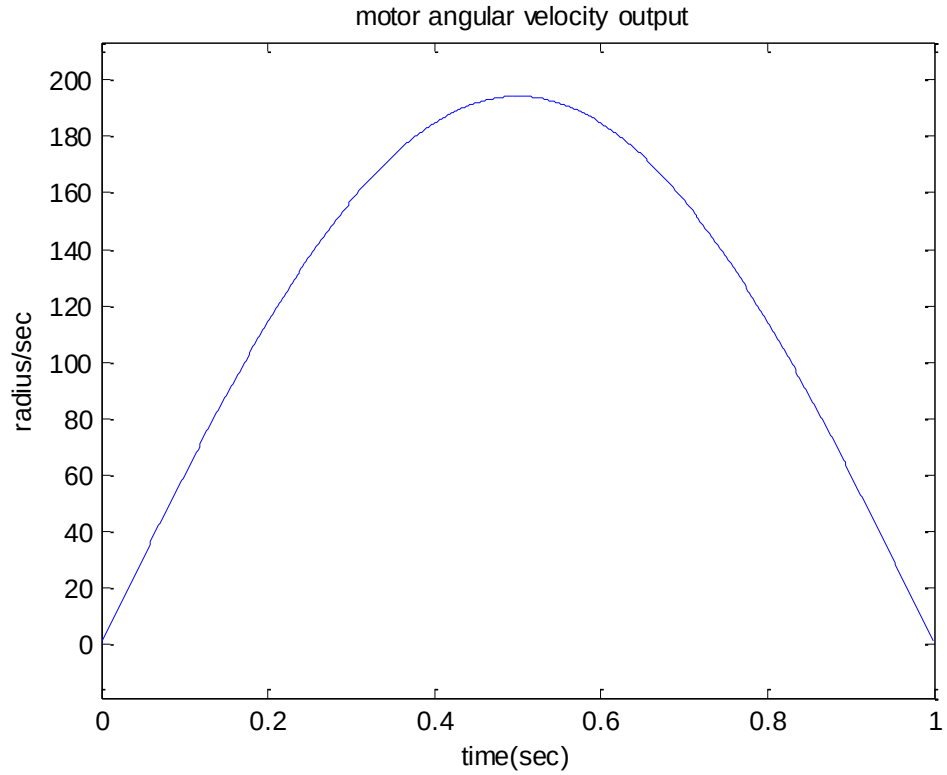

Figure 4.6 Sine velocity function for clenching subsystem moving upward (a) motor angular velocity

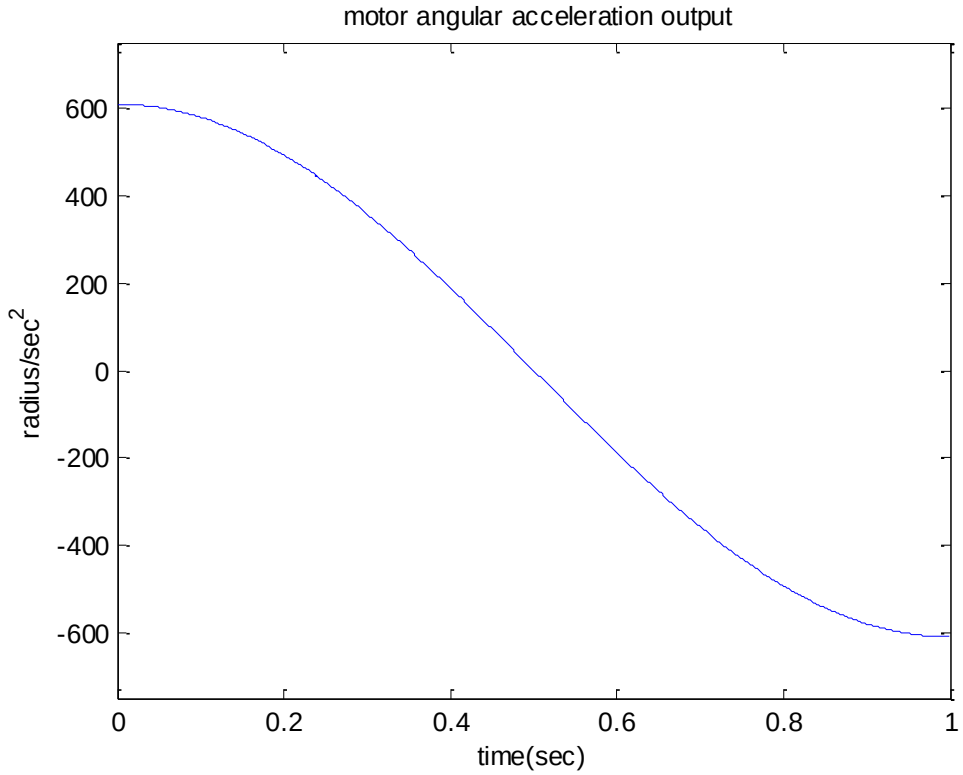

Figure. 4.6 Sine velocity function for clenching subsystem moving upward (b) motor angular acceleration

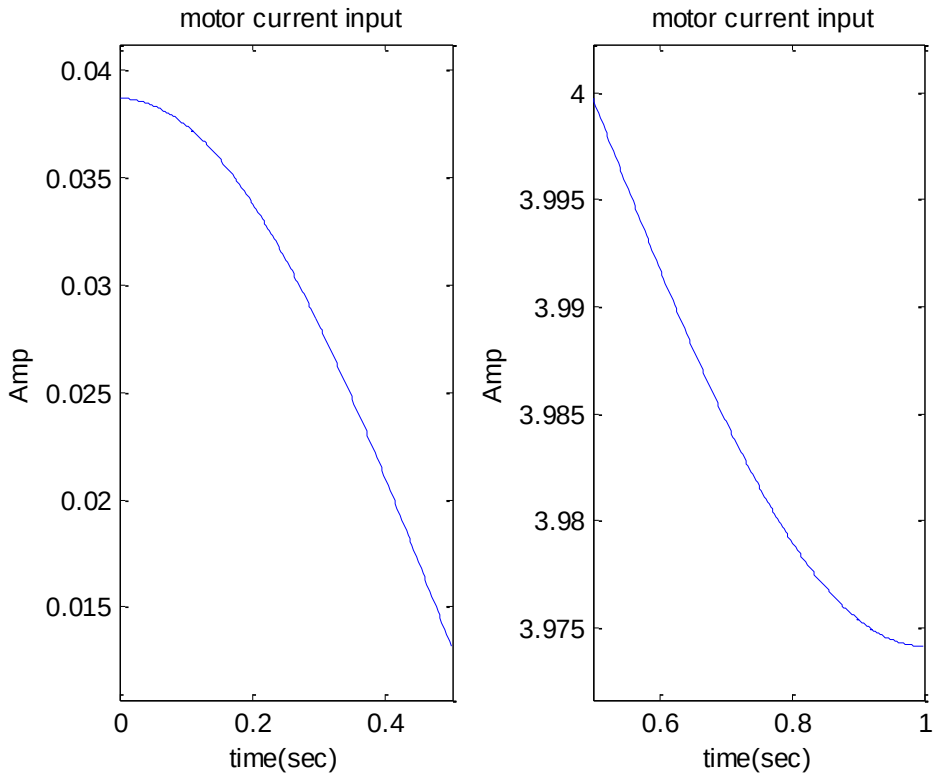

Figure 4.6 Sine velocity function for clenching subsystem moving upward
(c) motor angular currents using

4.3.4 Concluding Remarks

Based on the results shown in Table 4.1, the following discussion is separated into two based on the two conditions. First, with the jaw moving downward, the package load was constant and there is no external force exerting on it. The three different types of function generated the same results in the energy consumption for the DC motor. However, the motor using cubic velocity function spent the longest time and while the sine function takes the shortest time to accomplish this downward motion.

Secondly, with the jaw moving upward, there is an external force happening over

the second half of the trajectory, we have to consider increasing angular velocity and acceleration and also decreasing the cost in time. According to the results, for minimum energy consumption of motor, the angular velocity with a sine function is better than the cubic and the quadratic functions. Thus, in this case, the best energy saving is using sine equation for motor angular velocity output.

	Velocity function	Cost time	Energy consumption
Moving downward	$-9.9817t^3 - 121.0162t^2 + 237.1452t$	1.7166 sec	0.0015 J
	$-159.6377t^2 + 266.4277t$	1.6690 sec	0.0015 J
	$-131.0279\sin(-2.1187t - 364.4247)$	1.4828 sec	0.0015 J
Moving upward	$-470.216t^3 - 36.7845t^2 + 507.0005t$	1 sec	34.6861 J
	$-742.1085t^2 + 742.1085t$	1 sec	34.6861 J
	$194.2836\sin(-3.1416t + 3.1416)$	1 sec	34.6733J

Table 4.1: Minimum energy optimization results

Chapter 5

CONCLUSION AND SUGGESTION FOR FUTURE WORK

5.1 Conclusions

A novel design of a three degree-of-freedom mastication system for chewing assistance purpose has been presented. There were many proposed mechanical designs to assist in mandible functions or to help the jaw in chewing foods such as: the jaw simulator robot, robotic model of linear actuation and crank actuation. No matter how well they worked, they were all impractical due to their size and weight.

To solve this problem, a prototype of a new design for a mastication robot has been successfully constructed. Since the goal is to use the robot to fulfill mandible movement range and chewing force, the device prototype has been tested experimentally and has been shown to duplicate human jaw dynamic movements in the frontal plane. From the analysis and optimum simulation, the system has been shown to be able to exert the required output force while conserving input energy to the motors. This shows that by utilizing a novel mechanism with controls, it is possible to perform a similar human jaw movement and is sufficiently small and light for user applications.

5.2 Suggestion for Future Works

In the future, in order to improve on the robot function, a new prototype would be needed that has a higher gear ratio at the scotch yoke. The addition of a feed-back controller with a position sensor may also be useful to improve on motion accuracy. Improving the robot structure using the program Ansys as well as constructing a sturdier prototype for testing on a real human jaw would be the goal for future work.

Reference:

[1] W. L Xu, J. Bronlund: “Mastication Robots”, pp1-88, 170, 2010

[2] Galer, Hockenberry, et al.: “Human Jaw Motion Simulator”, pp7-51, 2007

[3] Gray, Henry, Anatomy of the Human Body, 20th ed. Philadelphia: Lea & Febiger, 1918.

[4] Takanobu, H., et al.: Mouth opening and closing training with 6-DOF parallel robot. In: Proceedings of the 2000 IEEE International Conference on Robotics & Automation, San Francisco, pp. 1384–1389 (2000)

[5] Takanobu, H., et al.: Jaw training robot and its clinical results. In: Proceedings of IEEE/ASME International Conference on Advanced Intelligent Mechatronics (AIM 2003), pp. 932–937 (2003)

[6] Takanobu, H., Takanishi, A.: Design of a Mastication Robot Mechanism Using a Human Skull Model. In: Proceedings of the 1993 IEEE/ RSJ International Conference on Intelligent Robots and Systems, Yokohama, Japan, July 26-30, 1993

[7] Xu, W.L., et al.: A robotic model of human masticatory system for reproducing chewing behaviors. IEEE Robotics Automation Mag. 12, 90–98 (2005)

[8] Torrance, J., et al.: Motion control of a chewing robot of 6 RSS parallel mechanism. In: Proceedings of International Conference on Autonomous Robotics

and Agents, pp.593–598. Palmerston North, New Zealand (2006)

[9] Waseda University, “Dental Robotics Groupe”, FEB 15, 2012 http://www.takanishi.mech.waseda.ac.jp/top/research/jaws/index.htm

[10] Takanobu, H., et al.: Mouth opening and closing training with 6-DOF parallel robot. In: Proceedings of the 2000 IEEE International Conference on Robotics & Automation, San Francisco, pp. 1384–1389 (2000)

[11] Takanobu, H., et al.: Mouth opening and closing training with 6-DOF parallel robot. In: Proceedings of the 2000 IEEE International Conference on Robotics & Automation, San Francisco, pp. 1384–1389 (2000)

[12] Takanobu, H., et al.: Integrated dental robot system for mouth opening and closing training. In: Proceedings of the 2002 IEEE International Conference on Robotics & Automation, Washington DC, pp. 1428–1433 (2002)

[13] Takanishi, A., et al.: Development of 3 DOF jaw robot WJ-2 as a human’s mastication simulator. In: Proceedings of Fifth International Conference on Advanced Robotics, Pisa, pp. 277–282 (1991)

[14] C. McNeill: “Science and Practice of Occlusion”, pp. 23-78, 193 (1997).

[15] Wikipedia, ” Temporomandibular joint”, MAR 03, 2012; http://en.wikipedia.org/wiki/Temporomandibular_joint

[16] K. D. Foster, A. Woda, M. A. Peyron: Effect of Texture of Plastic and Elastic Model Foods on the Parameters of Mastication, J Neurophysiol 95: 3469–3479, 2006

[17] P. Venkataraman: “Applied Optimization with Matlab Programming”, pp 1-11 & 369-376, 2008

[18] J. N. Nocedal and S. J. Wright. Numerical Optimization, chapters 12, 18. Prentice Hall, 1999.

Appendix A: Mastication Robot Model CAD Drawing

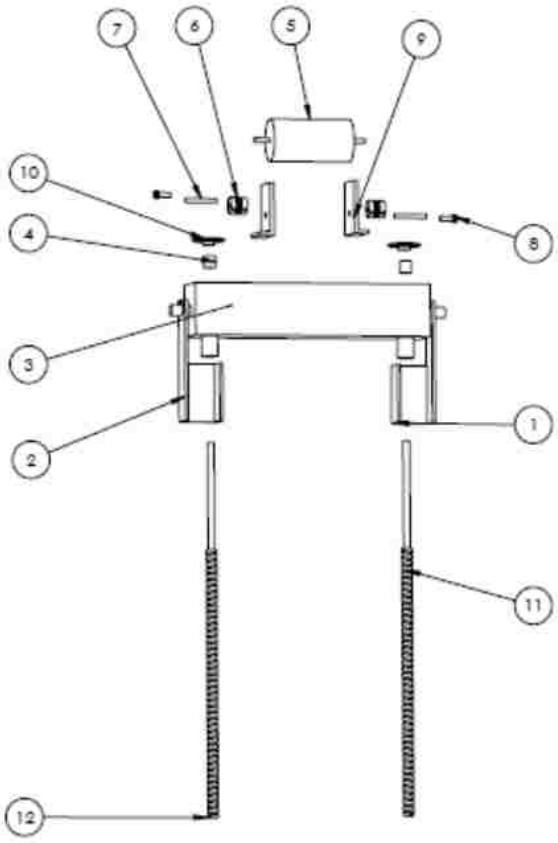

Figure Appendix A.1: clenching subsystem exploded view CAD drawing

Item No.	PART NAME	DESCRIPTION	QYT.
1	box support_Left	material: aluminum	1
2	box support_Right	material: aluminum	1
3	box	material: aluminum & acrylic	1
4	mount bearing	S99NH2-BN0814 from SDP Co.	2
5	double shaft motor	12V dc motor	1
6	rigid fairloc coupling	S51FCZ-125125 from SDP Co.	2
7	shaft	material: steel	2
8	pinion gear	12 DP , pinion from SDP Co.	1
9	main motor support	material: aluminum	2
10	bevel gear	60 DP , bevel from SDP Co.	1
11	LeadscrewR	BF6050 X 15” from Haydon Co	1
12	LeadscrewL	BF6050LH X 15” from Haydon Co	1

Table A.1: Bill of Material of clenching subsystem

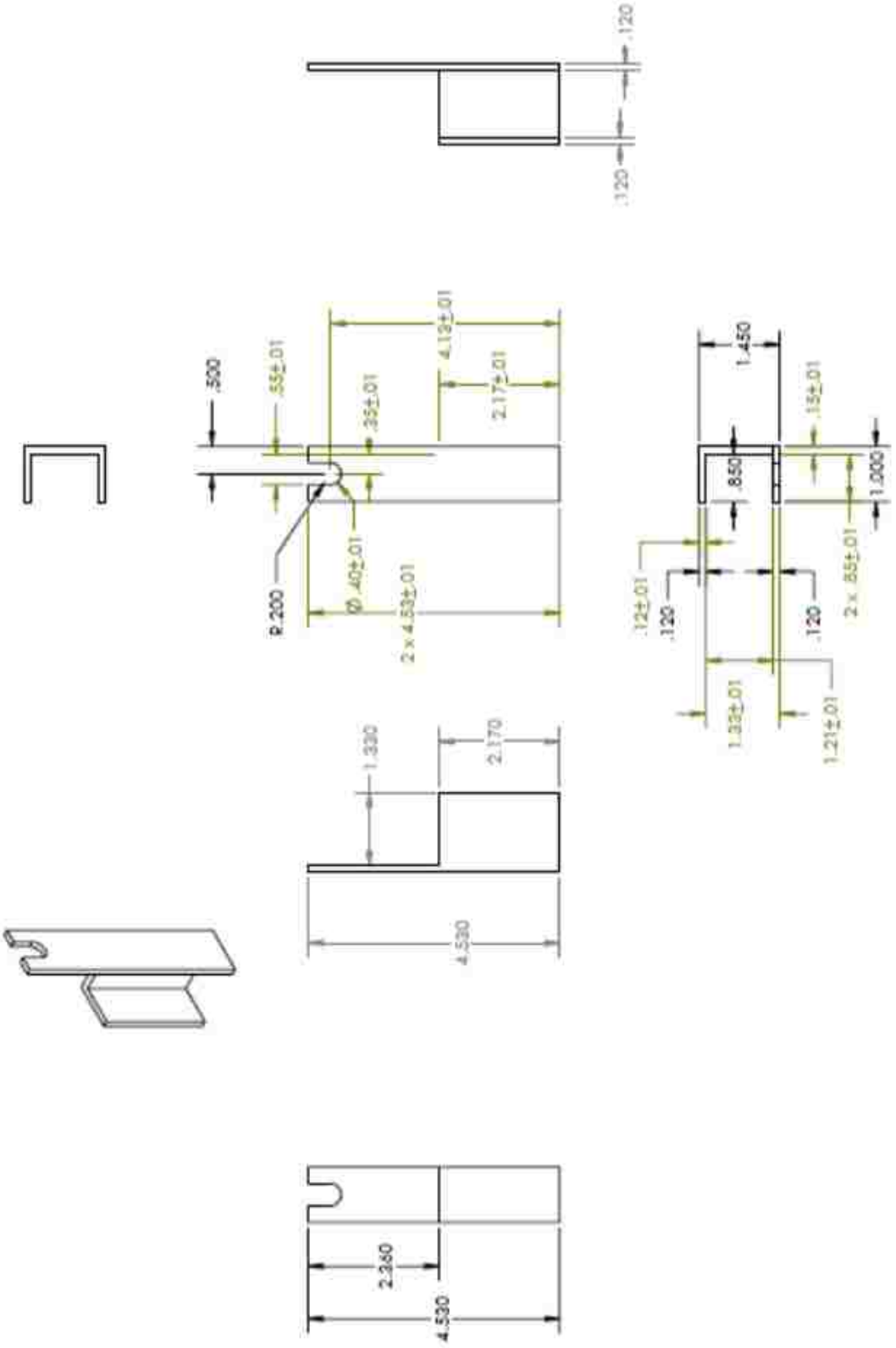

Figure Appendix A.2: Box support_Left

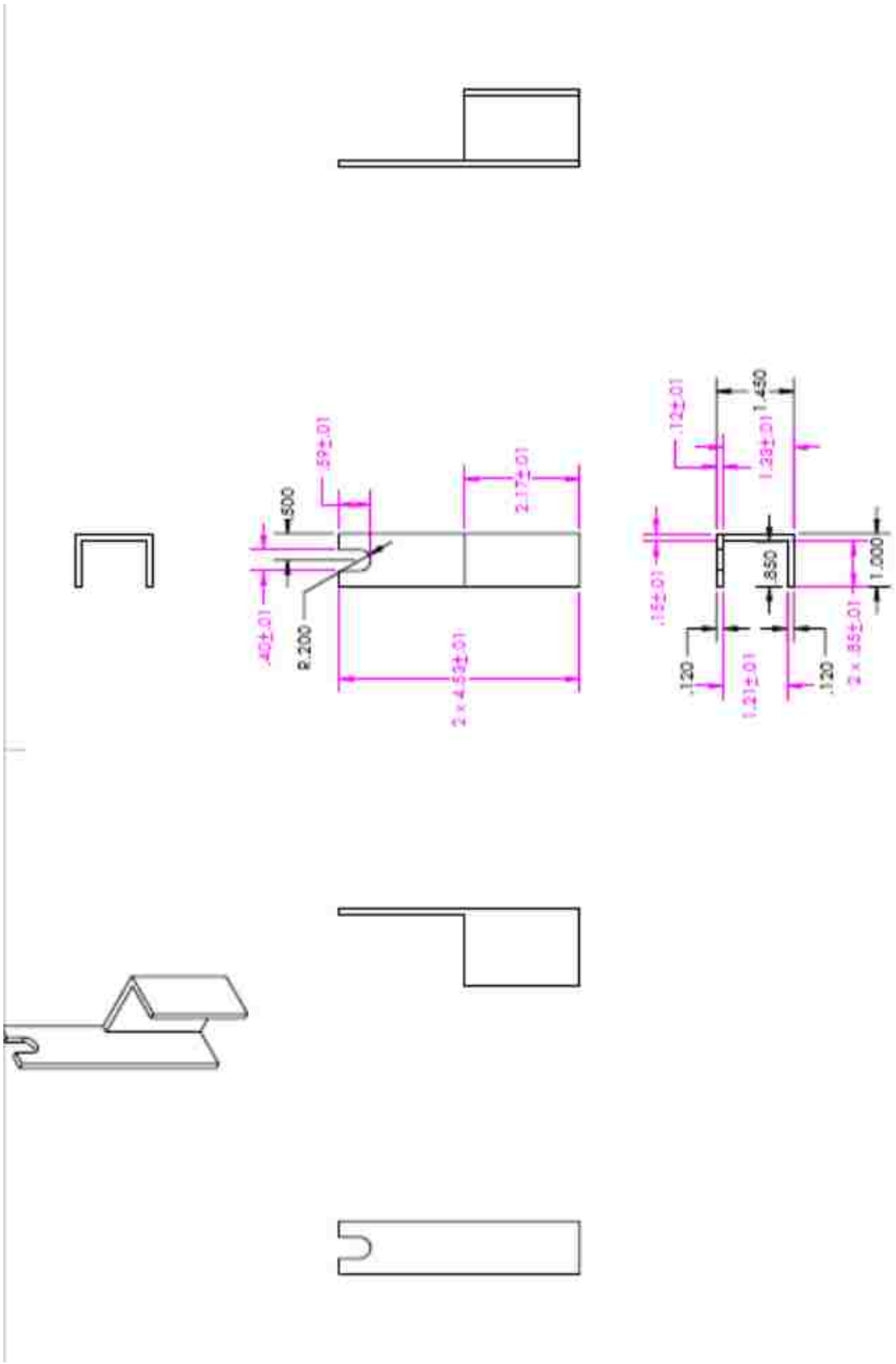

Figure Appendix A.3: Box support_Right

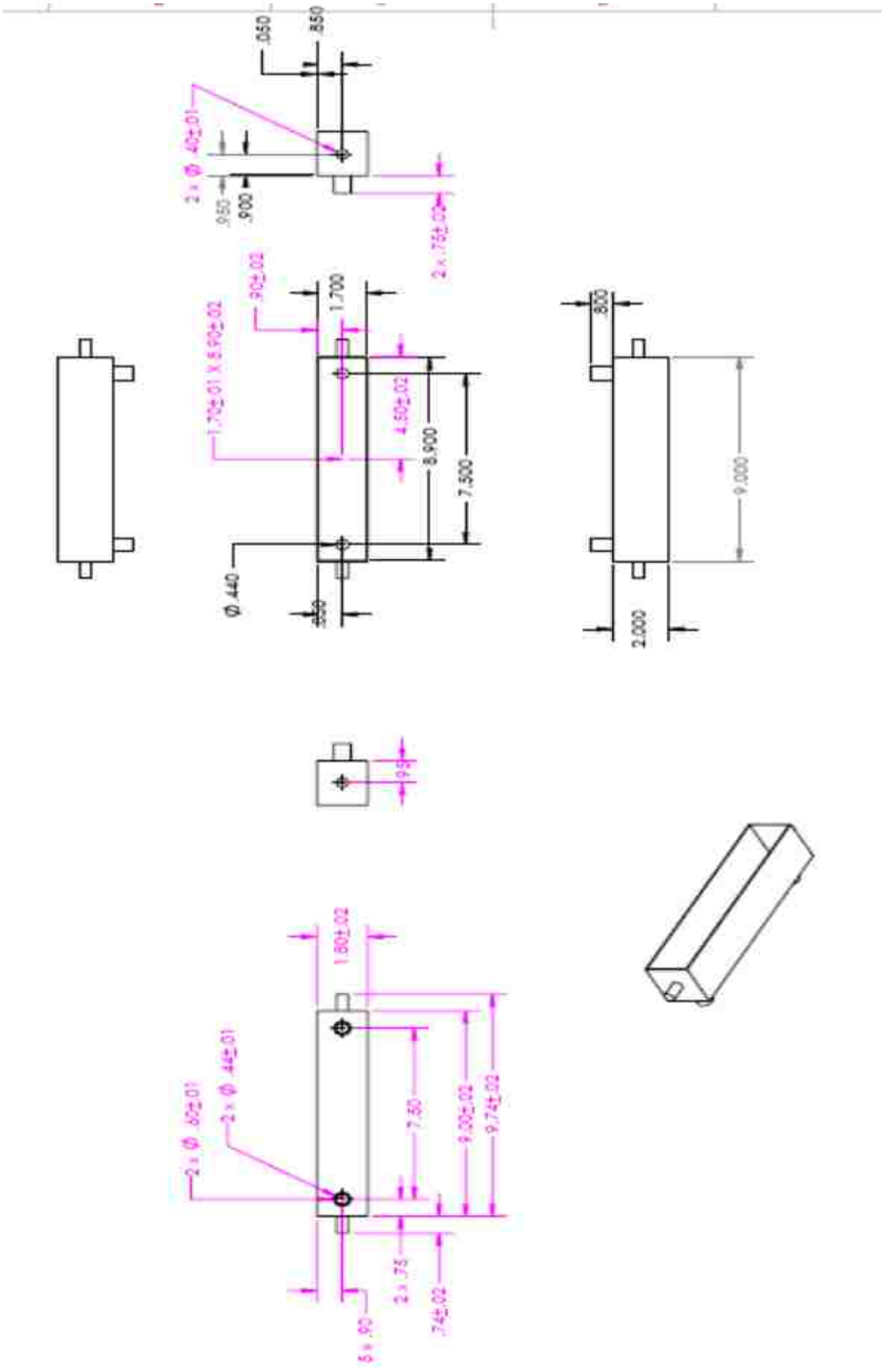

Figure Appendix A.4: Box

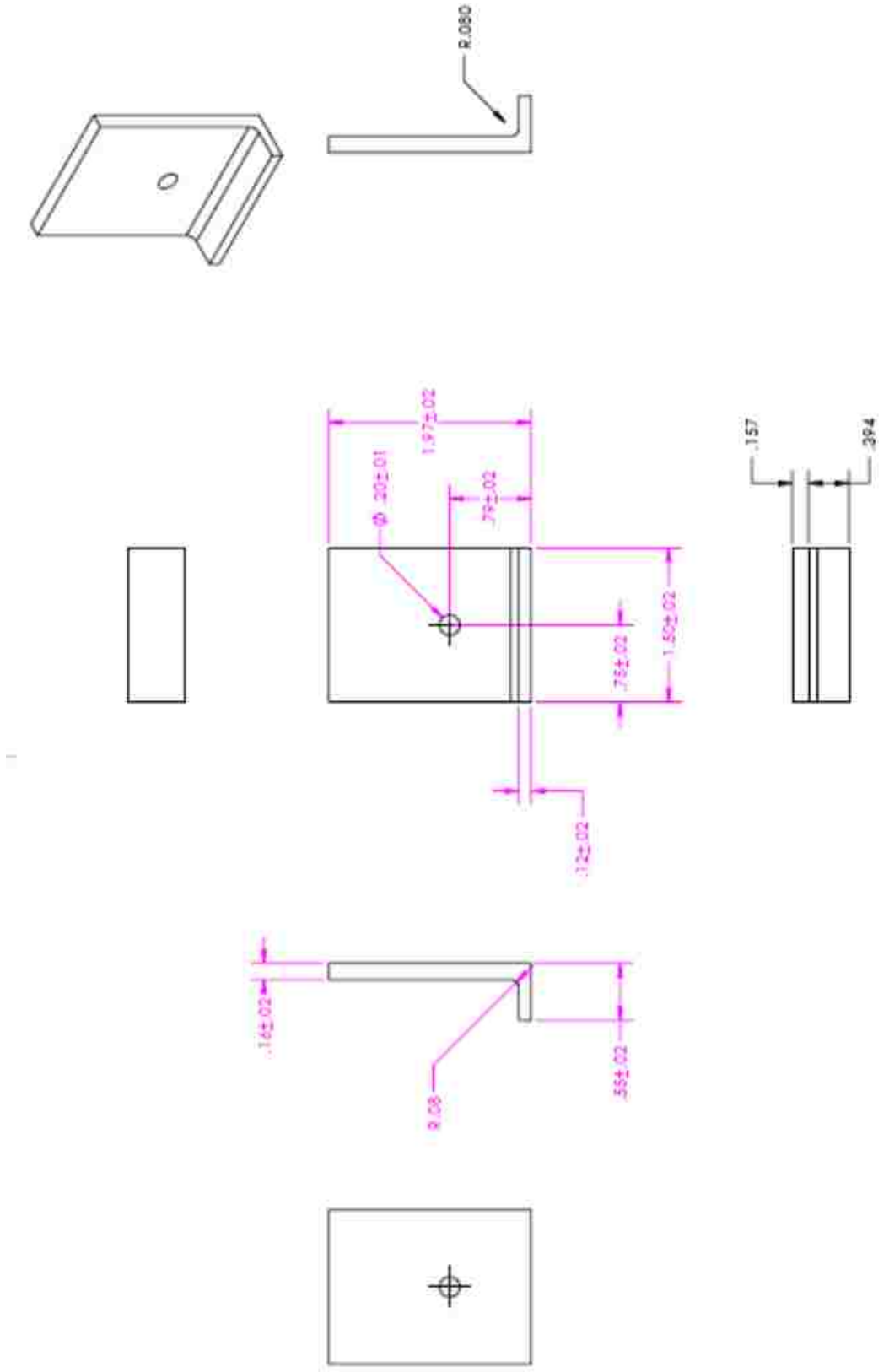

Figure Appendix A.5: Main motor support

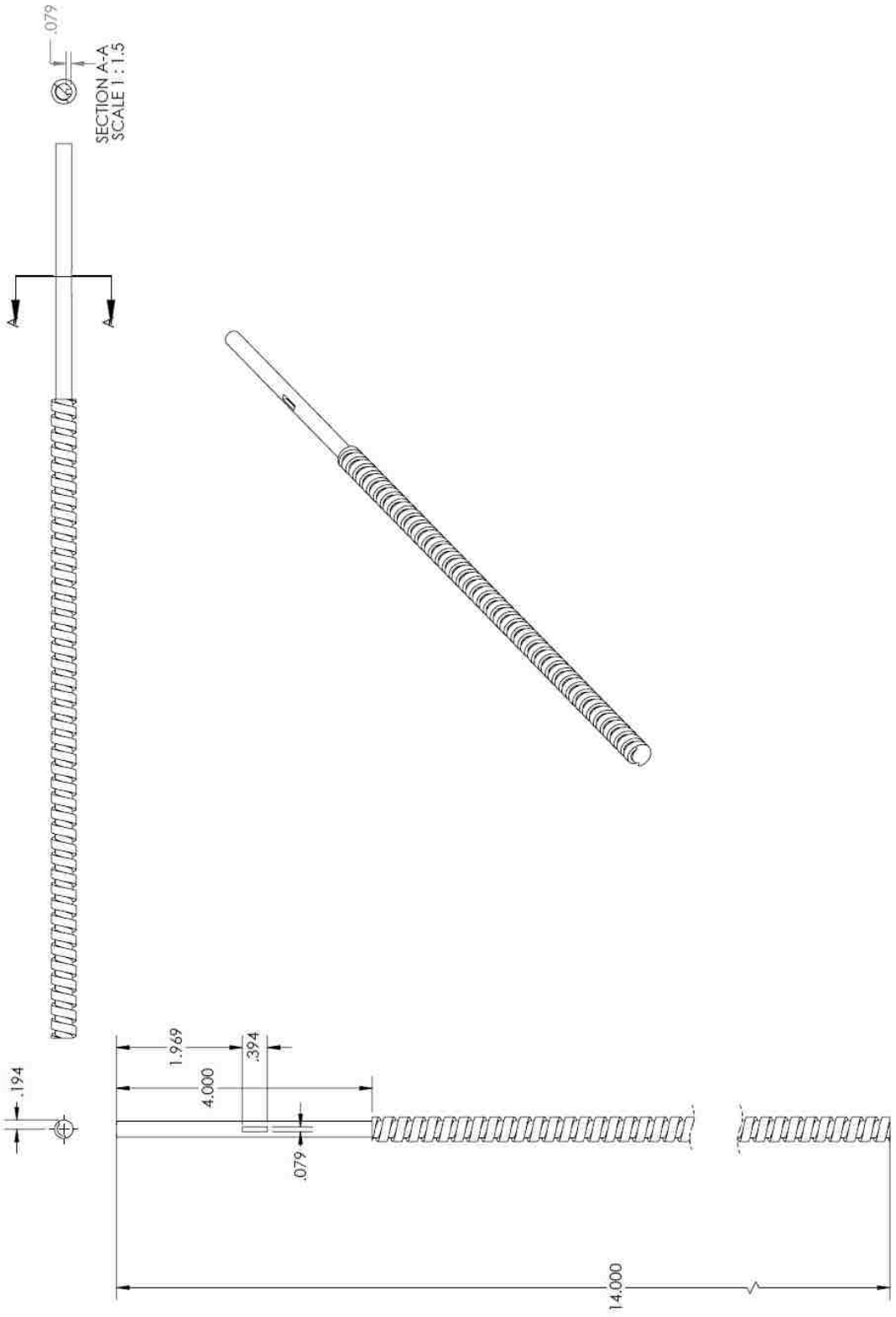

Figure Appendix A.6: Leadscrew RH

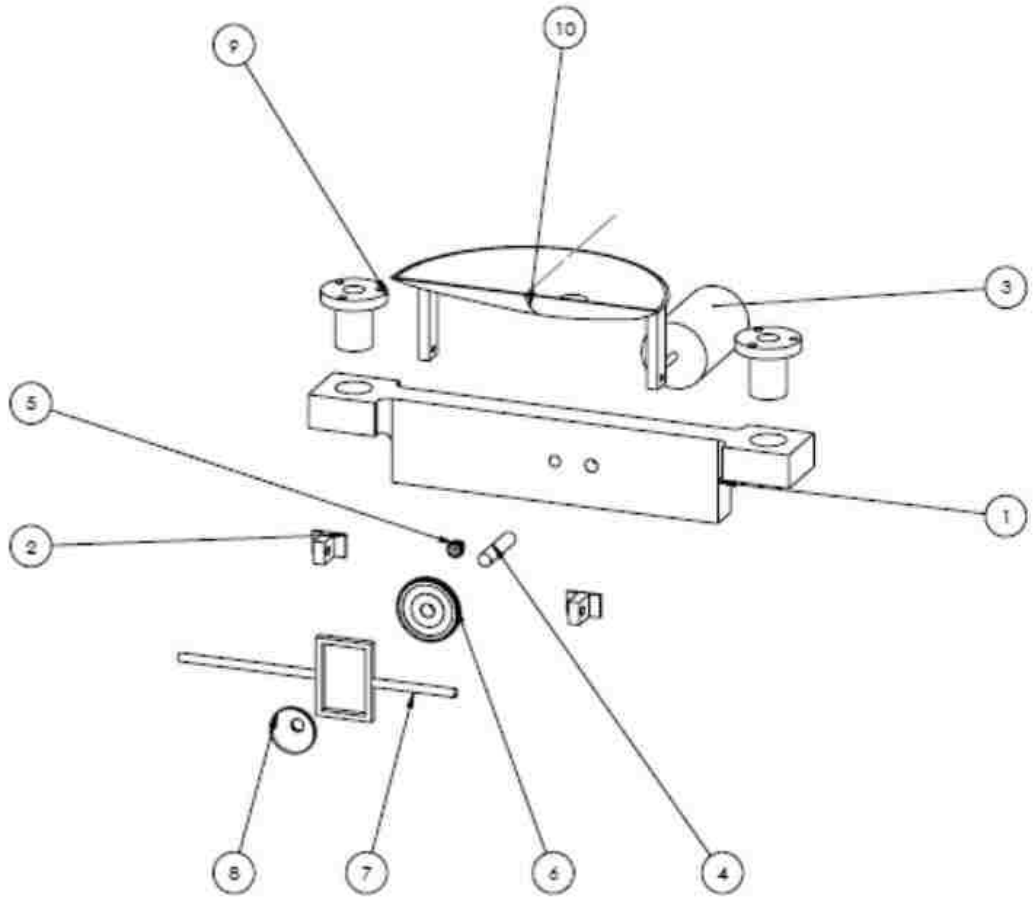

Figure Appendix A.6: Grinding subsystem exploded view CAD

Item No.	PART NAME	DESCRIPTION	QYT.
1	Grinding subsystem base board	material: acrylic	1
2	yoke support part	material: aluminum	2
3	second motor	24V dc motor	1
4	scotch-yoke shaft	material: steel	1
5	12 DP spur gear	A 1M 2MYZ05012 from SDP Co.	1
6	72 DP spur gear	A 1M 2MYH05072 from SDP Co.	1
7	yoke slider	material: aluminum & cooper	1
8	cam	material: acrylic	1
9	lead screw flange	BFWF-037-0500-BY18 from Haydon Co.	2
10	cap	material: aluminum	1

Table A.2: Bill of Material of Grinding subsystem

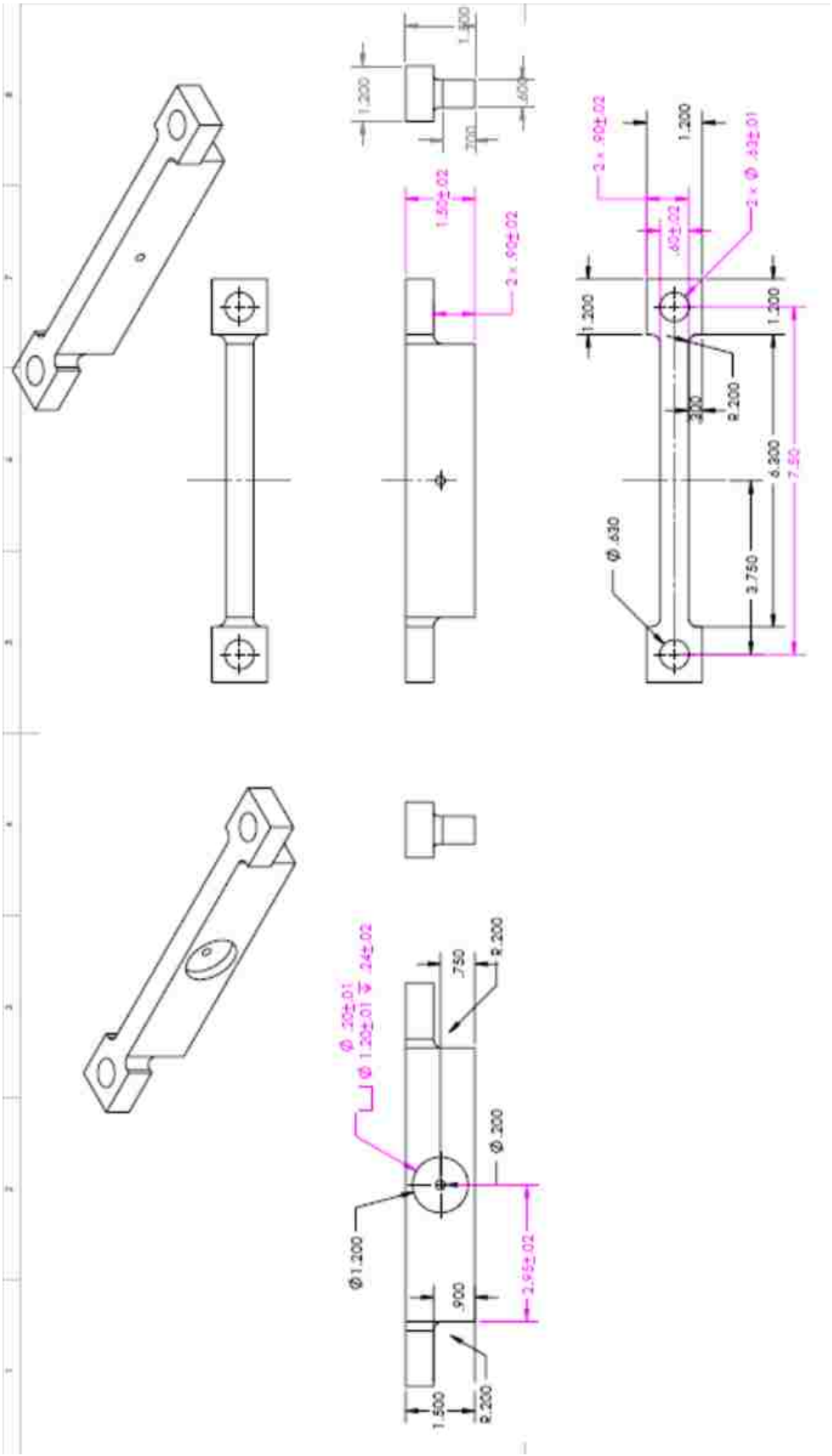

Figure Appendix A.7: Grinding subsystem base board

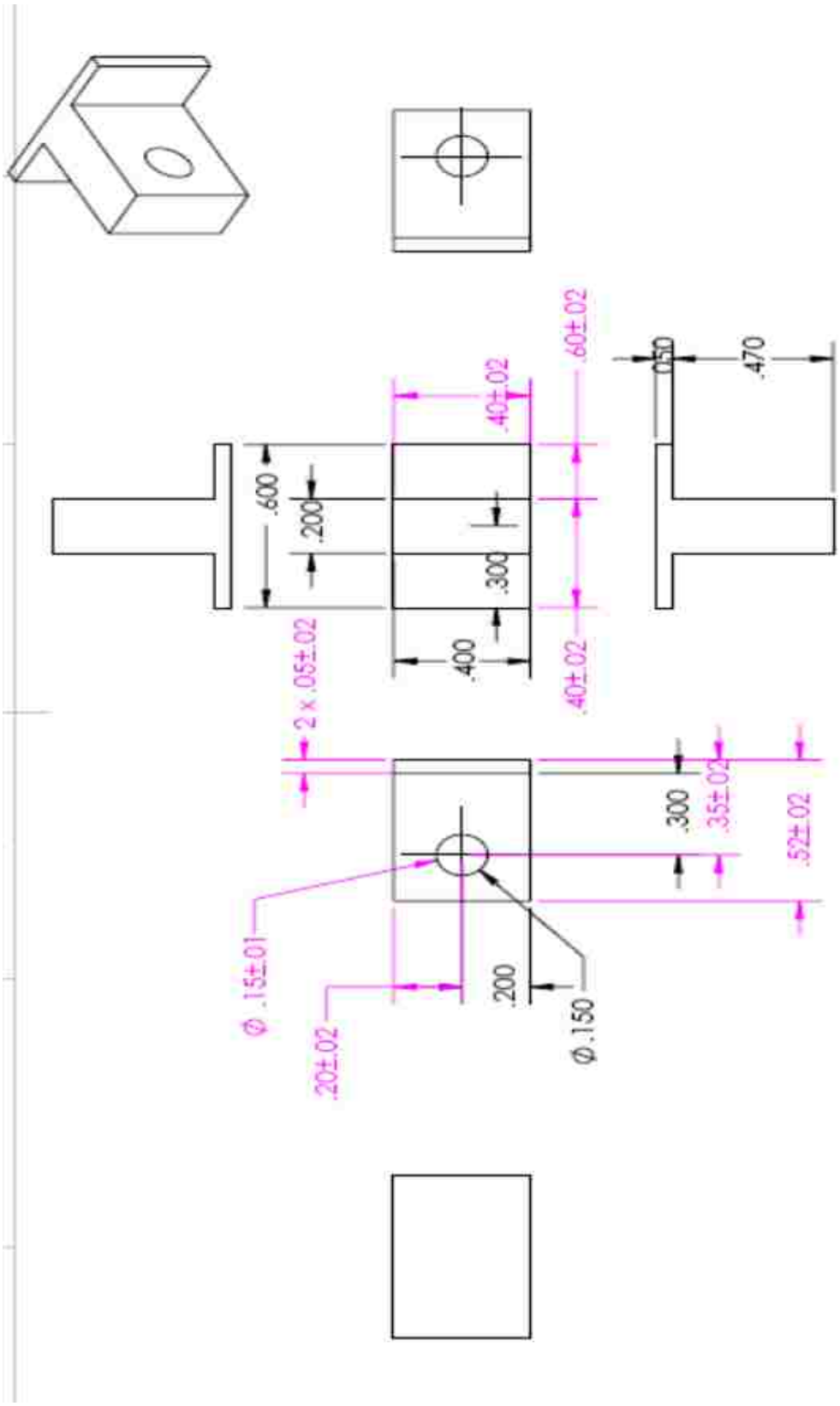

Figure Appendix A.8: Yoke support part

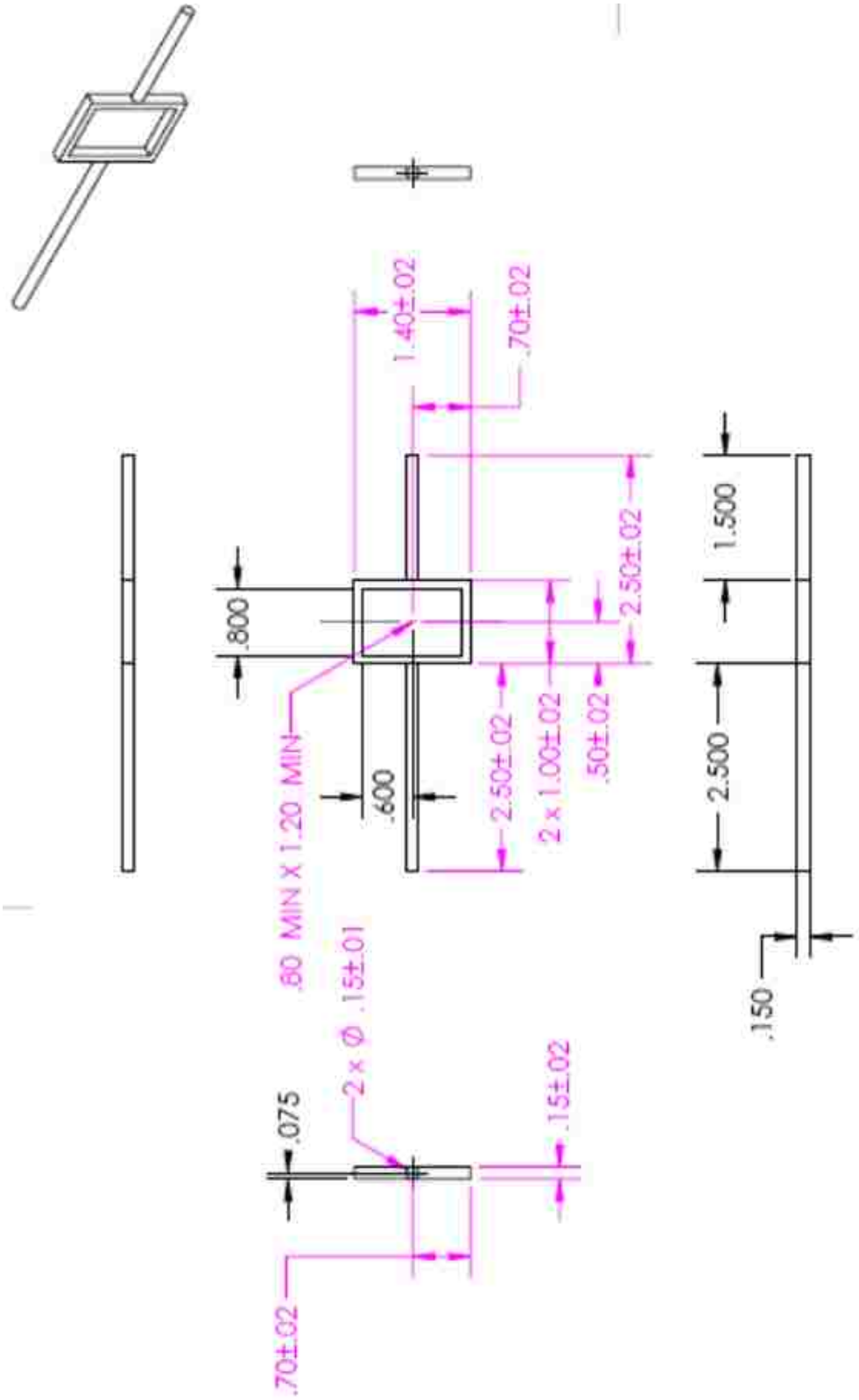

Figure Appendix A.9: Yoke slider

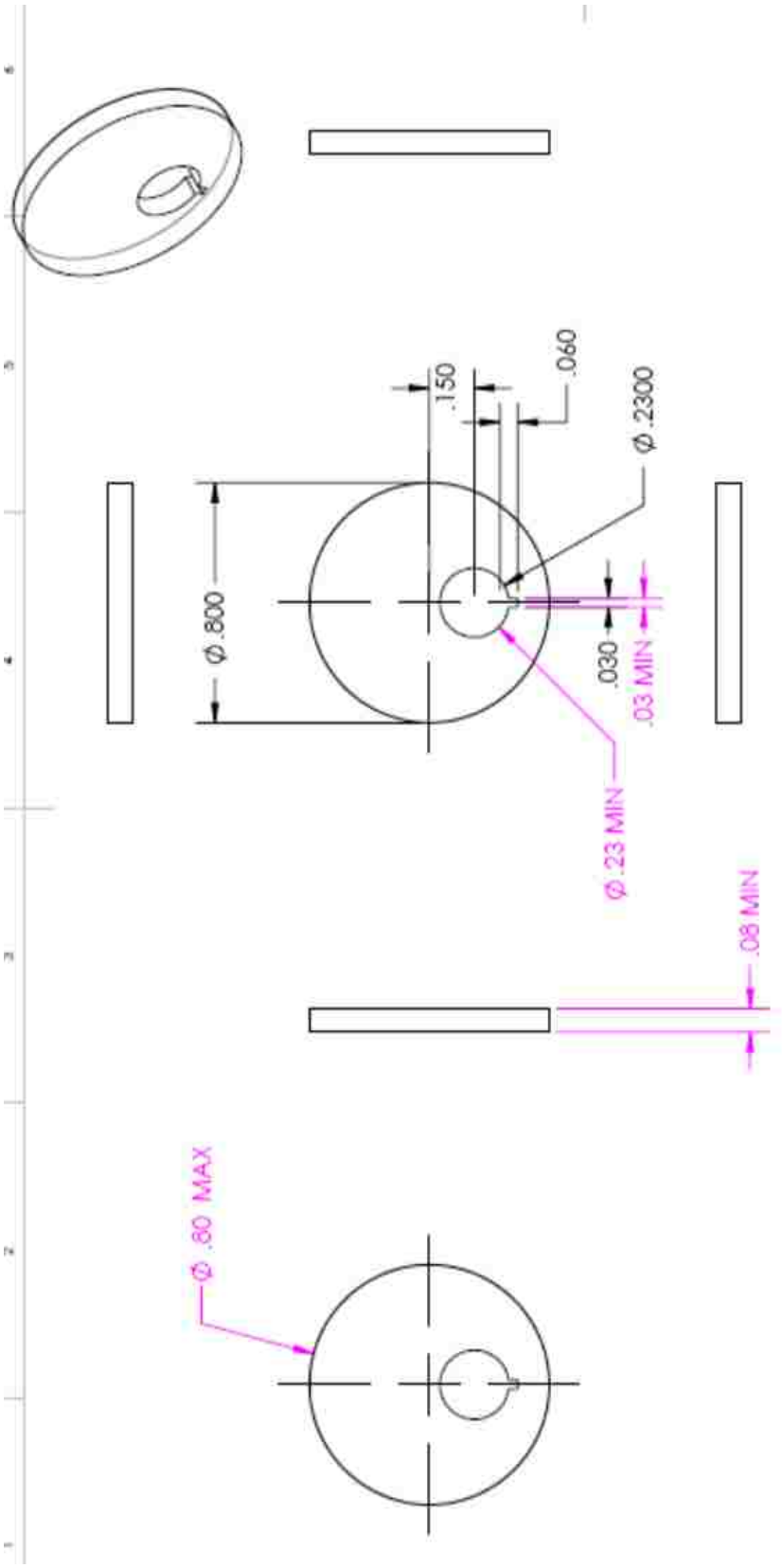

Figure Appendix A.10: Cam

Appendix B: Program of LabView applied in LVDT

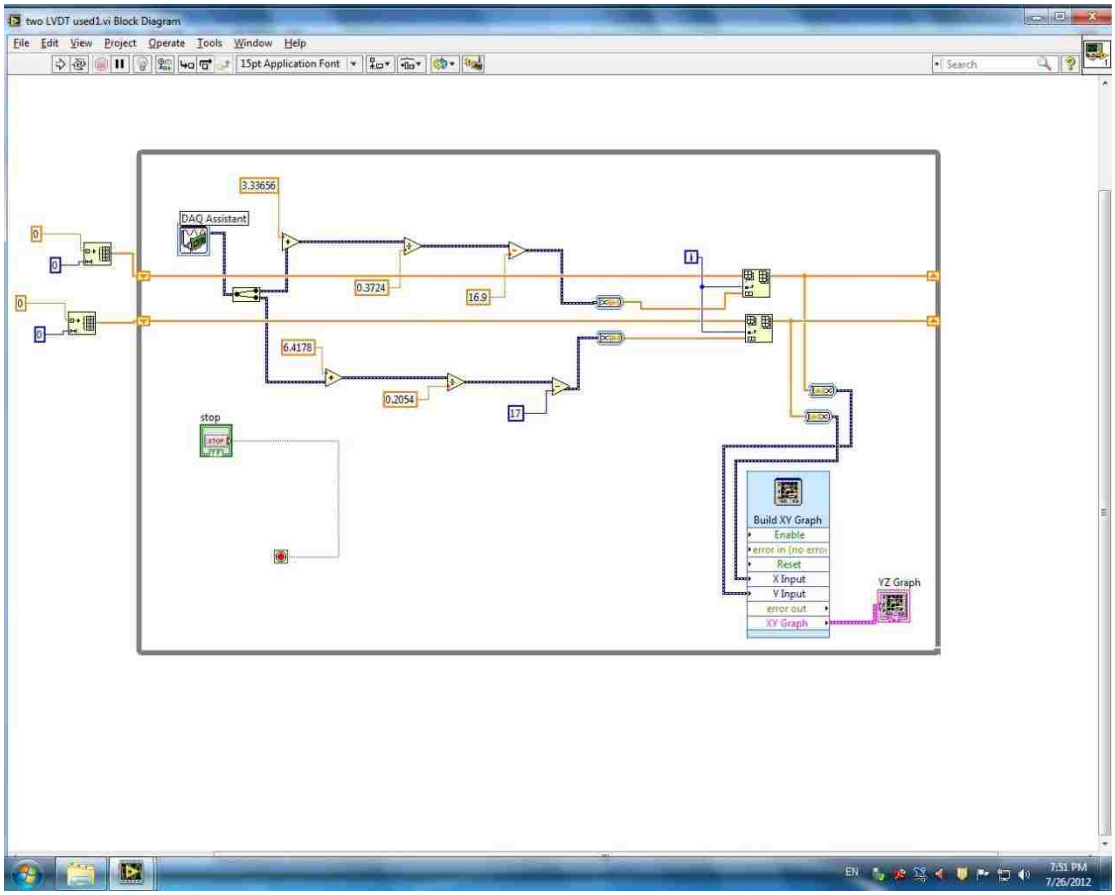

Figure Appendix B.1: Program of cam Recorded moving trajectory of the mastication robot in frontal plane

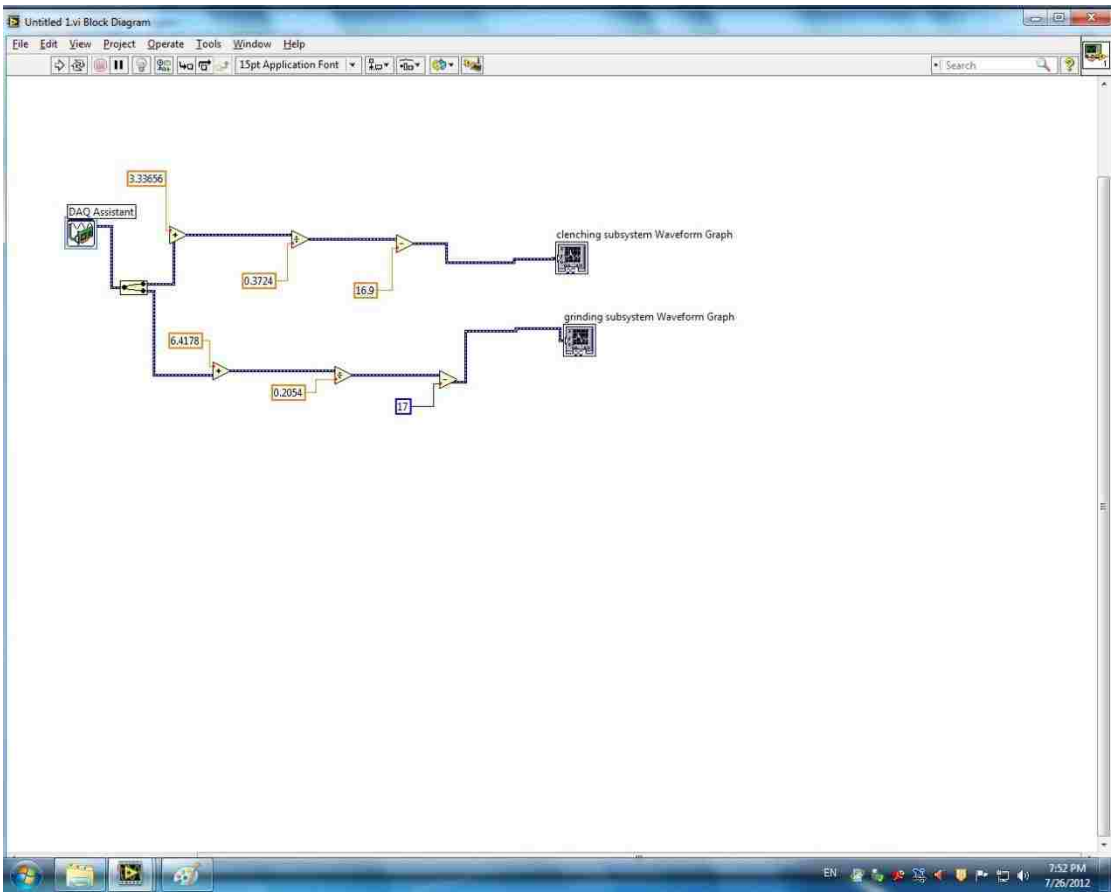

Figure Appendix B.2: Program of mastication robot moving trajectory in time

Appendix C:

Table C.1: Simulation model parameters for optimization analysis on mastication robot

Clenching subsystem motor:

k_m= 0.0338 N-m/amp

Rm =4.37 Ohm

Jm = 1.357×10^{-6} kg-m

Jc = 1.11×10^{-6} kg-m

Ng = 1/3

Lead screw of clenching subsystem:

l = 12.7 mm

W = 0.12 kg

e = 81%

D = 0.05 m

fc = 300 N

Vita

The author was born in Tainan, Taiwan on March 10, 1986 to Kuo-Hsin Chang and Yu-Siou Ciou. He earned a Bachelor of Science degree in the Department of Systems and Naval Mechatronic Engineering from National Cheng Kung University, Tainan City, Taiwan, in June 2008. The author studied in Mechanical Engineering and Mechanics Department, Lehigh University from 2010, and his research is supervised by the advisor, Dr. Meng-Sang Chew. The author's studies involve mechanical design and the application of control methods. He will receive his Master of Science degree in Mechanical Engineering and Mechanics in September, 2012.